7-30-2014 12:00 AM

Influence of approach flow conditions on urban street canyon flow

Karin Blackman
The University of Western Ontario

Supervisor
Dr. Eric Savory, P. Eng.
The University of Western Ontario

Graduate Program in Mechanical and Materials Engineering
A thesis submitted in partial fulfillment of the requirements for the degree in Master of Engineering Science
© Karin Blackman 2014

INFLUENCE OF APPROACH FLOW CONDITIONS ON URBAN STREET
CANYON FLOW

(Thesis format: Integrated Article)

by

Karin Blackman

Graduate Program in Mechanical and Materials Engineering

A thesis submitted in partial fulfillment
of the requirements for the degree of
Master's of Engineering Science

The School of Graduate and Postdoctoral Studies
The University of Western Ontario
London, Ontario, Canada

Abstract

The turbulent flow within a street canyon and the approaching boundary layer has been studied using idealized wind tunnel models and a semi-idealized field experiment conducted in Nantes, France. The effect of upstream roughness on street canyon flow (lateral length/height, L/h = 30) using either 3D (cube) or 2D (rectangular block) upstream roughness, of the same height as the canyon, has been studied for two streamwise canyon width to height aspect ratios (AR) of 1 and 3 using Particle Image Velocimetry. A further wind tunnel model of equivalent geometry to the field experiment was used to compare with flow data obtained using sonic anemometers within the field experiment. The results show that in both the field and wind tunnel there is a significant influence by the upstream roughness on the flow within the canyon with respect to the turbulence intensities, shear layer size, turbulence spectra and canyon ventilation.

Keywords

Co-Authorship Statement

The work presented here is a collaborative effort by the present author, Dr. Eric Savory, P. Eng. and Dr. Laurent Perret. The experiments were conducted at the Laboratoire de recherche en Hydrodynamique, Energétique et Environnement Atmosphérique (LHEEA) at École Centrale de Nantes (ECN) under the guidance of Dr. Perret. Dr. Perret coordinated the set-up of the wind tunnel experiments with the help of Mr. Thibaut Piquet. The field data used for comparison with the wind tunnel data was collected previously by Dr. Jean-Michel Rosant and Mr. Piquet in LHEEA while Dr. Perret and Mr. Piquet conducted initial selection of applicable data periods for analysis. The processing and data analysis of the wind tunnel and field data were conducted with guidance by Dr. Perret and Dr. Savory. Both articles were completed with the present author as the primary author, however both Dr. Savory and Dr. Perret provided feedback and guidance throughout the writing process. Particular assistance was given by Dr. Savory during the writing of the literature review found in Section 2.1 below. This included a recommendation for the outline of the literature review and a thorough discussion of relevant conclusions outlined by the present author. As well, an investigation of the internal boundary layer development in Chapter 2 was completed by Dr. Perret and is presented in Appendix A. A version of Chapter 2 has been submitted for review to the journal Environmental Fluid Mechanics and a version of Chapter 3 will be submitted for review to the journal Atmospheric Environment.

Acknowledgments

Table of Contents

List of Tables

List of Figures

Figure 11   Conceptual cartoon summarizing the unsteady flow dynamics above and within street canyons. Above the canyon turbulent organized structures in the form of low momentum regions (dark blue) and hairpin vortices (dark red) dominate transport. Q2 is an ejection event and Q4 is a sweep event. Eddies (dark green) are shed off of the vertical

List of Appendices

List of Abbreviations

2D	two-dimensional
3D	three-dimensional
ABL	atmospheric boundary layer
Ac. Fr	acquisition frequency
ACH	air exchange rate
ESDU	Engineering Sciences Data Unit
HWA	hot-wire anemometry
IBL	internal boundary layer
Instr.	instrumentation
Meas. Quan.	measured quantity
PIV	particle image velocimetry
r.m.s.	root mean square
Terr. Rough.	terrain roughness
TKE	turbulent kinetic energy
WT	wind tunnel

List of Notation

A_d total plan area

A_p plan area of obstacles

AR   aspect ratio (W/h)

AR_b aspect ratio of upstream roughness (W_b/L_b)

CO   carbon monoxide

CO_2 carbon dioxide

d   displacement height

δ_w vorticity thickness

FFT   number of fast Fourier transform points in spectra block length

h   height of the canyon

$\bar{k}$ time averaged quantity

<k>   spatially averaged quantity

L   length of the canyon

λ_p plan area packing density

λ_f frontal area packing density

L_u streamwise integral length scale

% difference $= \frac{field - WT}{WT} * 100$

q'   heat flux

R^2 variance

TKE	$= 0.5 * (\sigma_u{}^2 + \sigma_v{}^2 + \sigma_w{}^2)$
u_*	friction velocity
U_e	freestream velocity
U_g	gradient velocity
U_{10}	mast (S10) velocity
U, V, W	mean streamwise, spanwise and vertical velocity
u', v', w'	fluctuating component of streamwise, spanwise and vertical velocity
u, v, w	instantaneous streamwise, spanwise and vertical velocity
σ_u, σ_v, σ_w	streamwise, spanwise and vertical turbulence intensity
$\overline{u'w'}$	turbulent shear stress
Vel	velocity magnitude
W_b	width of the canyon
z_o	aerodynamic roughness length
z'/L	stability parameter

Chapter 1

1   Introduction

Poor urban air quality as a result of vehicle and building exhaust entrainment and re-circulation is a significant concern for human health. Deaths due to urban outdoor air pollution are estimated by the World Health Organization [15] to be 1.3 million worldwide per year. Particulate matter, ozone formed from nitrogen oxides, nitrogen dioxide and sulfur dioxide are all pollutants produced by the burning of fossil fuels such as in vehicular combustion engines [15]. These pollutants are known to increase the risk of serious health conditions such as cardiovascular and respiratory diseases, lung cancer and asthma [15]. With dense arrays of buildings and increased vehicular traffic, urban areas are at the highest risk for poor air quality. Many resources have been used to help mitigate the effects of poor air quality on the urban population, but in order to reduce the impact one must first understand the processes that govern the transport of pollutants.

1.1   Defining the street canyon model

1.1.1   Boundary layer

Urban structures that make up urban canyon arrays are classified as bluff bodies due to the separation and large wake that occur over the body. Eddies, which are turbulent structures, consist of rotating fluid that is present in sharp edged bluff body flow, such as that over a street canyon [3]. These structures are responsible for some transport of fluid and are present within the shear layer that is formed over the street canyon. Figure 1 shows these flow structures present in urban street canyon flow.
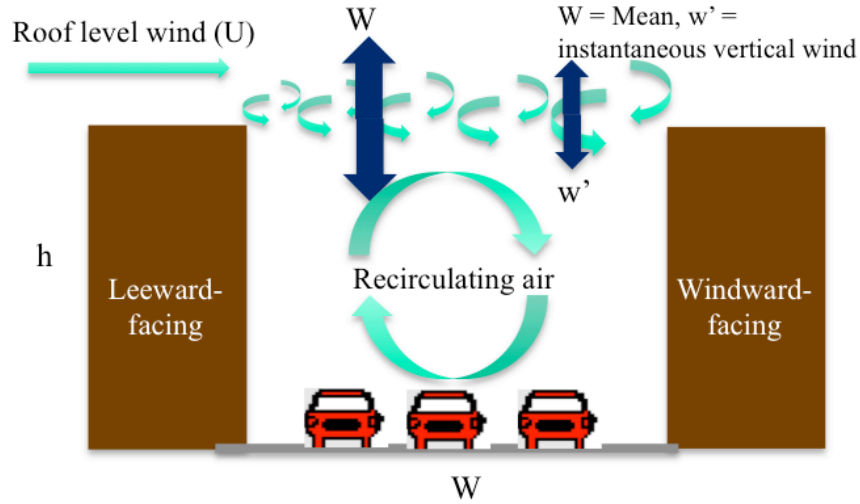
Figure 1   Mean flow pattern in urban street canyon

The behaviour of these turbulent structures forms the characteristics of the turbulent boundary layer. Boundary layers form over any surface, but in the urban environment the surface is sufficiently rough to create a complex boundary layer. There are two regions of a boundary layer. The first is the surface region where the flow is mostly dependent on the local effect of buildings [3]. The Ekman Layer is the remainder of the boundary layer, which can be defined by the log-law model [3]. The log law (Equation 1) uses the friction velocity (u_*), zero-plane displacement (d), and roughness length (z_o) to estimate the velocity at height z, where the friction velocity is a definition of shear stress in units of velocity, zero-plane displacement is the distance above the ground level that the wind is displaced upwards by the surface roughness and roughness length characterizes the roughness of the surface [3]. Another important parameter of the boundary layer is the freestream velocity (U_e) or gradient wind speed (U_g) in the atmospheric boundary layer (ABL), which is the velocity at a height that is no longer influenced by the ground roughness.

Equation 1   Log law

$$u_z = \frac{u_*}{k} \left[\ln \left(\frac{z-d}{z_o} \right) \right]$$

1.1.2   Surface roughness

The development of the boundary layer is significantly influenced by the surface characteristics [3]. Within the ABL these characteristics are defined as topography. Topography can be anything from gradual changes in elevation, escarpments or ridges, hills and valleys to fences, trees and buildings [3]. Within the wind tunnel upstream roughness arrays are used to simulate topography. Upstream roughness arrays are a series of elements that are used upstream of the canyon model to initiate and develop the approaching boundary layer. These arrays can be of any configuration or size, but generally there are three configurations used which are (1) two-dimensional bars, (2) three-dimensional staggered blocks or (3) three-dimensional aligned blocks (Figure 2). The aspect ratio (AR_b) of the 3D blocks can be defined as the ratio of width to length (W_b/L_b). The areal packing density (λ_p) of the roughness arrays can be defined as the ratio of the plan area of the obstacles (A_p) to the total plan area (A_d). Another parameter, the frontal area packing density (λ_f), which is the ratio of the frontal area of the obstacles (A_f) to the total frontal area (A_t), is used to define the upstream roughness.
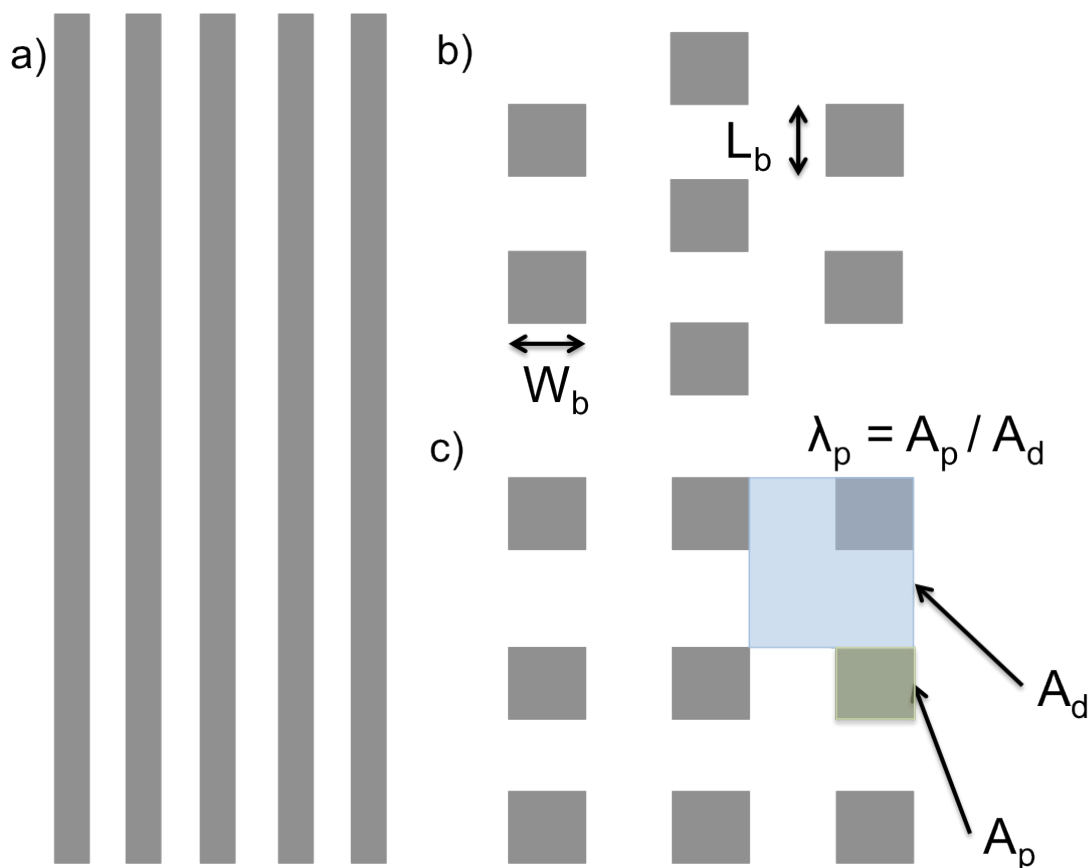
Figure 2   Upstream roughness array configurations; a) 2D bars; b) 3D staggered cubes; c) 3D aligned cubes

1.1.3   Street canyon

The urban environment is complex, but to understand the processes influencing the air quality of the entire city one can consider an individual street canyon. This allows us to investigate the fundamental physics and transport mechanisms governing ventilation of a street canyon immersed within an urban boundary layer. A street canyon is the area formed from a street between two rows of parallel buildings. Street canyons in urban areas can be defined by the same dimensions whether it be for a wind tunnel model or for a full-scale canyon. Figure 3 shows the dimensions used to define a street canyon including the length (L), height (h) and width (W). The aspect ratio (AR) of the canyon is defined as the ratio of the width to the height.

a)

Flow

L

b)

AR = W/h

h

W
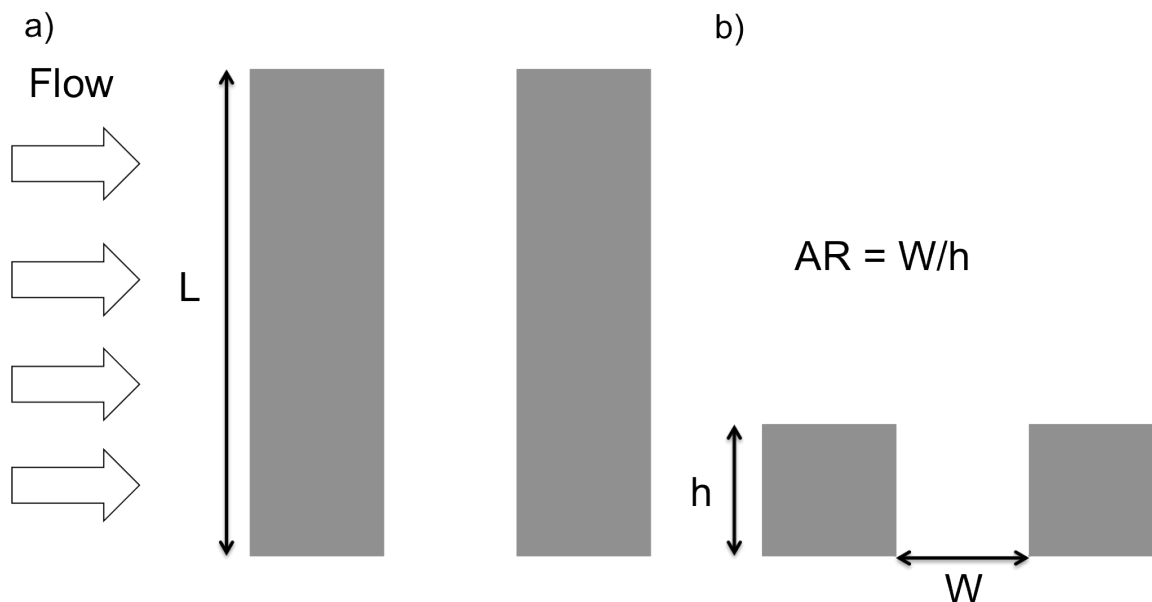
Figure 3   a) Plan view; b) side view of street canyon defining length, height, width and aspect ratio

1.2   Model approaches

Cities vary drastically from geographic region to region, for example cities in Europe are characterized by low buildings (5 storeys) with a dense packing structure, while tall buildings (100 storeys) characterize North American cities. One must consider carefully what method to use to model a street canyon based on what region one is interested in. There is always a trade-off between modeling a real city including geometric complexities and modeling a simplified version.

One method used to study real city street canyon flow and ventilation is conducting *in-situ* flow measurements within an existing urban environment (Figure 4). This figure shows flow measurement apparatus both within the canyon (Figure 4b) and on top of the enclosing buildings (Figure 4a) to collect flow measurements both within and above the canyon. Typically, with field measurements the measurement equipment consists of sonic anemometers, which can measure three-components of velocity at one point. Within the wind tunnel Particle Image Velocimetry (PIV), which utilizes a laser sheet, reflective particles and high-speed camera equipment, can be used to measure three-components of

velocity within a two-dimensional plane or three-dimensional box. *In-situ* flow measurements provide site-specific mean and turbulent flow statistics and can focus on specific areas of interest, such as; pedestrian level measurements or building exhaust locations. However, data logging times need to be long to obtain accurate statistics and flow measurements are limited to the number of instruments available. This means that profiles are limited and entire flow fields cannot be measured as they are with PIV in the wind tunnel. These studies are also difficult because the flow is highly dependent on weather conditions especially wind direction [10]. Obtaining an acceptable data set requires stringent data selection criteria and pre-treatment of those data [10]. Perhaps most importantly, as the flow dynamics are highly dependent on local building structure, *in-situ* measurements are not generally applicable to other sites and, therefore, cannot be used to understand the fundamental processes governing ventilation.

Figure 4   *In-situ* field study using sonic anemometers a) on building roof; b) within street canyon [4]

Conducting site-specific scaled wind tunnel model measurements can alleviate the measurement and data pre-treatment challenges (Figure 5). These site-specific models include the street canyon or area where measurements are desired as well as local buildings. The approaching boundary layer and freestream conditions can be controlled so there will be no variation in the data set, removing the requirement of pre-treatment [3]. As well, scaling boundary layers in the wind tunnel is well understood and results in a representative mean and turbulent flow structure for the site [3]. However, these

practices are not always implemented as will be elaborated upon in the present work. Although site-specific wind tunnel models yield realistic results the flows are difficult to interpret dynamically, thus rendering this approach unsuitable for understanding fundamental processes.

Figure 5   Site-specific wind tunnel model of 'Rue de Strasbourg' in Nantes and its surroundings [9]

Homogeneous models using simplified blocks to simulate ground roughness in the atmospheric boundary layer are a way of investigating canyon flow at the fundamental level to provide insight into urban areas (Figure 6). Although this method faces the same challenges with weather variation, data selection and pre-treatment there has been recent work using a PIV system to measure the flow field within an outdoor model [8, 14]. This improves the completeness of the information acquired. However careful attention must be paid when selecting a site to ensure that the approaching boundary layer represents the desired roughness terrain. This may require comparison of the approaching boundary

layer with the Engineering Sciences Data Unit (ESDU) information or other published data, which provides mean and turbulence profiles representative of boundary layer flow over different terrains [5, 6]. The simplified nature of the roughness elements allows this method to be used to investigate the fundamental flow processes.
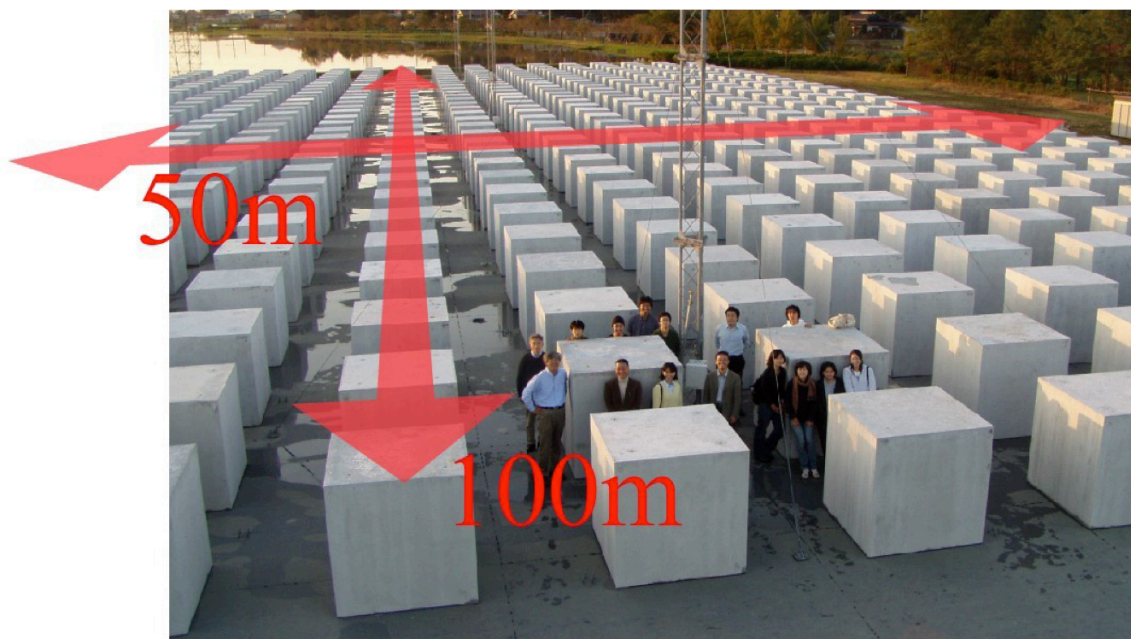
Figure 6   Homogeneous field model [8, 14]

Finally, wind tunnel models using simplified homogeneous roughness arrays and street canyons can be used to provide insight into the fundamental physics governing street canyon flow (Figure 7). These models can utilize measurement systems that provide relatively large spatial coverage such as PIV or high frequency acquisition such as hot-wire anemometry. As well, the boundary layer and inlet conditions can be controlled. However, as noted by Savory et al. [13] many street canyon flow studies conducted within the wind tunnel are not representative of full-scale boundary layers. As the flow dynamics are highly sensitive to the approaching boundary layer flow it is imperative to highlight the importance of accurately scaling the boundary layer and street canyon model [13].
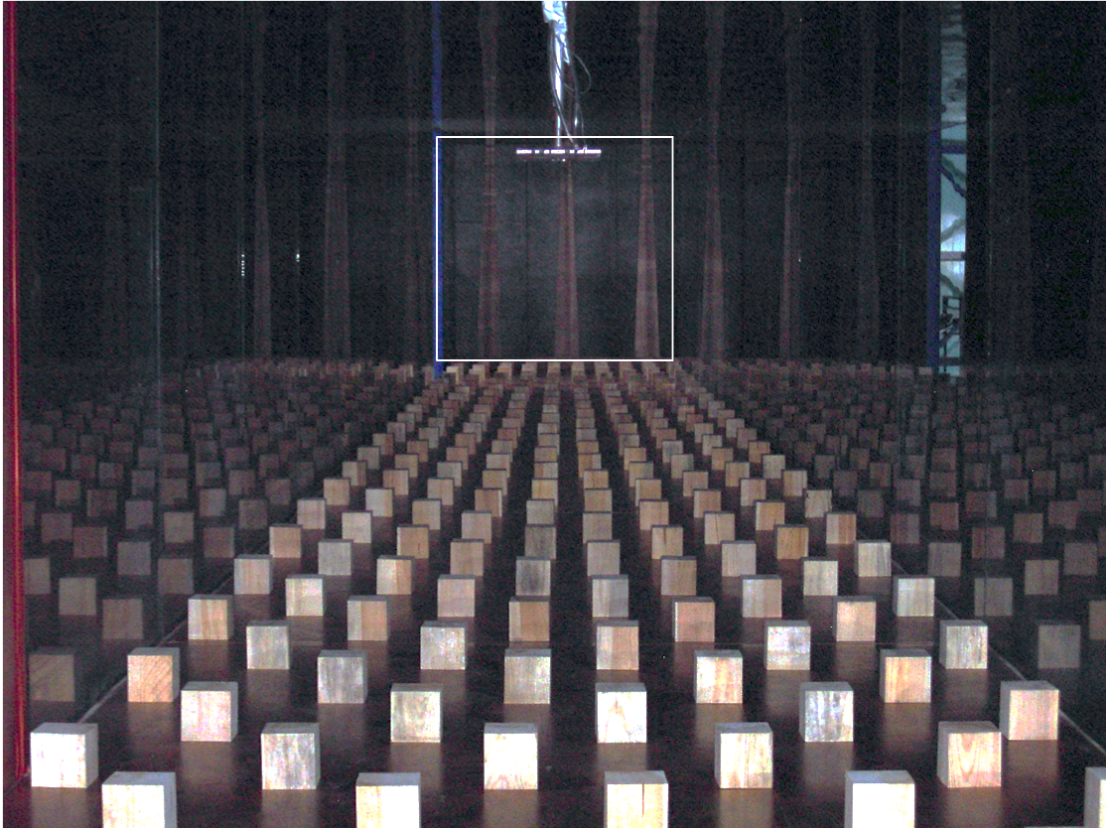
Figure 7   Homogeneous wind tunnel model at École Centrale de Nantes (France)

1.2.1   Model Scaling

When conducting both site-specific and simplified wind tunnel studies one must appropriately scale the approaching boundary layer and physical model considering three aspects of model similarity: geometric, kinematic, and dynamic. Geometric similarity is the scaling of all model dimensions to be a consistent ratio with that of the full-scale dimensions [3]. Kinematic similarity is the scaling of time as well as geometry and is achieved in the wind tunnel by matching Jensen number, Je, turbulent length scales, L_u, L_v and L_w, and turbulence spectra. The Jensen number is the ratio between the height of the obstacles, h, and the roughness length, z_o, and characterizes the upstream boundary layer. The boundary layer is further characterized by the size of the turbulent eddies described by turbulent length scales in the streamwise, L_u, spanwise, L_v, and vertical, L_w directions. Finally, the turbulence spectra, which describes the distribution of the energy containing turbulent eddies, should match full-scale when normalized. Dynamic

similarity is the scaling of all forces and is achieved by matching the dimensionless number Reynolds number, Re. This is difficult to achieve at small scales. However, it has been shown that flow over sharp edged bodies are not strongly Re dependent and similarity is achieved as long as sufficient Re is attained to generate turbulent flow.

These similarity requirements can be achieved using the guidelines specified by ESDU. ESDU provides empirically derived boundary layer profiles, including mean streamwise velocity, turbulence intensities, shear stress, integral length scale and turbulence spectra, for different terrain based on accumulated field data [5, 6]. These profiles can then be matched in the wind tunnel to achieve similarity using upstream roughness elements and turbulence generators such as fences and spires.

1.3   Turbulent canyon flow phenomena

The following section will describe current knowledge of the flow phenomena governing the ventilation of urban street canyons.

1.3.1   Sweeps and ejections

The turbulent interaction between the canyon flow and the overlying boundary layer is responsible for the ventilation of the canyon. This interaction causes two types of events: sweeps and ejections (Figure 8). A sweep is an event where fluid and momentum enter the canyon from the shear layer, while an ejection is an event where fluid and momentum leave the canyon and enter the shear layer. As fluid always has a tendency to move from areas of high momentum to areas of low momentum this suggests that there is a relationship between sweeps, ejections and turbulent momentum gradients across the shear layer and street canyon.
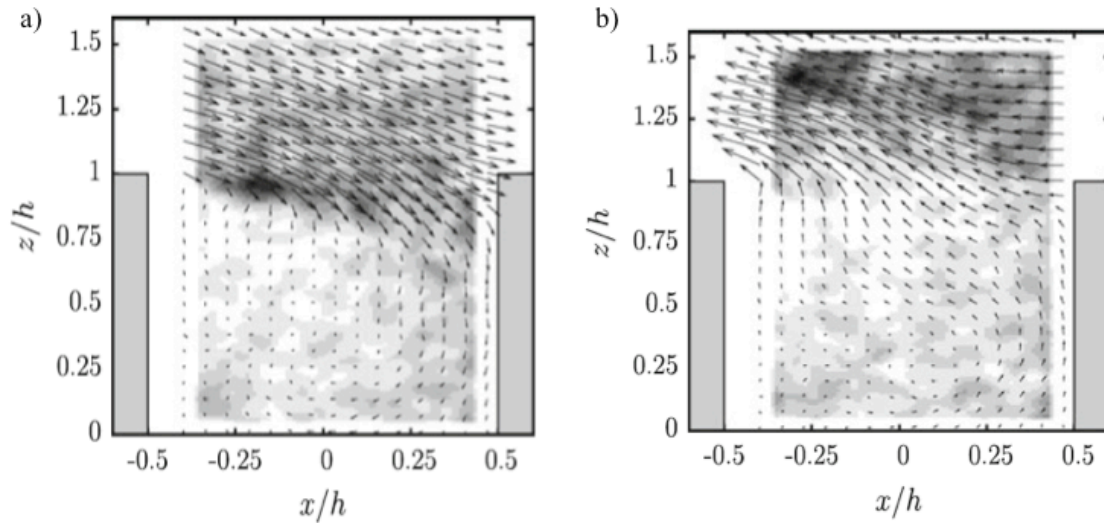
Figure 8 Example of phase averaged velocity fields corresponding to a) sweep event; b) ejection event. Where the approach flow is left to right, the arrows represent the velocity vectors and the contours are the phase-averaged swirling strength from white as zero to black as high value [12]

1.3.2 Shear layer

The shear layer above an urban street canyon is where exchange of momentum and fluid between the canyon and the overlying atmospheric boundary layer takes place. It is formed by separation at the upstream sharp edge of the obstacle and eddies that are formed along the upstream roof of the obstacle and shed periodically at the downstream edge. The shape of the shear layer is dependent on the flow regime of the canyon; skimming flow, wake interference flow or isolated roughness flow regime (Figure 9) [11]. Unlike the wake interference and isolated roughness regimes, within the skimming flow regime there is no penetration of the shear layer into the canyon, so there is a decoupling of the overlying boundary layer and shear layer with the canyon flow [13]. This suggests that ventilation is dependent only on the intermittent sweep and ejection events. However, flapping of the shear layer, which is caused by the periodic shedding of eddies from the upstream obstacle roof, has been documented and correlated with sweep and ejection events [13, 14]. Furthermore, sweep and ejection events have been

correlated with strong rotational motion within the shear layer when the approaching freestream flow is perpendicular to the canyon length [13].
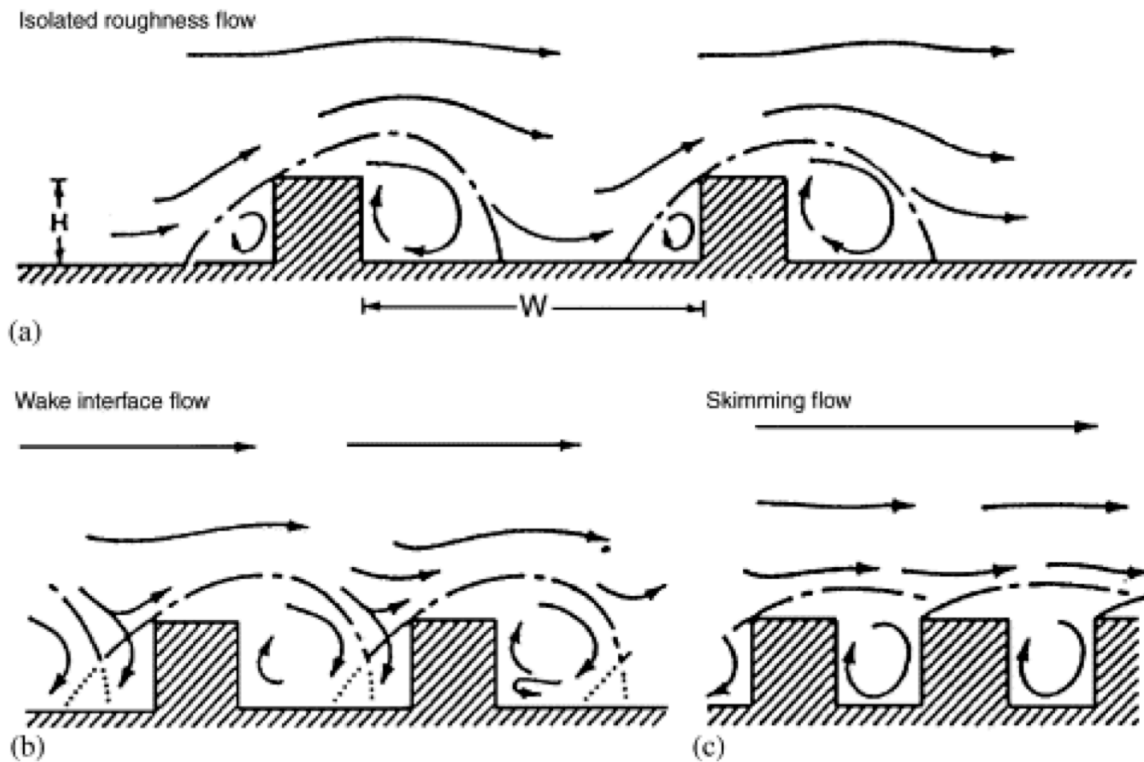
Figure 9 Flow regimes: a) isolated roughness flow; b) wake interference flow; c) skimming flow [11]

1.3.3 Coherent structures and low momentum regions

Ejection events are the process of transferring fluid from areas of high momentum within the canyon to areas of low momentum within the overlying boundary layer. Several studies have shown that ejection events are correlated with low momentum regions [8, 14]. Low momentum regions are areas of lower velocity than the surrounding flow. Coceal et al. [1] detected large-scale structures described as low momentum regions or low speed streaks (Figure 10). These structures are ever-present, thus demonstrating that they are persistent, coherent features [1]. Coherent structures are defined as 'a connected turbulent fluid mass with instantaneously phase-correlated vorticity over its spatial extent [7]. This means that although turbulence itself is a three-dimensional random process, coherent structures have a large-scale vorticity component that is instantaneously

consistent over the spatial extent of the structure [7]. This large-scale vorticity component is called the coherent vorticity and is the primary identifier of coherent structures [7].
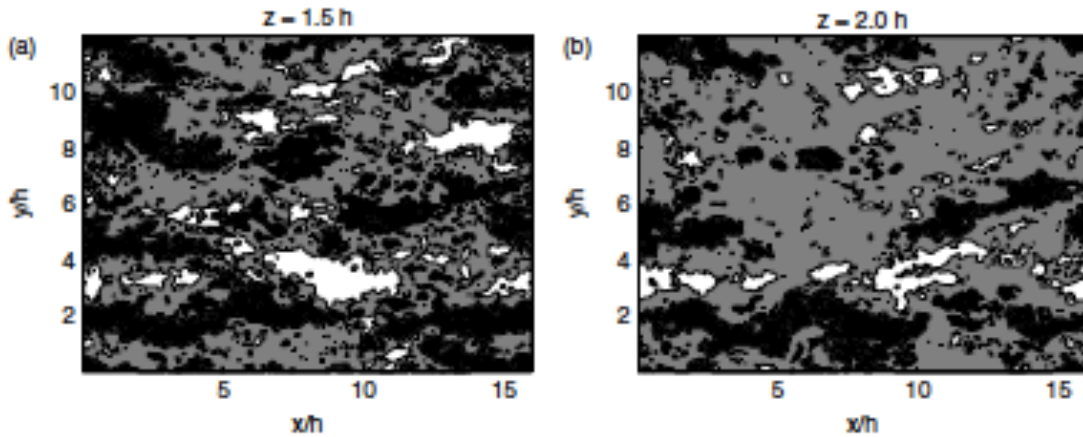
Figure 10 Instantaneous flow visualization of low momentum regions in a horizontal plane above a cubical array with black regions $u < 0.8u_m$, white regions $u > 1.2u_m$ where u_m is the local mean velocity [1]

It is suspected that low speed streaks are the result of groups of coherent hairpin vortices [1]. These hairpin vortices are generated from a strong ejection event from an unspecified source which restricts spanwise vortex lines. These are then rotated and stretched by the mean shear. The result of this phenomenon is an inclined primary vortex that resembles a horseshoe or hairpin shape. This vortex then produces strong ejections, which repeat the process, thus creating a group of hairpin vortices. This group results in the appearance of a low momentum region that is much longer than the length scale of the individual hairpin vortex [1]. The process of production of these hairpin vortices is little understood. What is understood is that these structures have a significant effect on the frequency and strength of sweep and ejection events that ventilate the canyon.

1.4 Canyon flow summary

The transport of pollutants within a single street canyon can be conceptually described by Figure 11 [2]. The figure shows three regimes, the first being turbulent organized structures along with hairpin vortices well above the canyon (dark blue and dark red,

respectively). The Q2 and Q4 events are ejection and sweep events, respectively, and are responsible for the intermittent exchange of pollutants between the canyon and the overlying boundary layer. The second is a strong shear layer formed over the top of the upstream building (white) and the third is a recirculation within the canyon (black). These three regimes are responsible for the ventilation of the street canyon. This is a simplified conceptual model and does not describe the complexity of the flow, but acts to give a summary of the flow structures that have a role in the ventilation of urban street canyons. The transport of pollutants in urban street canyons governs the overall air quality of an urban environment. Thus, it is important to study the roles and relationships between all of the turbulent structures and processes that influence the ventilation of urban street canyons.
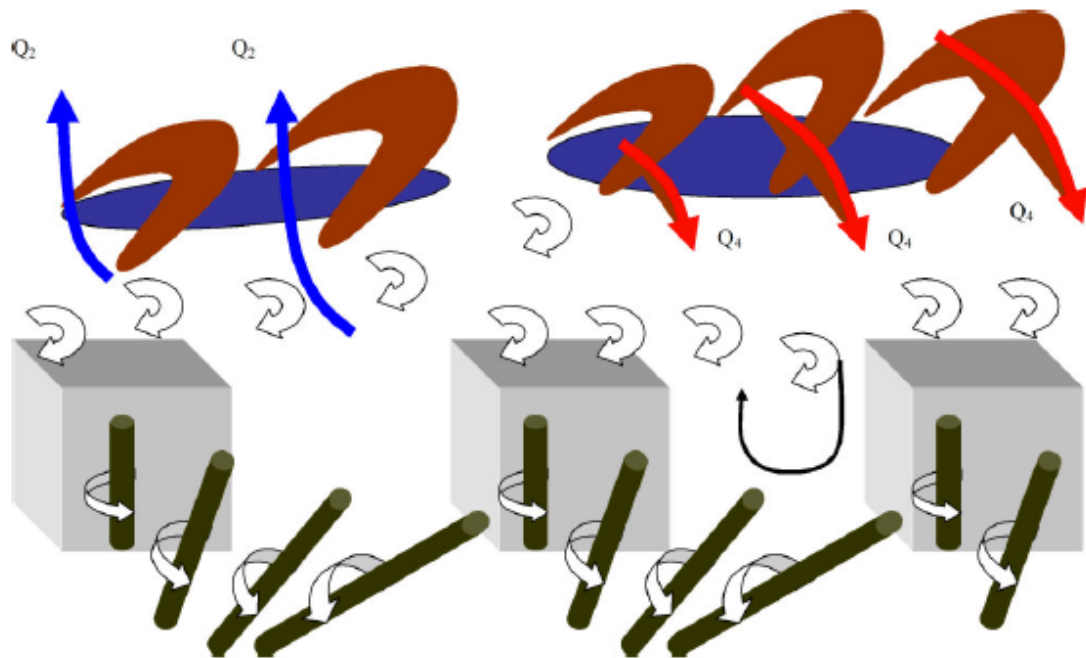
Figure 11 Conceptual cartoon summarizing the unsteady flow dynamics above and within street canyons. Above the canyon turbulent organized structures in the form of low momentum regions (dark blue) and hairpin vortices (dark red) dominate transport. Q2 is an ejection event and Q4 is a sweep event. Eddies (dark green) are shed off of the vertical sides of the building. A shear layer (white) is created by eddies forming along the roof of the building, which drives the recirculation zone (black) within the canyon [2]

1.5   Objective of the thesis

The flow phenomena discussed above are known to influence the ventilation of urban street canyons. However, the interaction and development of these flow structures is poorly understood and little work has been completed to quantify the transport events. The challenges faced when modeling this problem, including the scaling of the boundary layer, have prevented a thorough investigation of the subject. This research program aims to improve the understanding of the fundamental physics governing street canyon ventilation through quantification of the turbulent flow dynamics. The current research aims to provide sufficient setting for studying the canyon flow dynamics by, (1) understanding the effects of upstream roughness on canyon flow regimes and, (2) quantifying the relationship between mean and unsteady wind flows in a wind tunnel and at full-scale.

1.6   Structure of the thesis

The following sections include two articles that describe the research completed. The first is an investigation of the effect of upstream roughness array on street canyon flow mean turbulence statistics using simplified wind tunnel roughness arrays and nominally two-dimensional canyons. The second describes a study on the quantitative relationship of the mean and turbulent wind flow between a wind tunnel and full-scale street canyon model of equivalent geometry. A final section discusses the results of these two studies and the insights they provide into the understanding of the ventilation of urban street canyons.

1.7   Summary

Poor air quality is a significant concern for human health in urban areas [15]. Although much work has been done investigating the mean flow structure in street canyons, the dynamic structures and processes responsible for ventilation are poorly understood quantitatively. The current research aims to improve the understanding of these processes at a fundamental level by using simplified representations of urban street canyons and terrain. The following chapter will discuss the effect of upstream roughness on the canyon flow turbulence statistics related to canyon ventilation.

1.8 References

1. Coceal O, Dobre A, Thomas TG, Belcher SE (2007) Structure of turbulent flow over regular arrays of cubical roughness. J Fluid Mech 589:375-409

2. Coceal O, Dobre A, Thomas TG (2007) Unsteady dynamics and organized structures from DNS over an idealized building canopy. Int J Climatol 27:1943-1953

3. Cook NJ (1985) The designer's guide to wind loading of building structures: Part 1. The University Press, Cambridge

4. Eliasson I, Offerle B, Grimmond CSB, Lindqvist S (2006) Wind fields and turbulence statistics in an urban street canyon. Atmos Environ 40:1-16

5. ESDU (1982) Strong winds in the atmospheric boundary layer. Part I: mean-hourly wind speeds. Data Item 82026 (amended 1993), Engineering Sciences Data Unit International

6. ESDU (1985) Characteristics of atmospheric turbulence near the ground. Part II: single point data for strong winds (neutral atmosphere. Data Item 852020 (amended 1993), Engineering Sciences Data Unit International

7. Hussain AKMF (1986) Coherent structures and turbulence. J Fluid Mech 173: 303-356

8. Inagaki A, Castillo MCL, Yamashita Y, Kanda M, Takimoto H (2012) Large-eddy simulation of coherent flow structures within a cubical canopy. Bound Layer Meteorol 142:207-222

9. Kastner-Klein P, Rotach MW (2004) Mean flow and turbulence characteristics in an urban roughness sublayer. Bound Layer Meteorol 111:55-84

10. Liu HY, Bo TL, Wang GH, Zheng XJ (2014) The analysis of turbulence intensity and Reynolds shear stress in wall-bounded turbulent flows at high Reynolds numbers. Bound Layer Meteorol 150:33-47

11. Oke TR (1988) The urban energy balance. Prog Phys Geogr 12:471-508

12. Perret L, Savory E (2013) Large-scale structures over a single street canyon immersed in an urban-type boundary layer. Bound Layer Meteorol 148:111-131

13. Savory E, Perret L, Rivet C (2011) Modelling considerations for examining the mean and unsteady flow in a simple urban-type street canyon. Meteorol and Atmos Phys 121:1-16

14. Takimoto H, Sato A, Barlow JF, Moriwaki R, Inagaki A, Onomura S, Kanda M (2011) Particle Image Velocimetry measurements of turbulent flow within outdoor and indoor urban scale models and flushing motions in urban canopy layers. Bound Layer Meteorol 140:295-314

15. World Health Organization (2014) Ambient (outdoor) air quality and health: fact sheet 313. http://www.who.int/mediacentre/factsheets/fs313/en/. Accessed 14 March 2014

Chapter 2

2 Effect of upstream flow regime on street canyon flow mean turbulence statistics

The following chapter describes an investigation of the effect of upstream roughness on the canyon flow mean turbulence statistics. First a detailed literature review will be presented, followed by the experimental details and finally, a discussion and conclusions of the results obtained.

2.1 Introduction

A simple street canyon model reproduces the main features of most common street configurations, specifically for the case for which the upstream wind is perpendicular to the street axis. When modeling this configuration in the wind tunnel, Savory et al. [30] have noted, firstly, it is crucial to match the non-dimensional parameters of roughness length z_o/h, (where z_o is the aerodynamic roughness length and h is the height of the canyon) and integral length scale (L_u/h), within a factor of 2-3, between the model and full-scale to ensure the terrain type is essentially equal in both cases. Secondly, the geometry of the roughness used to generate the boundary layer is important as 2D block arrays enforce 2D behaviour of the large coherent structures generated whereas 3D arrangements reproduce more closely the 3D turbulent structure of the atmospheric boundary layer (ABL). Finally, comparison between different wind tunnel experiments of the same configuration can only be made quantitatively for those cases where the normalized displacement height (d/h) is approximately the same. These observations demonstrate the importance of aerodynamic scaling when modeling street canyons and the sensitivity of the canyon flow to the approaching boundary conditions, characterized, in particular, by z_o. Besides aerodynamic parameters such z_o/h and d/h, two other important parameters emerge from the literature: the aspect ratio AR = W/h (where W is the canyon streamwise width) of the studied street canyon and the roughness plan area density (defined as the ratio of the plan area of the roughness elements to the total plan area $\lambda_p = A_p/A_d$) of the roughness array over which the flow develops. The steady flow regimes of street canyons, with varying aspect ratio AR, have been well studied,

including the steady flow regimes, "skimming", "wake interference" and "isolated roughness" [22], classified by Grimmond and Oke [7] and Macdonald et al. [18] both as a function of W/h and also in terms of the effects of z_o/h, d/h and λ_p.

Although λ_p has been shown by Grimmond and Oke [7] to have a significant impact on the flow within a canyon, it is postulated here that the roughness geometry (two or three dimensional (2D or 3D) elements) employed to generate the flow in which the studied canyon is immersed also has an important effect. The present study is a comparative analysis of aerodynamically scaled boundary layers with modified upstream configurations, including both 3D and 2D roughness elements, and their effect on the flow in 2D canyons of different aspect ratio. The roughness plan area density λ_p and AR are modified for the upstream roughness and for the canyon, respectively, to include both skimming and wake interference regimes. The following review concerns experimental studies except where stated otherwise. Issues with aerodynamic scaling in previous studies are well documented by Savory et al. [30] and are, therefore, not discussed here.

The mean flow of street canyons in roughness arrays can be defined based on vertical profiles of horizontal streamwise averages of mean velocity, turbulence statistics, integral length scales and mass flux all spatially averaged across the canyon opening. Very few studies have examined the effect of varying the geometry (2D or 3D) of the roughness elements on the boundary layer flow, and it is difficult to compare them as the nature of the roughness differs for each study (see list of previous studies and their configurations in Table 1). The configurations used in these studies provide limited information, as they do not use multiple configurations with varying λ_p for each type of roughness, 3D or 2D. In their study of the pollutant removal from a street canyon of AR = 1, Michioka and Sato [21] did study two geometries, both within the skimming flow regime. When using the mean velocity at z = 2h, they found that the Reynolds shear stress increases from 2D to 3D configurations, as does the friction velocity. This change of geometry has a small effect on the mean velocity profiles within the canopy. Similarly, the friction velocity and shear stress (normalized by the freestream velocity) were found to increase from 2D to 3D configurations throughout the boundary layer by Volino et al. [33]. Lee et al. [15] found a similar trend when the streamwise spacing of roughness elements was smaller

than 5h but the opposite when the spacing increases. No clear information about the influence of λ_p was given. The influence of varying the roughness geometry on the turbulence integral length scales was also investigated. Volino et al. [33] and Lee et al. [14, 15] found that this change of geometry has a strong influence, with larger length scales above the roughness for 2D cases than 3D cases [33], but Takimoto et al. [32] show no consistent variation of integral length scales between the 2D and 3D cases. Of the studies presented here, Volino et al. [33] makes the most definitive conclusions concerning integral length scales. However, those conclusions are founded upon a limited number of configurations, only one 2D and 3D case, with the 3D case consisting of a rectangular mesh formed from circular section elements compared to the 2D square bars. Other researchers have studied only 2D or 3D arrays, with the work tending to focus on the effect of roughness aspect ratio or plan area density.

Table 1   Relevant literature (* A = aligned, S = staggered)

Reference	Method	2D or 3D	Array*	λ_p	Canyon AR	U_e (m/s)	u_* (m/s)	Compared Quantities
Barlow and Leitl [1]	Exp.	2D	-	63%, 50%	-	6	0.44, 0.44	
Cheng et al. [3]	Exp.		A	6.25%, 25%	-		0.65, 0.68	
		3D	S	6.25%, 25%	-	10	0.73, 0.71	z_o, $\overline{\langle u'w'\rangle}$
Coceal et al. [4]	DNS	3D	S	25%	-	-	-	-
Hagishima et al. [8]	Exp.		A	25%	-		-	
		3D	S	25%	-	8	-	z_o
Ho and Liu [9]	Exp.	2D	-	50%, 3%, 25%, 11%, 9%, 8%	-	2.5	-	ACH
Huq and Franzese [10]	Exp.	3D	A	13%, 25%, 19%	-	0.078, 0.094, 0.11	-	$\overline{U}$, σ_u
Kanda et al. [11]	LES	3D	A	0%, 44%	-	1	-	z_o
Kanda [12]	LES	3D	S	0%, 44%	-	1	-	-

Reference	Method	2D or 3D	Array[*]	λ_p	Canyon AR	U_e (m/s)	u_* (m/s)	Compared Quantities
Lee et al. [14]	Exp.	3D	S	4%	-	-	-	
		2D	-	11%	-	-	-	L_u
Lee et al. [15]	DNS	2D		25%				
		3D		12.5%	-	-	-	-
Liu et al. [16]	LES	2D	-	66%, 50%, 33%	-	-	-	
Macdonald [17] and Macdonald et al. [18, 19]	Exp.	3D	A	5%, 33%	-	1.5	0.2, 0.24	
			S	5%, 33%	-		0.22, 0.24	z_o
Marciotto and Fisch [20]	Exp.	2D	-	11%, 14%, 20%	-	10	0.62, 0.62, 0.81	-
Michioka and Sato [21]	LES	3D	A	25%	1		0.099	$<\overline{U}>$, $<\overline{u'w'}>$
		2D	-	50%, 33%	1	1	0.067, 0.092	
Rafailidis [24]	Exp.	2D	-	66%, 50%	-	5	-	σ_u
Ricciardelli and Polimeno [25]	Exp.	3D	A	36%	-	10	-	-
Rivet [26]	Exp.	3D	S	25%	-	5.9	0.38	$<\overline{U}>$, $\overline{U}$, σ_u, $<\overline{u'w'}>$
Salizzoni et al. [28]	Exp.	2D	-	25%, 33%, 40%, 50%	1	6.75	0.46, 0.41, 0.36, 0.33	$\overline{U}$, σ_u
Sato et al. [29]	Exp.	3D	A	11%, 25%, 44%	1	0.65	0.065	$\overline{U}$, σ_u
Savory et al. [30]	Exp.	3D	S	6.25%	-	5.9	0.345	z_o, $\overline{U}$, σ_u
Takimoto et al. [32]	Exp.	3D	A	44%, 25%, 18%	-	2	0.22, 0.27, 0.27	
		2D	-	50%	-		0.15	L_u
Volino et al. [33]	Exp.	3D	A	-	-	1.247	0.0603	
		2D	-	11%	-	0.5	0.0341	L_u

2D roughness can also be used to represent a street canyon and using this configuration reproduces the important flow mechanisms, such as turbulent organized structures, sweeps and ejections and a separated shear layer, while a *priori* reducing complexity [23]. Here, those papers that have used 2D square bar roughness to represent street canyons and those that have used them simply for roughness arrays are examined. Each of the following cases used roughness elements and canyons of equal height. The turbulent eddies defined by integral length scales within the skimming flow regime were found to be limited or suppressed within and above the roughness by the large λ_p [9, 28]. This is further confirmed by Rafailidis [24] who noted that λ_p within the skimming flow regime has only a mild effect on the turbulence statistics at $z/h = 1$ and above. On the contrary, the turbulence is increased at $z/h = 1$ by the flow impinging on the windward face in the isolated roughness regime [9]. Salizzoni et al. [28] also noted that in the wake interference regime the turbulent structures and turbulence intensity are larger than in the skimming flow regime above the roughness. The shear stress was found to vary with λ_p within and above the roughness up to a height of approximately 5h [28]. When investigating the shear layer size no significant difference was found between the skimming and wake interference regimes. Finally, for all cases they found that the dynamics of the shear layer and the flow, characterized by the r.m.s. of the streamwise and vertical velocity fluctuations, within the cavity is significantly influenced by the turbulent kinetic energy (TKE) in the external flow.

Arrays of 3D roughness elements have been used to reproduce the three-dimensionality of the turbulence near the ground within the atmospheric boundary layer. The height below which the boundary layer is influenced by the roughness was found to be approximately 4h by Cheng et al. [3]. This is slightly higher than the value of 3h found for a 2D case in skimming flow [24]. The spatially averaged vertical profiles of streamwise velocity do not differ significantly between aligned and staggered configurations [17]. The effect of alignment (staggered or aligned) on the spatially averaged turbulent shear stress near the ground for all λ_p, as well as above the roughness for low λ_p, is significant, as found by Cheng et al. [3]. Huq and Franzese [10] determined that near the ground this stress is comparable for all aligned cases tested of varying λ_p. As well, Cheng et al. [3] showed that the shear stress is dependent on λ_p for aligned cases

and not significantly dependent for staggered cases above the roughness height and within the shear layer. However, it was determined that the relationship between λ_p and turbulence statistics is insignificant for aligned arrays above the roughness, but significant within the roughness [11]. Salizzoni et al. [28] determined that the shear stress is dependent on λ_p, whereas Marciotto and Fisch, who also studied 2D arrays [20], found it is not. Of the studies including aligned arrays some determined that shear stress is not dependent [10] on λ_p while others found it was [3]. There is much inconsistency in regard to the relationship between shear stress and λ_p, therefore no definite conclusion can be drawn from the available studies. Through quadrant analysis at z/h = 1 Kanda et al. [12] suggest that the ventilation determined by quadrant analysis of aligned arrays is sensitive to λ_p, whereas it is not for staggered arrays. Finally, z_o is shown to be higher for staggered arrays than aligned cases for all λ_p [8, 18]. Grimmond and Oke [7] do not distinguish between aligned and staggered 3D arrays in their study of the effects on z_o of λ_p. In both 2D and 3D cases it is shown that the vertical profiles of streamwise velocity increase in magnitude with increasing λ_p [11, 28].

From the above review several conclusions can be drawn with respect to the differences between 2D and 3D configurations from studies using only 2D configurations or only 3D configurations. The spatially averaged shear stress is higher above the roughness in the 3D case, but configuration type has negligible impact within the roughness [3, 21]. Studies of turbulence intensity show contradictory results as it is larger above the roughness in 2D than 3D configurations when comparing the results of some studies [10, 24], but it is also noted to be similar above the roughness when comparing others [10, 28]. A similar discrepancy is apparent in the vertical profiles of streamwise mean velocity with 2D cases having higher values than 3D cases [4, 28] or *vice versa* [10, 28].

Ho and Liu [9] and Liu et al. [16] include analysis of the mass flux, which is based on the time-averaged flow rate across the 2D canyon opening and can be separated into the mean, turbulent and total components, which can be used as a measurement of the ventilation rate. Both studies determined that the mass flux increases with decreasing λ_p [9, 16]. Ho and Liu [9] also found that the turbulent fluctuations dominate the total mass flux for all cases tested. Liu et al. [16] compared very dense arrays (λ_p = 67%, 50%) with

a slightly less dense array (λ_p = 33%) and found that the former cases had approximately equal mass flux, but the latter case had greater mass flux than that of the other two cases by a factor of 2 as it falls within the wake interference regime compared to the other skimming flow regime cases.

The interaction between the boundary layer over roughness arrays with different λ_p and canyons with different AR has not been previously studied extensively through experiments in the same facility and with a comprehensive range of configurations. In particular, the role of the effect of turbulence generated locally and in the oncoming boundary layer upon the flow in the canyon and its ventilation characteristics remain unclear. Recently, Marciotto and Fisch [20] investigated a 2D canyon with varying AR = 4, 6, and 8 and surprisingly concluded that "the flow within the canyon is little sensitive to the turbulence level of the flow above" a statement which is claimed to be supported by Ricciardelli and Polimeno [25], but is contradicted by Salizzoni et al. [28] who found that the structure of the external flow influences the structure of the cavity flow. Although Ricciardelli and Polimeno [25] noted that the mean and fluctuating characteristics of canyon flow are more dependent on local geometry than that of the oncoming flow, that observation was made on the basis of measurements within large obstacles in only two boundary layers, one with a smooth ground plane and one with very small roughness elements when compared with the measurement roughness obstacles. This meant that not only were the oncoming flows insufficiently turbulent, but their study did not cover a wide enough range of configurations to provide sufficient evidence for such a claim. Ricciardelli and Polimeno [25] also state that the turbulence within the canyon seems to be "a superposition of the oncoming large-scale turbulence and of the locally generated small-scale turbulence". However, previous evidence has shown that there is coupling rather than merely "superposition", between the local and oncoming turbulent flow characteristics [2, 8, 13, 23, 28].

From this present overview it may be seen that many studies have investigated roughness arrays through a variety of methods and at different model scales. Discrepancies are apparent when comparing 2D and 3D cases of equal λ_p using statistics such as turbulence intensity, integral length scale, streamwise velocity, and Reynolds shear stress. The

spatially averaged turbulent shear stress above staggered arrays has been shown to be insensitive to λ_p, while the shear stress, above but not within of aligned arrays, has been shown to be sensitive to λ_p. Additionally, z_o is shown to be higher for staggered than aligned 3D arrays. However, each of these studies lack a significant range of configurations, including both 2D and 3D arrays falling within both the skimming flow regime and the wake interference regime, to determine the effects of upstream roughness on the canyon flow. Furthermore, several of the studies have not used proper aerodynamic scaling for them to simulate realistic urban arrays or street canyons. From this review several questions still remain:

- What is the impact of using aligned versus staggered arrays on the turbulence statistics within and above the canyon?
- What is the effect of using 2D versus 3D obstacle arrays on the turbulence statistics within the canyon, the shear layer and the overlying boundary layer?
- What is the effect of λ_p on the turbulence statistics throughout the boundary layer within both the skimming flow regime and the wake interference regime?

The overall goal of the present research is to determine the oncoming boundary layer mean flow and turbulence statistics and those of street canyons for realistic scales and a range of configurations in order to; (a) determine the differences between the boundary layer produced by 2D and 3D obstacle arrays with equal λ_p and their interaction with canyons of AR representing two different regimes (skimming and wake interference) according to the Oke [22] categorization and (b) to investigate the dynamics of the flow and structure of the turbulence. Chapter 2 focuses on part (a).

2.2 Experimental details

The experiments were conducted in the low-speed, suck-down boundary layer wind tunnel in the LHEEA at École Centrale de Nantes (Figure 12), which has working section dimensions of 2 m (width) x 2 m (height) x 24 m length and a 5:1 ratio inlet contraction. The empty-tunnel has a free-stream turbulence intensity of 0.5% over a wind speed range of 3-10 m/s with good spanwise uniformity to within ±5% [30]. The experiments used five 800 mm high vertical tapered spires located immediately downstream of the

contraction and a 200 mm high solid fence across the working section 750 mm downstream of the spires to initiate the boundary layer development. These were followed by an initial 13 m fetch of 50 mm staggered cube roughness elements with a plan area density of 25% to initiate boundary layer development. The canyon flow measurement tests were taken 5.5 m downstream of this initial development region whilst the roughness arrays over this last portion of the wind tunnel floor were either 50 mm cubes arranged in a staggered array with $\lambda p = 25\%$ or 50 mm square section, two-dimensional bars that spanned the width of the tunnel, with an element spacing of either 1h or 3h. Six flow configurations were investigated: two canyon widths of W/h = 1 or 3, with 3 different types of upstream roughness elements (Table 2). The measurement canyons are referred to as Cnh with n = 1 or 3, and the upstream roughness (Rm) is staggered cubes (m = cu) or 2D bars with m = 1h or 3h. The canyon building length was L = 30h, with the canyon height h = 50 mm.
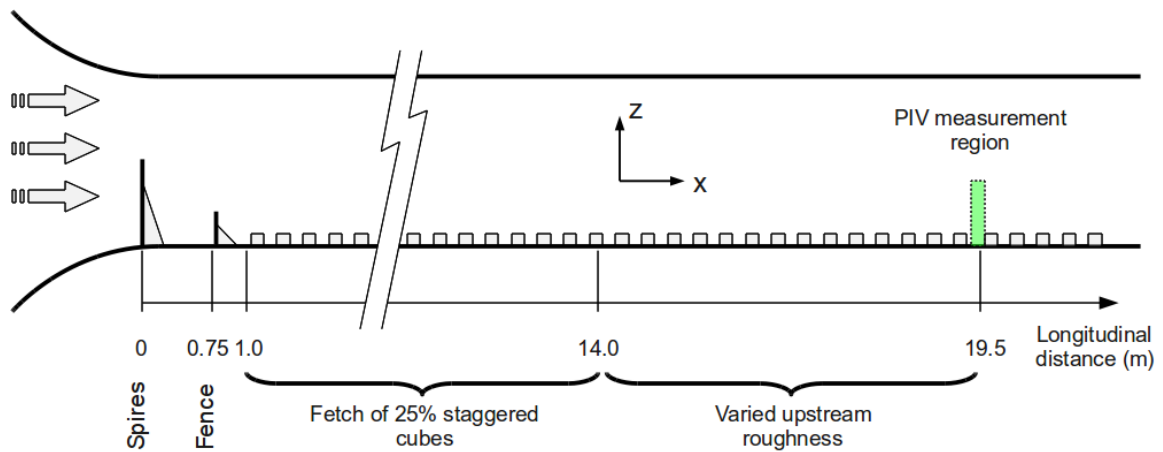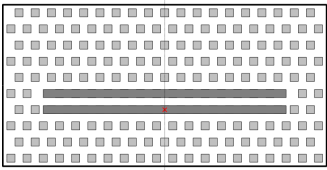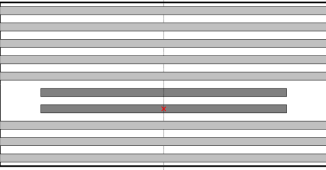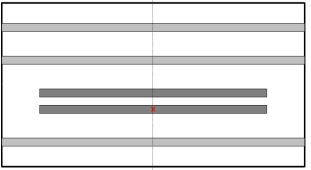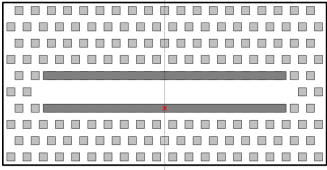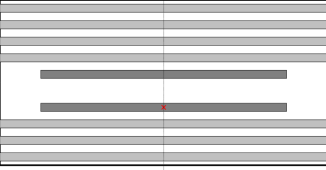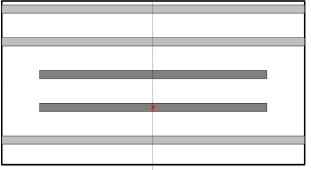
Figure 12 Wind tunnel set-up

Table 2   Canyon configurations studied in the present work

Roughness	25% Staggered cubes (Rcu) λ_p = 25%	2D bars, spacing: 1h (R1h) λ_p = 50%	2D bars, spacing: 3h (R3h) λ_p = 25%
Canyon width	C1hRcu	C1hR1h	C1hR3h
W = 1h (C1h)			
W = 3h (C3h)	C3hRcu	C3hR1h	C3hR3h

The velocity fields were measured in a vertical plane in the centre of the canyon aligned with the free stream flow direction (Figure 13). A Dantec Particle Image Velocimetry (PIV) system set up in stereoscopic configuration and located beneath the wind tunnel floor was used to measure the three velocity components. A commercially available smoke generator was used to seed the flow with water-glycol droplets of a diameter with distribution mean of 1 μm. To ensure proper seeding of the lower part of the boundary layer the seeding particles were introduced just downstream of the contraction section of the wind tunnel. The particles were illuminated for PIV measurement using a light sheet generated by a Litron double cavity Nd-YAG laser (2 x 200 mJ). A frequency of 7 Hz was used between pairs of pulses and two CCD cameras with a 60 mm objective lens were used to record pairs of images. A time-step of 400 μs was set between two images of the same pair. The synchronization of the cameras and laser was controlled using Dantec Dynamic Studio software, which was also used to perform the PIV analysis of the recorded images. 5000 pairs of images were recorded for each flow configuration and the multi-pass cross-correlation PIV processing resulted in a final interrogation window size of 16 x 16 pixels with an overlap of 50%. For all the configurations, the final spatial

resolution was 0.83 mm and 1.68 mm in the longitudinal and vertical directions, respectively. In addition, two single hot-wire anemometer probes (HWA) were used to measure the streamwise velocity component above the downstream canyon block at heights of 1.2h and 4h (Figure 13). These measurements, synchronized with the PIV system to allow for accurate correlation, were performed with a sampling rate of 10 kHz. The maximum standard deviation of the main statistics due to statistical error were estimated by making the assumptions that the velocity distributions are Gaussian and were found to be of 0.0041, 0.0029 and 0.0002 for the mean velocity, velocity standard deviation and turbulent shear stress normalized by freestream velocity, respectively. The error of repeatability of the experiments can be estimated by comparing the flow statistics obtained for the same upstream roughness elements and different canyon width in the upper region where the canyon geometry influence is expected to be negligible. This error was found to be smaller than that due to the statistical convergence. All the experiments were performed with the same free-stream velocity U_e = 5.9 m s^{-1} measured with a pitot tube located at x = 15 m, y = 0 m and z = 1.5 m, giving a Reynolds number, based on canyon height, of Re_h = 1.9x10^4.

The spanwise homogeneity was investigated by Rivet et al. [26] over the cube array (Rcu) for z/h > 2. It was determined that the turbulence statistics taken at three spanwise measurement locations were in agreement, to within 5% [26]. In addition, Savory et al. [30] showed that the centre-line mean flow profiles were dependent of canyon length when L/h > 9 and the canyon length in the present work (L/h = 30) greatly exceeds that value. Finally, since the upstream roughness changes between x = 1-14 m and x = 14-19.5 m for the R1h and R3h cases an analysis of the internal boundary layer (IBL) development is provided in Appendix A. It was determined that at the location of the canyon the IBL is in equilibrium with the boundary layer.
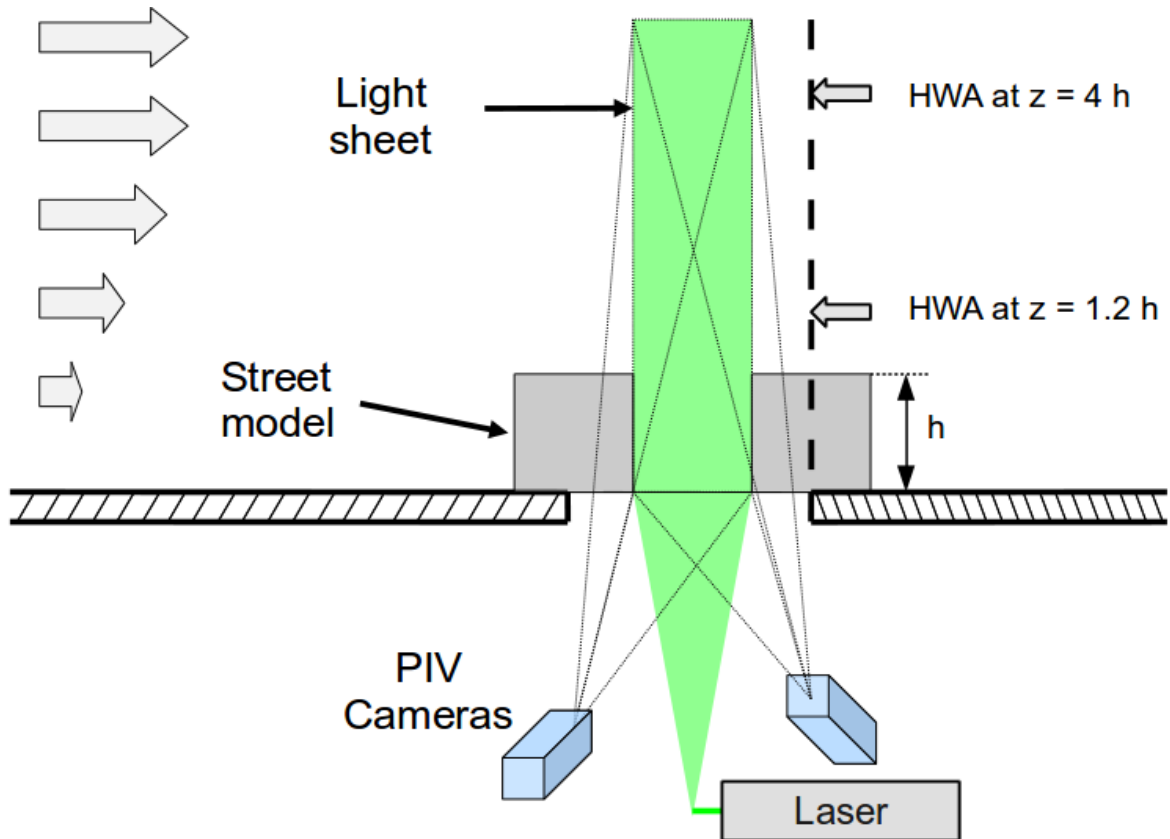
Figure 13   Stereoscopic PIV set-up

2.3   Results and discussion

The following section will first describe the scaling of the three approaching boundary layers considered in the present work to determine what full-scale cases are being represented. This is followed by an investigation of the approaching boundary layers to determine the influence of packing density λ_p and array obstacle configuration on the mean turbulence statistics of the roughness including a comparison with literature. Finally, the role of the canyon AR will be investigated, using all six configurations from the present work, along with those from the literature.

2.3.1   Scaling of the approaching boundary layers

The PIV profiles taken at x = 19.5 m were compared with ESDU, which provides generic representations of atmospheric boundary layer (ABL) profiles based on full-scale field data [5, 6]. The profiles used are vertical profiles at the centre of the roughness elements

(midpoint between the successive rows of roughness elements and the wind tunnel in the spanwise direction). The log law parameters z_o and d were determined by fitting the vertical streamwise velocity profile to the log law equation (Equation 2) with u_* estimated from the vertical profile of the Reynolds shear stress in the constant stress region located just above the roughness height (Figure 18b).

Equation 2   Log law

$$U(z) = \frac{u_*}{k} \left[\ln \left(\frac{z-d}{z_o} \right) \right]$$

The integral length scales of the streamwise velocity were estimated from the temporal correlation coefficient from the PIV data and mean streamwise velocity at the corresponding height using Taylor's hypothesis of frozen turbulence (Equation 3).

Equation 3   Taylor's hypothesis of frozen turbulence

$$L_u(z) = \int R_{uu}(z,\tau)d\tau * U(z)$$

Given the low time-resolution of the PIV system (7 Hz), the integral time scale was estimated by fitting an exponential decaying function to the temporal correlation obtained from the PIV. To assess the validity of the method, an example of a computed temporal correlation is shown in Figure 14, together with the same quantity obtained from well time-resolved hot-wire measurements and the exponential fit. The best match scale of the boundary layer configurations are 1:100, 1:200, and 1:100 for R1h, Rcu, and R3h, respectively. When using z_o as an indicator, the terrains vary, with R1h being rural (z_o = 0.03 m), Rcu being between outskirts or suburban (z_o = 0.2 m), and R3h being urban (z_o = 0.7 m). The profiles are shown in Figure 15 along with the corresponding ESDU profiles. The integral length scale is not precisely modeled in the higher altitudes, which is typically the case in wind tunnel simulations as the size of the eddies is limited by the cross-sectional dimensions of the wind tunnel, the size of the vorticity generators at the entrance of the working section and the thickness of the boundary layer that can be generated over the available fetch length. From a comparison with the spectral density it

is evident that the turbulence is modeled well within the boundary layer (z - d < 5h) (Figure 16). The Jensen number scaling results in an approximate scaling of 1:250 or a full-scale building height of 12.5 m for all three boundary layers within an acceptable factor of 2-3. Thus, the profile scaling with ESDU would suggest a full-scale building height of 5 m for R1h and R3h and 10 m for Rcu.
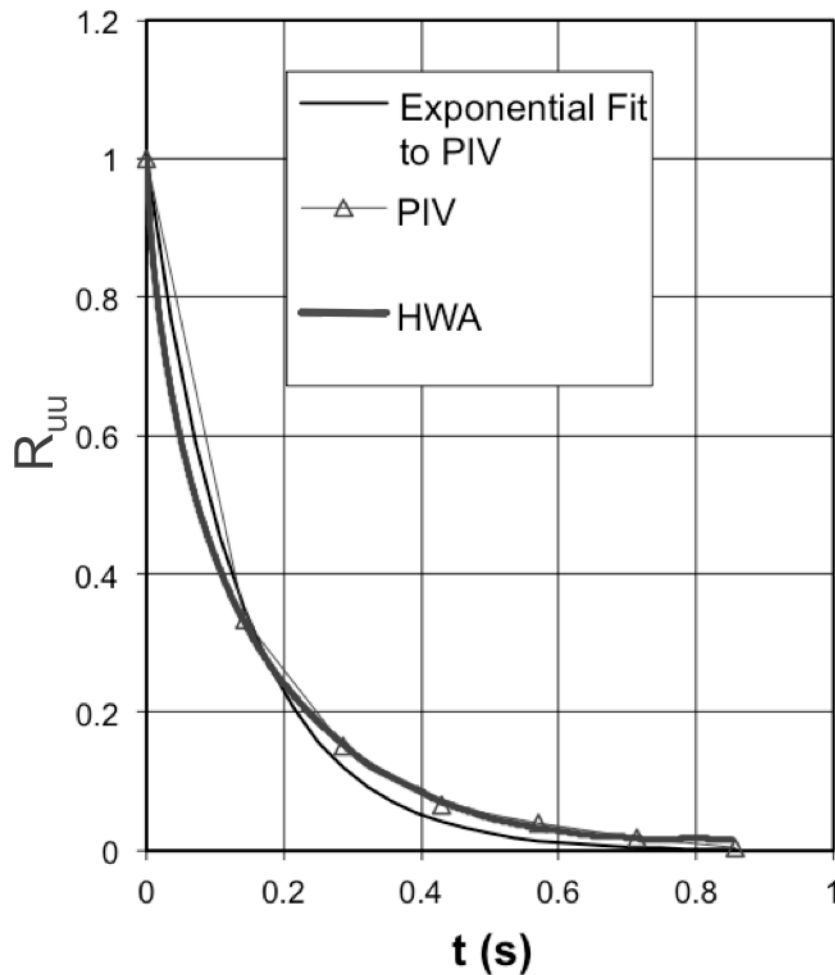
Figure 14   Example of temporal correlation obtained at z = 4h from PIV (Δ) and HWA (—). Solid line exponential fit to the PIV results
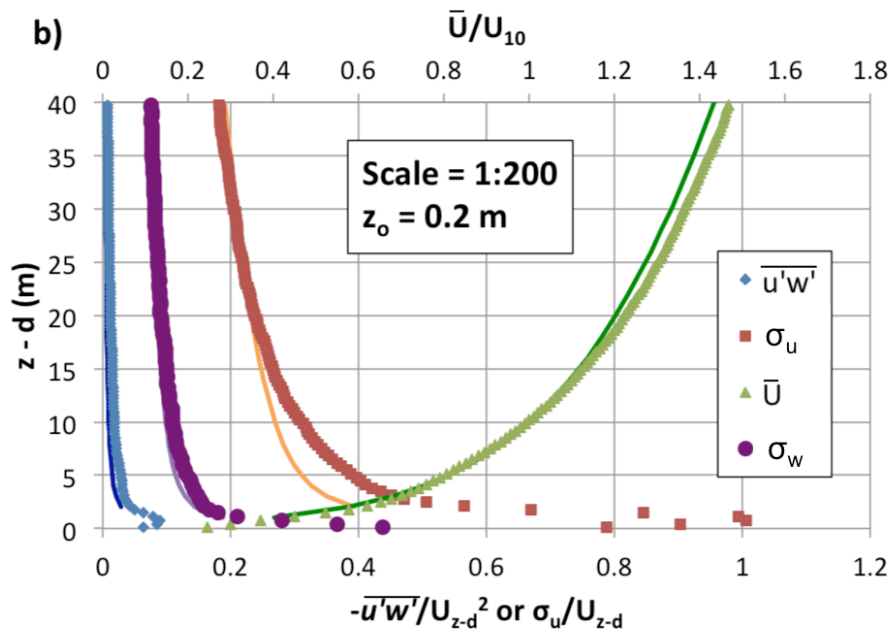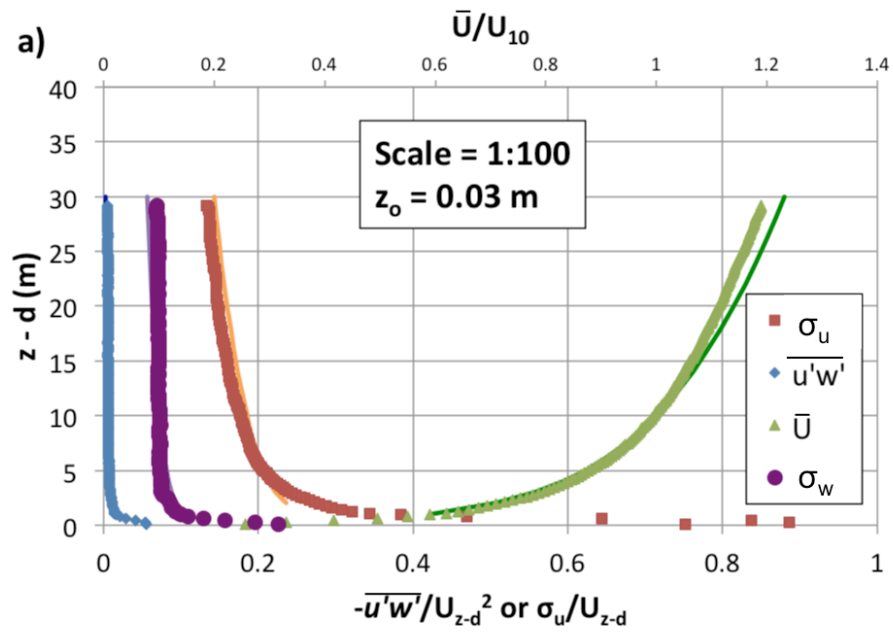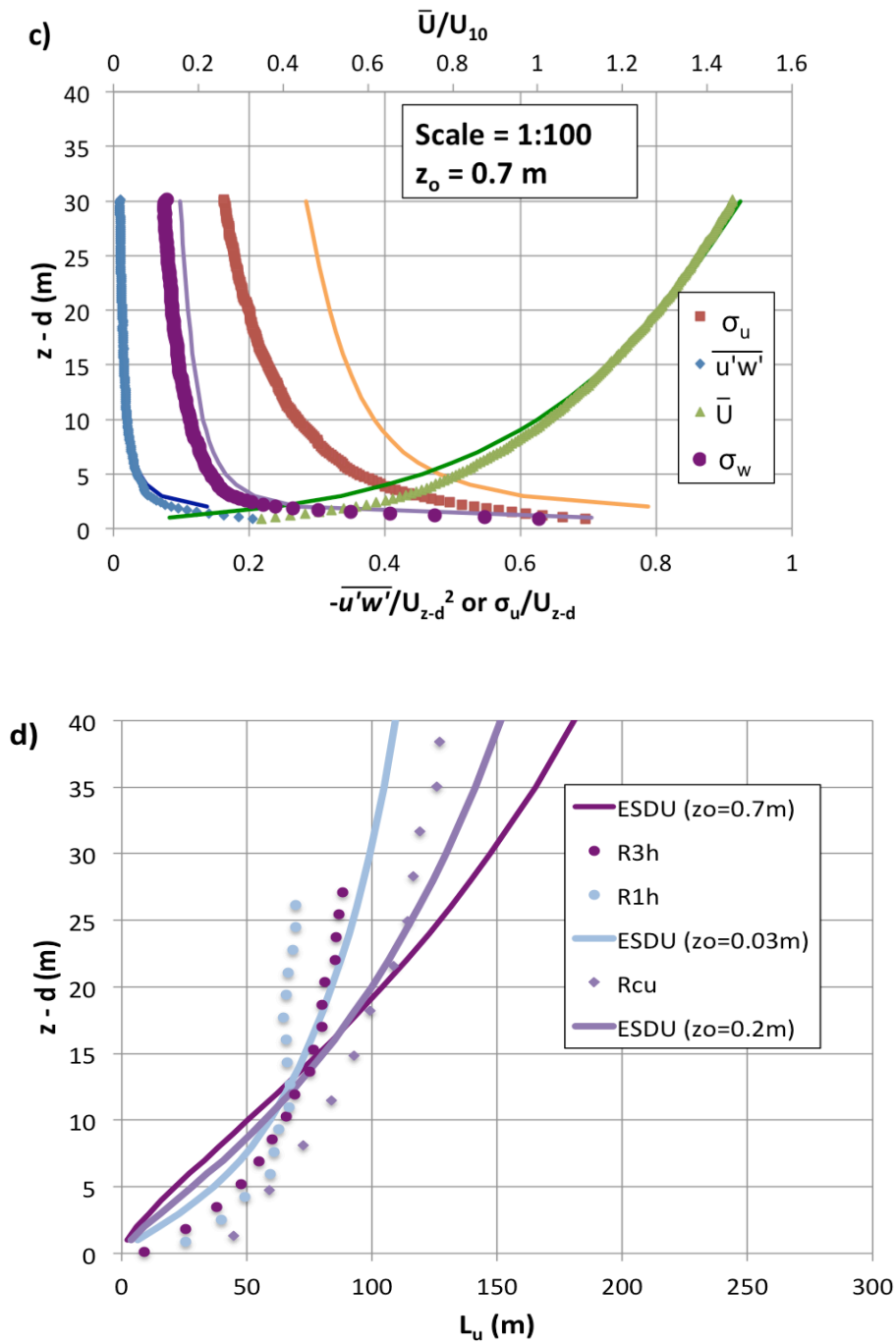
Figure 15 Comparison between ESDU [5, 6] boundary layer profiles and centre vertical PIV profiles for different scaling factors a) R1h; b) Rcu; c) R3h; d) streamwise integral length scales. Lines denote ESDU profiles and points denote experimental data
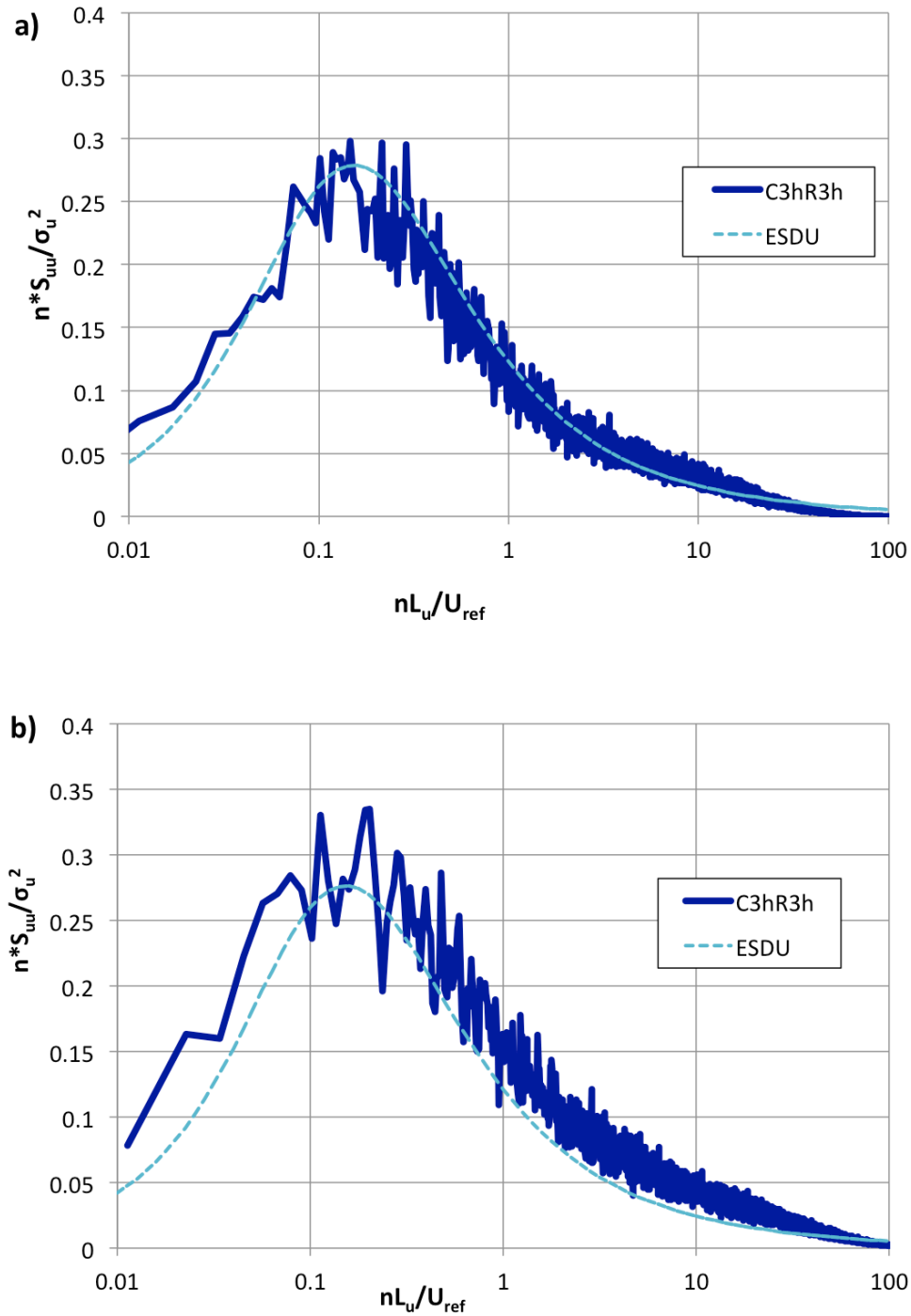
Figure 16   Spectral density of the streamwise velocity obtained at height a) z = 2h; b) z = 4h from HWA (—) compared to the ESDU [5, 6] model (---) for C3hR3h

2.3.2 Comparison of boundary layer characteristics for different upstream roughness

The following section considers only the three upstream boundary layers studied, which are Rcu, R1h and R3h. For the R1h and R3h cases measurements were taken above the canyon, which is of equal AR to the roughness elements and for the Rcu case, measurements were taken above the cube roughness.

2.3.2.1 Boundary layer characteristics

The boundary layer characteristics provide insight into the effects of varying the roughness density and configuration. These characteristics were calculated using both the spatially averaged vertical profile across the width of the canyon and the centre vertical profile as specified in Section 2. When using the friction velocity to normalize other quantities the value used corresponds to the vertical profile, either spatially averaged or centre. When considering the spatially averaged values with increased plan area density, from Rcu and R3h to R1h, the friction velocity and roughness length decrease while the zero-plane displacement increases. This is a result of the increased plan area density of R1h and the skimming flow regime. When comparing the centre values the same pattern is evident for the friction velocity, which suggests the evolution of this parameter with λ_p is not sensitive to spatial averaging. Although the roughness length exhibits the same trend there is some variability between the spatially averaged and centre profiles suggesting that this value is sensitive to spatial averaging. Finally, the centre zero-plane displacement results in significantly different values between the spatially averaged and centre values again suggesting sensitivity to spatial averaging. Grimmond and Oke [7] modeled the z_o and d as a function of the λ_p. These values are shown in Figure 17 along with the current data and other studies of different configurations including 2D, 3D aligned [8, 11, 18] and 3D staggered [3, 30]. All of the results shown are calculated from spatially averaged vertical streamwise velocity profiles including those values taken from the literature. It is evident that 2D roughness arrays result in higher z_o than 3D roughness arrays of equal λ_p. As well, staggered 3D arrays result in higher z_o than aligned, with this difference being greater with lower λ_p. In the present case, the R1h and R3h configurations have a plan area density of 50% and 25%, respectively. When compared

to those from the model of Grimmond and Oke [7], the roughness parameters found in the present study vary significantly. However, the cases with $\lambda_p = 25\%$ lie within the outer limits provided by Grimmond and Oke [7] based on all the data they compiled, whereas the 2D $\lambda_p = 50\%$ case does not lie within the outer limits provided. The discrepancy is likely to be the result of the differences in roughness configuration between the cases as can be seen when comparing 2D and 3D configurations that have the same plan area density. Thus, not only do the boundary layer parameters depend on the plan area density, but also on the geometry of the roughness elements.

Table 3 Boundary layer characteristics, where SA and C denote the values derived from spatially averaged and centre vertical velocity profiles, respectively

Roughness	Profile	u_* / U_e	d / h	z_o / h
Staggered cubes (Rcu)	SA	0.066	0.892	0.061
	C	0.064	0.900	0.060
2D bars, 1h spacing (R1h)	SA	0.047	0.980	0.008
			0.927	0.015
2D bars, 3h spacing (R3h)	SA	0.072	0.552	0.143
	C	0.070	0.725	0.125
$\lambda_p = 25\%$ [7]		-	0.600	0.120
$\lambda_p = 50\%$ [7]		-	0.800	0.080
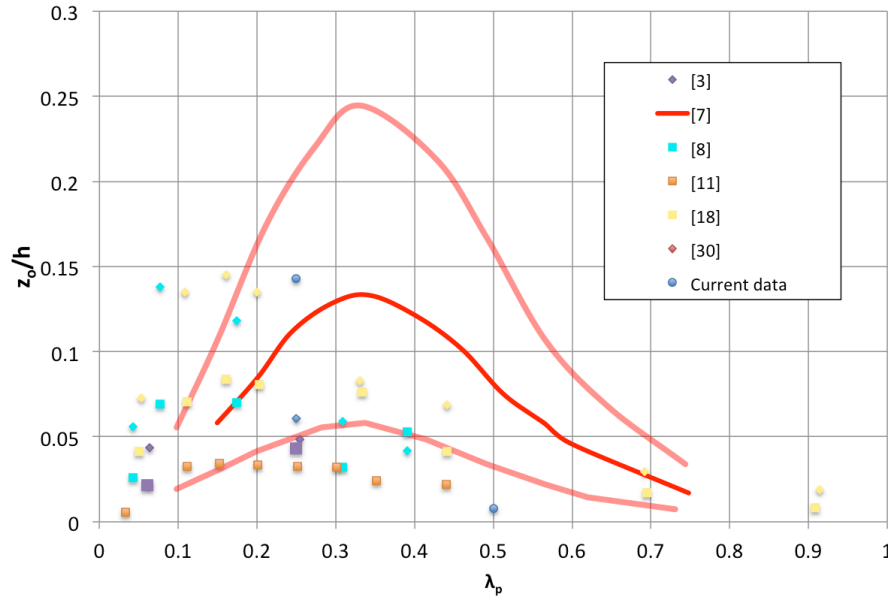
Figure 17 Boundary layer roughness length of the present study (blue) compared with the review from Grimmond and Oke [7] (dark line: mean values, light lines: outer limits) and experimental data from the literature [3, 8, 11, 18, 30]. Circles: 2D configurations; Squares: 3D aligned configurations; Diamonds: 3D staggered configurations; each colour denotes one reference

2.3.2.2   Spatially averaged turbulence statistics

The mean statistics of the roughness boundary layers, including vertical profiles of mean streamwise velocity and Reynolds shear stress were spatially averaged across the width of the canyon and normalized by the freestream velocity to give a representative profile for each boundary layer studied. The mean velocity profiles (Figure 18a) show that in the skimming flow regime case (R1h) the mean velocity is larger than that of R3h, which is in the wake interference regime. With equal λ_p the 3D configuration results in larger streamwise velocity than the 2D configuration, which is likely a result of obstacle spacing making the 3D configuration a skimming flow. The results of Michioka and Sato [21] do not show a significant trend between cases, which may be a result of all of their configurations laying within the skimming flow regime. From the earlier review, there is no significant difference in the mean velocity profiles between aligned and staggered 3D arrays [17]. As well, the magnitude of the velocity depends on λ_p for 2D cases [11, 28]

and the current results confirm this observation. The spatially averaged shear stress shows the opposite trend with the higher AR having a larger shear stress, which is confirmed by the results of Michioka and Sato [21] (Figure 18b). Salizzoni et al. [28] also confirm this pattern, but Marciotto and Fisch [20] found that the shear stress is not dependent on λ_p. 3D configurations of aligned and staggered arrays show, that in both cases, an increase in λ_p results in an increase in the shear stress [3]. When comparing the current study's 3D configuration with the 2D configuration of equal λ_p the 3D configuration results in lower magnitudes of shear stress. This suggests that the 3D configuration is within the skimming flow regime. This is confirmed by Michioka and Sato [21] who found that with equal AR the shear stress increases from 2D to 3D, but contradicted by Lee et al. [14] and Volino et al. [33] who found the opposite to be true. This contradiction may be attributed to the flow regime. Within the skimming flow regime 3D configurations have a larger magnitude of shear stress than 2D configurations, but within the wake interference regime 3D configurations have smaller magnitudes of shear stress than 2D configurations.

2.3.2.3   Centre turbulence statistics

The centre vertical profiles of the mean streamwise velocity and streamwise turbulence intensity are normalized by the friction velocity derived from the centre vertical profiles (Figure 18c, Figure 18d). The centre mean velocity profiles follow the same pattern as the spatially averaged profiles with an increase in AR resulting in decreased velocity [21]. There is a significant difference between the results of the current study and those of Salizzoni et al. [28] and Sato et al. [29] for 2D configurations of equal AR. 3D arrays were found to have the opposite pattern to 2D arrays with the larger AR resulting in larger velocities [10]. The streamwise turbulence intensity (σ_u) above the roughness array is similar for both 2D configurations of the current study where σ_u is governed by the boundary layer simulation conditions, but within the roughness array the wake interference regime case has larger σ_u. This suggests that in the skimming flow regime there is less turbulence produced in the lower part of the boundary layer. Turbulence is generated from the mean shear. Skimming flow produces less mean shear at the downstream canyon obstacle where flow impinges at the top of the wall, whereas, wake

interference has strong separation and, hence, stronger mean velocity gradients at the leading corner of the downstream canyon obstacle. The apparent similarity of the streamwise turbulence intensity above the canyon between the two 2D configurations of the present work is contradicted by Salizzoni et al. [28] and Huq and Franzese [10] who determined that σ_u increases with increasing AR. Furthermore, it contradicts the observations made in previous studies which found that σ_u is suppressed in the skimming flow regime, resulting in higher magnitudes above the roughness array in the wake interference regime [9, 16, 28]. However, the 3D configuration results in slightly lower σ_u magnitudes above the roughness array. When compared with other studies of the same configurations there is some discrepancy [24, 28, 29]. The differences between skimming flow regime cases are less than the wake interference cases as skimming flow is less sensitive to boundary layer conditions.

b)

c)
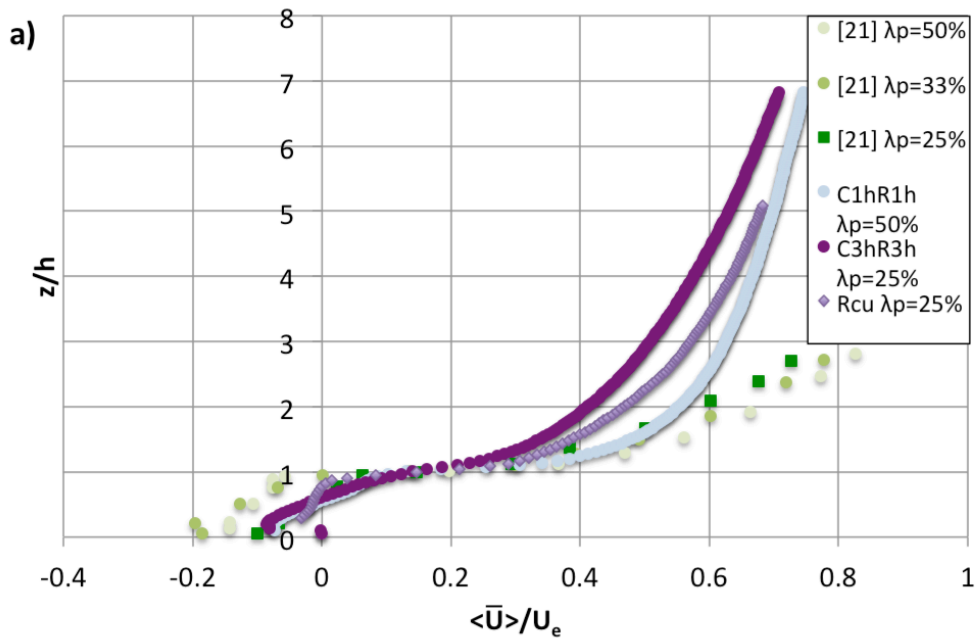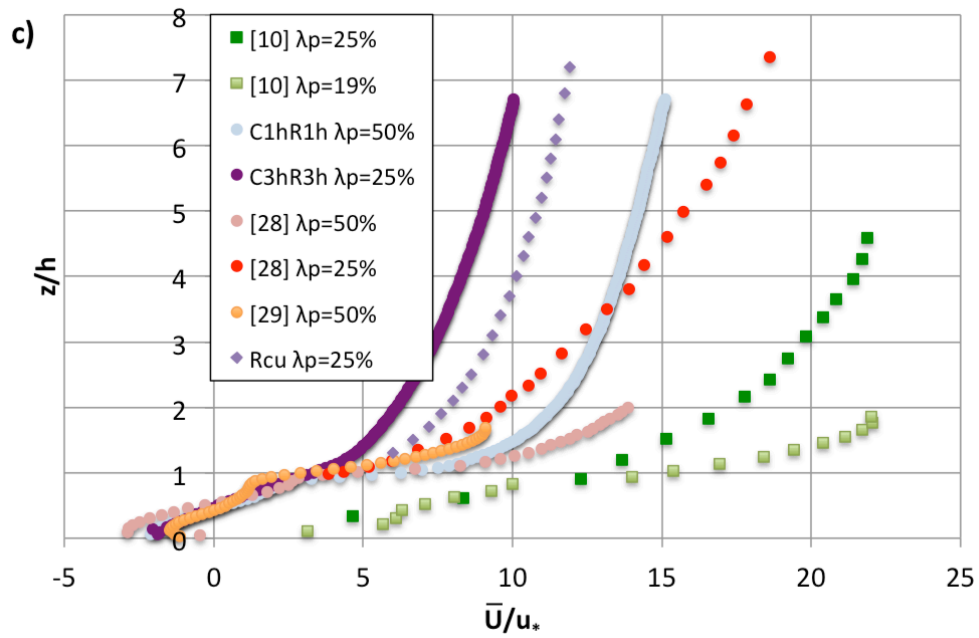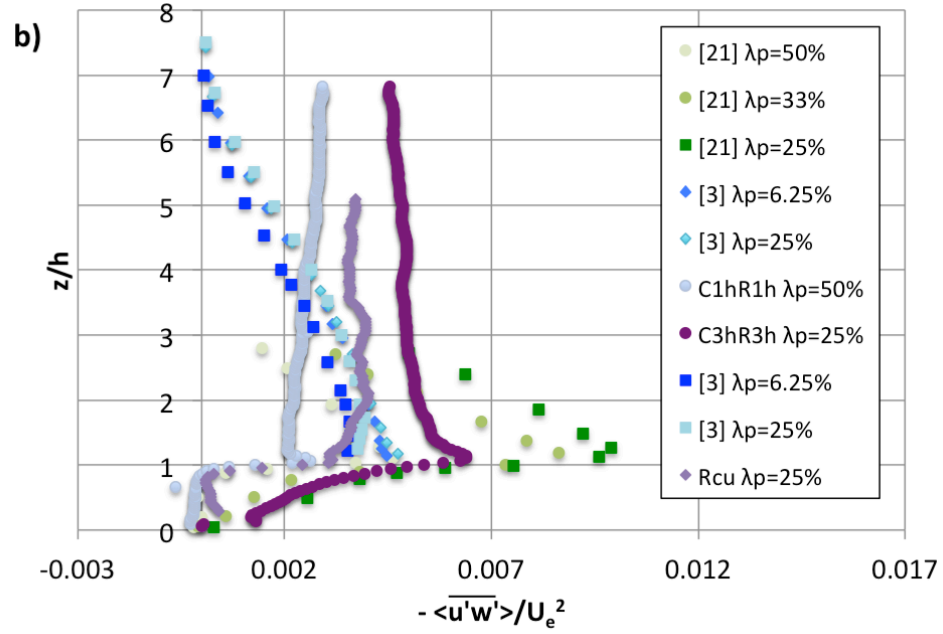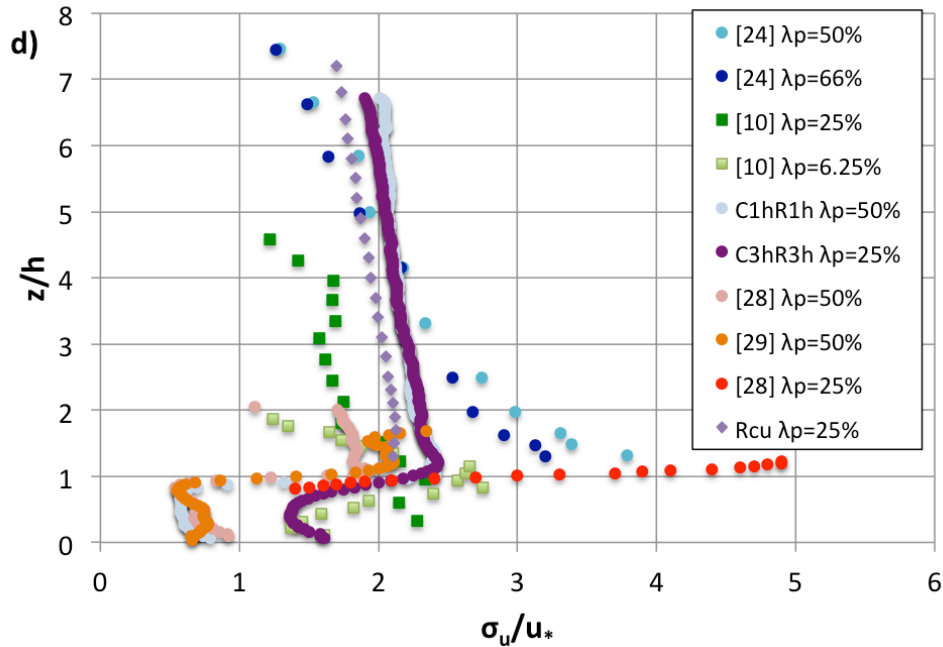
Figure 18   Comparison of approaching boundary layer flow statistics from the present study with results from literature for a) spatially averaged mean streamwise velocity [21]; b) spatially averaged Reynolds shear stress [3, 21]; c) centre mean streamwise velocity [10, 28, 29]; d) centre streamwise turbulence intensity [10, 24, 28, 29]. Spatially averaged quantities are normalized by freestream velocity and centre quantities are normalized by friction velocity derived from centre profiles. Circles: 2D configurations; Squares: 3D aligned configurations; Diamonds: 3D staggered configurations

2.3.2.4   Turbulent kinetic energy

The TKE and the relative contribution of each orthogonal component was analyzed for the three upstream roughness configurations (Figure 19). The streamwise component of velocity contributes most to the total TKE with the vertical component contributing the least. A field experiment conducted in Zurich, Switzerland, supports this result [27]. Figure 19d shows the relative contribution of each velocity component to the total TKE within the roughness ($z/h = 0 - 1$), within the shear layer ($z/h = 1 – 2$) and above the shear layer ($z/h = 2 – 6$). The values were taken as averages across each of the regions. The proportion of the streamwise velocity component is highest within the shear layer and in

the overlying boundary layer. However, within the roughness the contribution of the spanwise and vertical components are increased and the streamwise contribution is decreased. The large magnitudes of relative contribution within the roughness are a result of low magnitudes of total TKE present within the roughness. The results also show that an increase in λ_p results in decreased streamwise TKE, but increased spanwise and vertical TKE, specifically in the outer region. The effect of array obstacle configuration is also apparent within the shear layer as the 3D Rcu case results in decreased streamwise and spanwise TKE and increased vertical TKE compared to the 2D case of equal λ_p. These results demonstrate that 2D and 3D configurations of equal λ_p do not result in similar relative contribution to total TKE profiles. When compared to the results of Macdonald [19] for an aligned 3D array with $\lambda_p = 25\%$ the current results have larger magnitudes for the streamwise TKE for all configurations. The results correspond well to the R3h case for the vertical component to a height of approximately $z/h = 4$, but then begin to decrease [19]. This may be a consequence of simulation method as no fence was used by Macdonald [19]. The spanwise contribution is higher than the current results by a significant amount. It is apparent that the contributions of each velocity component to the total TKE of aligned and staggered cube arrays are not the same.

b)

c)
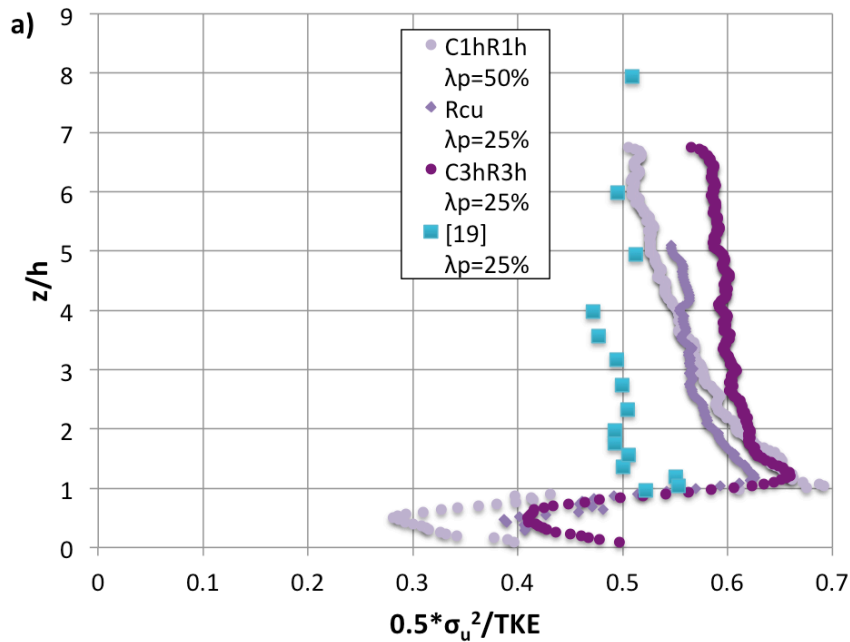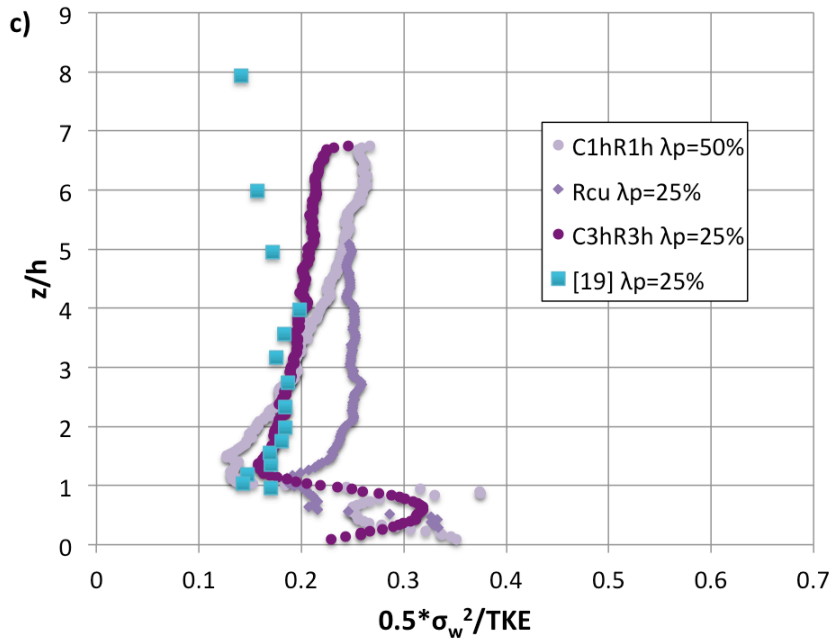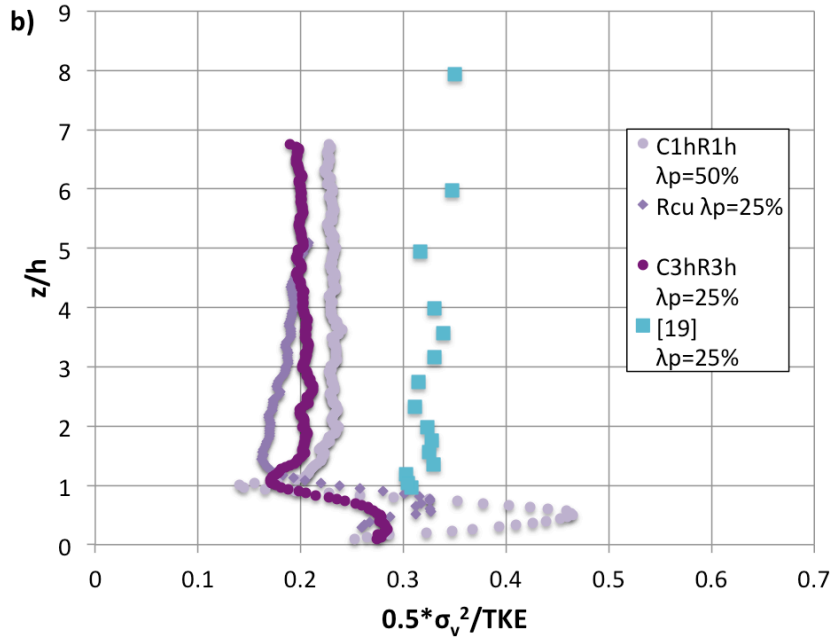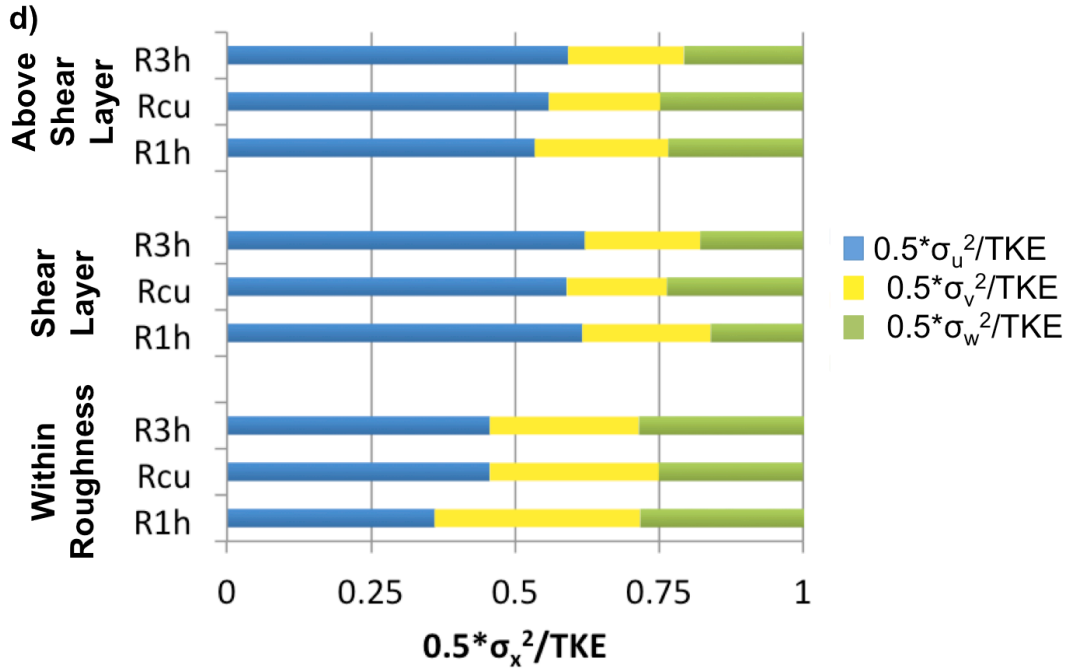
Figure 19 Comparison of contribution to total TKE of a) streamwise velocity component; b) vertical velocity component; c) spanwise velocity component with literature [19]; d) proportion of each TKE component with height. Circles: 2D configurations; Squares: 3D aligned configurations; Diamonds: 3D staggered configurations

2.3.2.5 Streamwise integral length scale

The influence of the geometry of the upstream roughness elements is also assessed via the estimation of the streamwise integral length scale (L_u), which is an important parameter when classifying boundary layers and is calculated as outlined in Section 3.1. In the region just above the roughness to a height of approximately 3h, the length scales for R3h and R1h are of similar size, while in the Rcu case the scales are smaller (Figure 20). At heights above 3h the length scales of the Rcu are again the smallest, but there is some deviation between the R3h and R1h cases with the lower AR configuration having smaller length scales. This deviation is likely to be due to the different growth rates of the internal boundary layers that develop after the change of roughness geometry: the rougher the surface, the faster the growth. Nevertheless, the present results agree with those of Volino et al. [33] who found that the length scales of the 2D roughness case were

significantly higher than the 3D case throughout the height of the boundary layer. Conversely, the present results and those of Volino et al. [33] are contradicted by Takimoto et al. [32] whose results show that 3D configurations result in larger L_u than those of 2D configurations with equal AR. This discrepancy may be a result of simulation method leading to a smaller boundary layer to building height ratio as no spires were used by Takimoto et al. [32] to produce turbulence and it is clear that L_u tapers off to very small values with increasing height in their work. All results seem to approach a similar value as z/h approaches unity except the 2D configuration of Volino et al. [33] with a high AR.
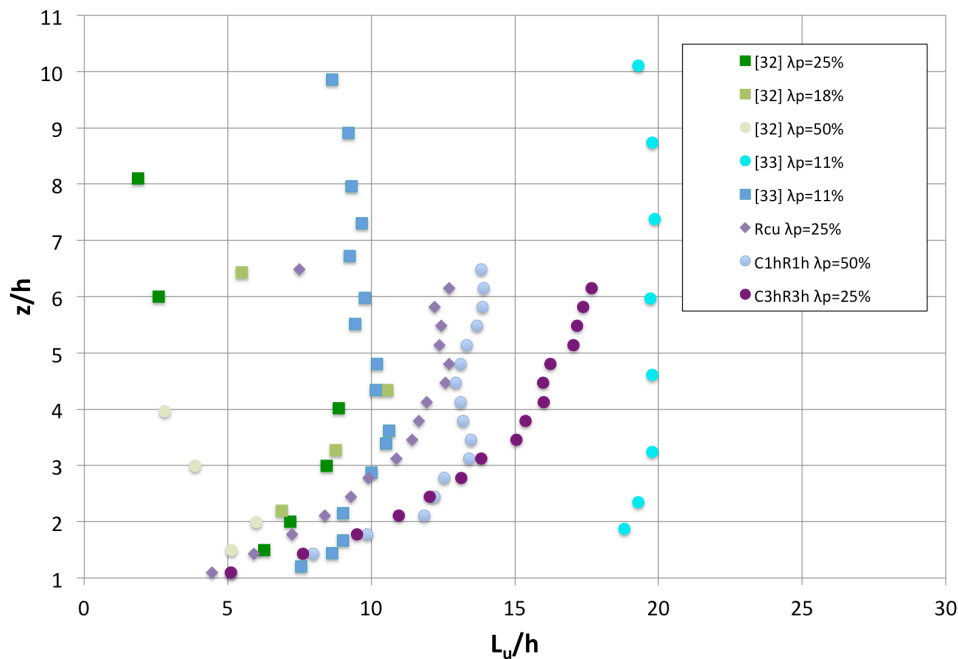
Figure 20   Streamwise integral length scales compared with data from literature [32, 33]. Circles: 2D configurations; Squares: 3D aligned configurations; Diamonds: 3D staggered configurations

2.3.3   Comparison of canyon flow regimes

Previous work attempting to classify the canyon dynamics of varying upstream roughness spacing are compared to the present work, normalized by the friction velocity derived from the centre vertical shear stress profiles (Figure 21). These profiles are measured

with the 2D test canyon for all three upstream roughness configurations. When comparing the mean streamwise velocity centre profiles there is no significant difference between the canyons of AR = 1 and 3 (C1h and C3h) configurations for each respective upstream roughness. The differences between canyon configurations are also not significant above the shear layer in the σ_u centre profiles. However, the σ_u peaks are larger for all C3h compared to C1h configurations within the shear layer. This suggests that the size of the measurement canyon has little impact on the turbulence statistics above the canyon, which are mostly influenced by the upstream roughness configuration, but does have a significant impact on the shear layer.

a)

Legend:
- C1hRcu λp=25%
- C1hR1h λp=50%
- C1hR3h λp=25%
- [28] λp=50%
- [28] λp=25%
- [29] λp=50%
- [30] λp=6.25%
- C3hR3h λp=25%
- C3hRcu λp=25%
- C3hR1h λp=50%

z/h

$\bar{U}/u_*$
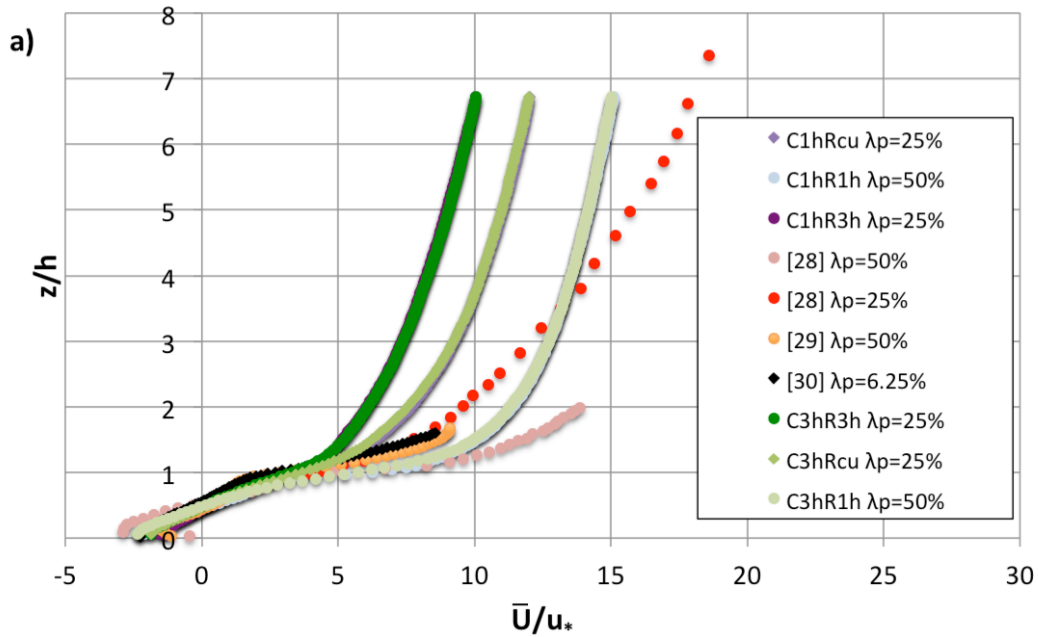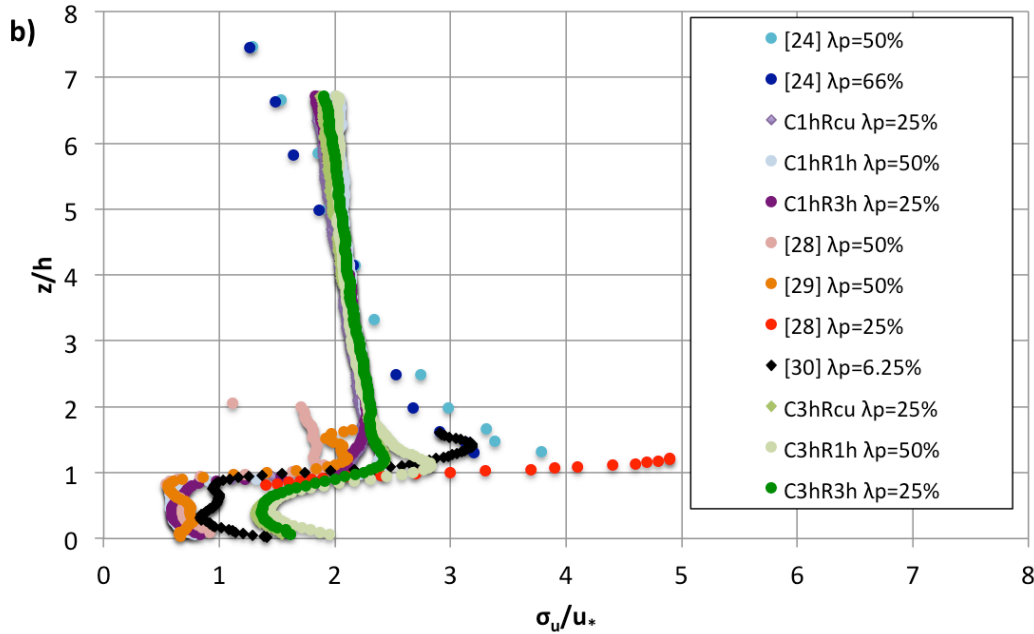
Figure 21 a) Centre streamwise mean velocity measured within the canyon normalized by friction velocity derived from centre profiles compared with literature [28, 29, 30]; b) turbulence intensity normalized by friction velocity derived from centre profiles measured within the canyon compared with literature [24, 28, 29, 30]. Circles: 2D configurations; Squares: 3D aligned configurations; Diamonds: 3D staggered configurations

The vorticity thickness (δ_w) of a mixing layer is a measure of the vertical extent of the shear layer over the canyon. It was calculated by determining the maximum velocity gradient over the canyon opening using the finite difference method and the velocity difference, which was selected to be between the free streamwise velocity and zero at the bottom of the canyon (Equation 4). The location of the maximum gradient was recorded and the location and boundaries of the shear layer were determined by adding and subtracting half of the vorticity thickness from the location of the maximum gradient.

Equation 4 Vorticity thickness

$$\delta_w = \frac{\Delta U}{(^{dU}/_{dy})_{max}}$$

Comparing the shear layers of the different configurations shows that the C3h results in much wider shear layers than C1h with greater penetration into the canyon (Figure 22a and b). It is evident in both the C1h and C3h cases that the upstream roughness changes the shape and size of the shear layer. Rcu and R3h result in similarly sized and shaped shear layers, whereas the R1h results in slightly smaller shear layers in both canyon configurations. This is interesting to note as both R3h and Rcu have the same plan area density (25%), which may explain the similarity.
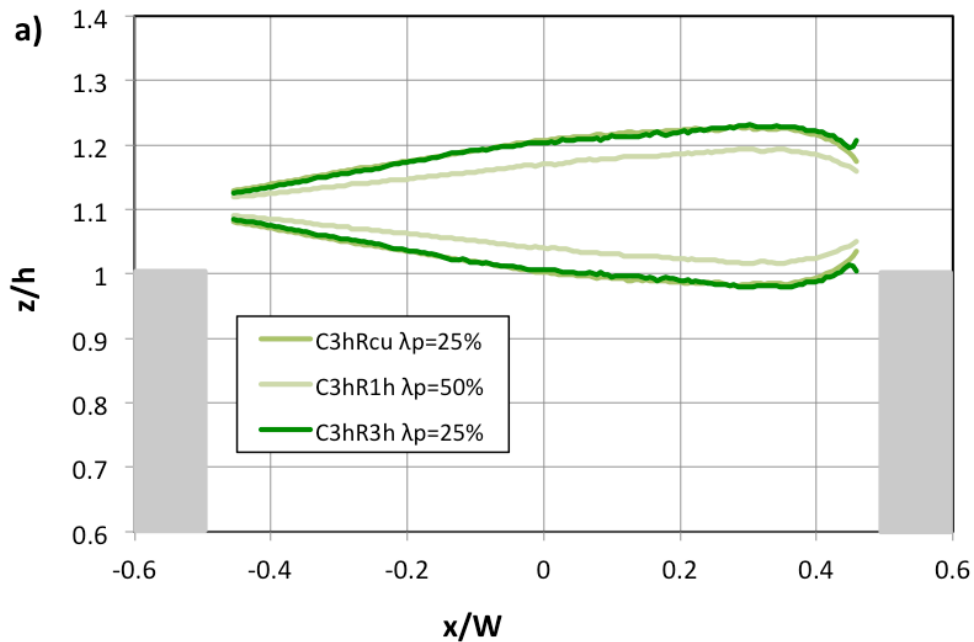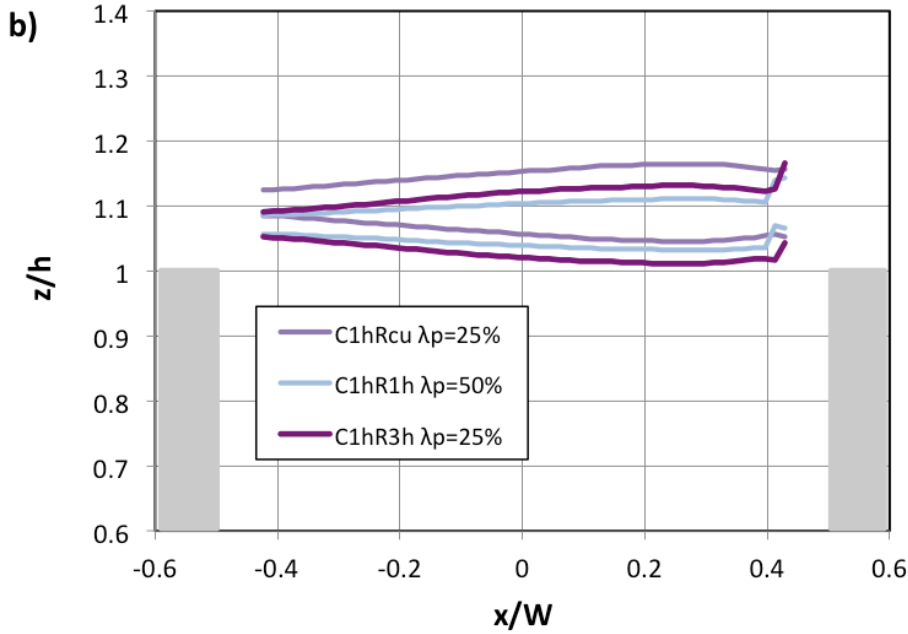
Figure 22 Shear layer boundaries of a) the C3h; b) C1h canyon configurations for the 3 different types of approaching flows

The shear layer TKE production can also be used to determine the shear layer boundaries (Equation 5). The gradient of the TKE production is then used to define the boundaries with a threshold value. This threshold value is not given by Salizzoni et al. [28] and was determined in the present case as the value at the base of the peak in the TKE production gradient.

Equation 5 Turbulent kinetic energy production

$$P = \overline{u'u'}\frac{\partial \overline{u}}{\partial x} + \overline{u'w'}\frac{\partial \overline{u}}{\partial z} + \overline{w'u'}\frac{\partial \overline{w}}{\partial x} + \overline{w'w'}\frac{\partial \overline{w}}{\partial z}$$

This method is used with the current results for comparison purposes (Figure 23). From the comparison it is evident that the shear layers of all three configurations are similar with only a slightly higher boundary in the C1hR3h configuration. The configurations of Salizzoni et al. [28] result in lower and thinner shear layers, which agrees with the larger peak in the turbulence intensity profiles shown previously. This may be a result of

differences in the height of turbulence generators used as the present study used generators of approximately 16h compared to 8h used by Salizzoni et al. [28].
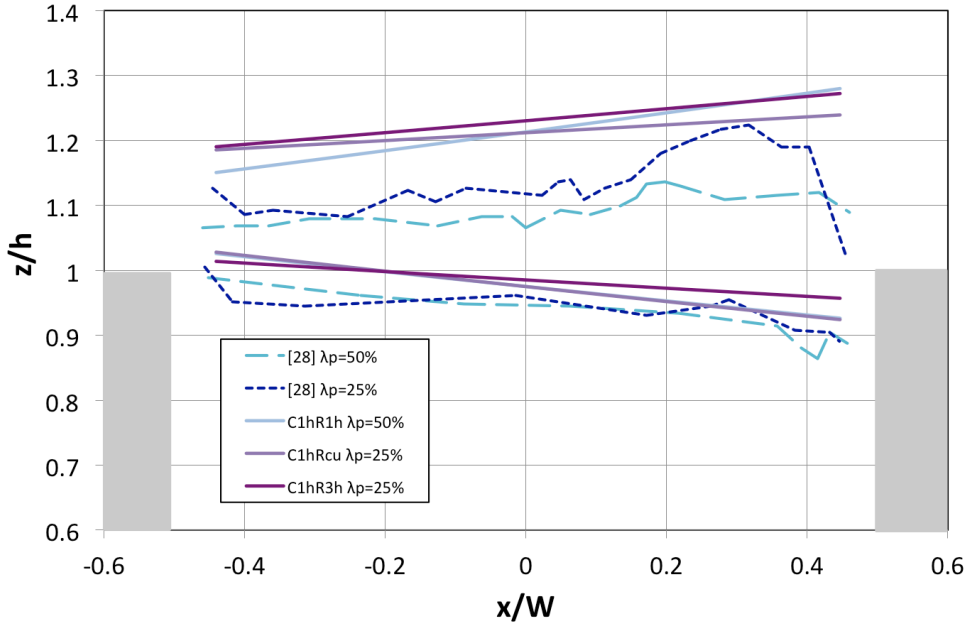
Figure 23   Shear layer boundaries of C1h canyon configurations for the 3 different types of approaching flows using TKE Production method compared with [28]

In order to further quantify the effect of the upstream roughness configuration on the canyon flow, the time-averaged vertical flow rate across the canyon opening was computed as:

Equation 6   Time-averaged vertical flow rate

$$Q = \frac{L}{N} \sum_{j=1}^{N} \int_{x=-W/2}^{x=W/2} w(z = h, t_j)\,dx$$

where w is the instantaneous vertical velocity, W is the canyon width, L is the canyon lateral length and N is the number of PIV images used for averaging. The computation was performed on the centre of the canyon (y = 0). The total flow rate, Q, was decomposed into its positive (upward) and negative (downward) contributions. Using w

= W + w', the contribution of both the mean (W) and the fluctuating (w') velocities to the positive and negative flow rates were estimated. The results are shown in Figure 24a. For both canyon AR studied, changing from a skimming to a wake interference flow regime in the upstream roughness and in agreement with the shear layer analysis, increases the magnitude of the total positive and negative flow rates (filled triangles), which is due to both an increase of the contribution of the mean flow and the fluctuating velocity. An increase of three times canyon AR results in an increase of approximately 1.5 times the total positive and negative flow rates. When comparing the present configurations with equal λ_p the 2D configuration has a higher flow rate than the 3D case. This is due to the transition from skimming flow in the 3D case to wake interference flow in the 2D case. The results are compared to those of Ho and Liu [9] (Figure 24b) and it is evident that the current configurations result in lower magnitudes for the total flow rate and the turbulent flow rate. It is apparent that for all configurations the majority of the instantaneous flow rate across the canyon is due to the turbulence fluctuations.

Given the high aspect ratio L/h of the investigated canyons, one could expect the flow to be statistically homogeneous in the transverse direction. The combination of this hypothesis with the configuration of the canyon axis perpendicular to the main flow leads to a zero contribution of the mean flow to the total flow rate at the canyon opening. The results presented in Figure 24a show a small positive contribution of the mean flow to the total flow rate (x). These values correspond to mean vertical velocities of the order of magnitude of the statistical error (Section 2). The possibilities of the canyon being slightly off with its theoretical axis or of a slight misalignment of the measurement plane with the main flow were investigated by estimating the mean transversal flow rate needed to compensate the non-zero vertical flow rate. It was found to correspond to angular offset lower that 0.7°, a value smaller than the accuracy that can be achieved in setting up such experiment. The non-zero values of the mean total rate are therefore considered to have no statistical significance. Mass transfer between the canyon and the boundary layer should, therefore, be considered as being caused by turbulent fluctuations.
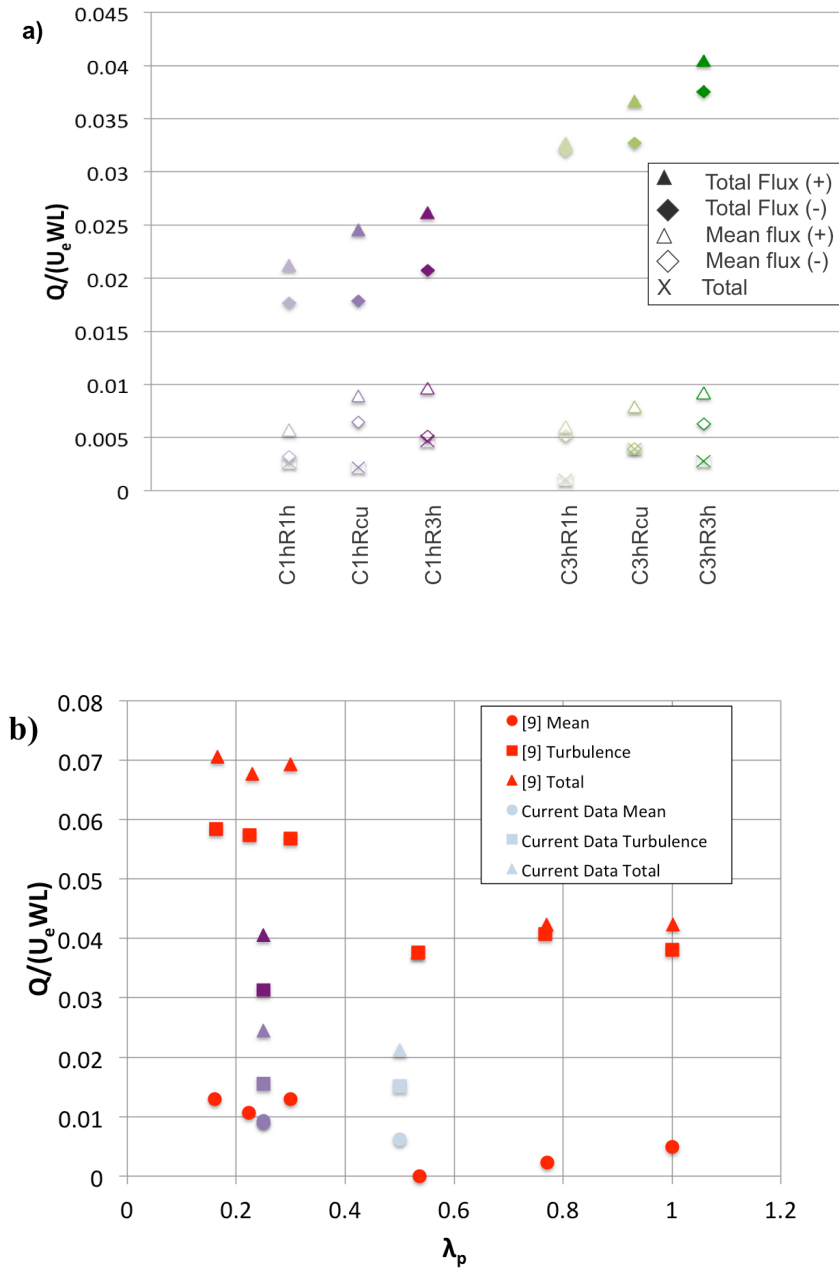
Figure 24 a) Positive flow rate across the canyon (▲), negative flow rate across the canyon (♦) and total flow rate across the canyon (×) flow rates Q/U_eWL across the canyon for the 6 different configurations; open symbols: contribution of the mean flow to the flow rate; filled symbols: contribution of both the mean flow and fluctuation to the flow rate; b) Air Exchange Rate (ACH) of present results compared with [9] with contribution from mean (circles), turbulence (squares) and total (triangles) for three configurations

2.4 Conclusions

The geometry of the roughness elements (cubes or 2D bars with different streamwise spacing) in the upstream roughness used to simulate an atmospheric boundary layer was found to have a non-negligible influence on the characteristics of the boundary layer. The effect of roughness plan area density (λ_p) is evident within the vertical profiles of mean streamwise velocity, shear stress, turbulence intensity and integral length scales. The current results agree with previous work, which found that the mean streamwise velocity for configurations of equal λ_p is higher in the 3D than 2D configuration [10, 28]. The relative contribution of the three orthogonal components to the total turbulent kinetic energy (TKE) also agrees with published data and demonstrates that staggered and aligned arrays or 2D and 3D arrays of equal λ_p do not generate the same profiles of TKE [19, 27]. The current results show that the integral length scale is larger in 2D than 3D cases of equal λ_p and confirms that the integral length scale also increases with increasing AR in 2D configurations [33]. The spatially averaged turbulent shear stress increases with decreasing λ_p for 2D configurations, as confirmed by the literature [21]. The spatially averaged shear stress is also shown to increase from the 3D to 2D configuration of equal λ_p, in contradiction to previous work [21]. The current results show that the canyon ventilation flow rate increases from 3D to 2D configurations of equal λ_p and increases with decreasing λ_p. This is due to the transition from skimming to wake interference regimes. Comparing the roughness length (z_o) for 2D and 3D configurations of equal λ_p shows that 2D configurations result in larger magnitudes. ESDU scaling was used to classify the three upstream roughness configurations. The scaling suggests that the R1h configuration represents a scenario that is not applicable to the study of street canyon ventilation and, thus, this configuration should not be used in further studies wishing to investigate urban street canyon flows. This is confirmed by the very high value of the displacement height ($d/h > 0.98$), which appears not to be compatible with the estimated nature of the terrain (rural).

The influence of the different approach flows on the flow inside a street canyon model was investigated for two different canyon streamwise widths (W). An increase in canyon width resulted in higher turbulence intensity peaks within the shear layer and increased

vertical canyon ventilation rate. However, there is a negligible effect on the streamwise velocity and turbulence intensity above the canyon, which suggests that these parameters and the outer flow are mostly influenced by the upstream roughness. The increased canyon width resulted in a larger shear layer with all upstream roughness configurations and it is also evident that the 2D R1h (square section obstacles spaced at 1h) configuration results in a slightly smaller shear layer with both measurement canyon configurations. The ventilation of the canyon, estimated via the computation of positive and negative flow rate across the canyon opening, was found to be influenced by the upstream flow regime, even with a canyon with $W/h = 1$. An upstream wake-interference flow regime leads to stronger exchanges between the canyon and the flow above by enhancing both the turbulence and the mean flow contribution to the flow rate. Thus, it is evident that care must be taken when selecting the upstream roughness element configuration for a given wind tunnel study, depending on which regime (wake interference or skimming) is desired for the oncoming flow and, separately, for the test canyon.

2.5 Summary

The use of idealized roughness arrays and canyons within the wind tunnel produces scaled boundary layers applicable to the study of urban street canyon ventilation. The following chapter uses field data from an idealized canyon to examine whether an idealized wind tunnel model reproduces the main turbulence characteristics and what the influence of upstream conditions are on the flow within the canyon.

2.6 References

1. Barlow JF, Leitl B (2007) Effect of roof shapes on unsteady flow dynamics in street canyons. International Workshop on Physical Modelling of Flow and Dispersion Phenomena (PHYSMOD) August 2007, Orléans, France

2. Chang K, Constantinescu G, Park S (2006) Analysis of the flow and mass transfer processes for the incompressible flow past an open cavity with a laminar and a fully turbulent incoming boundary layer. J Fluid Mech 561:113-145

3. Cheng H, Hayden P, Robins AG, Castro IP (2007) Flow over cube arrays of different packing densities. J Wind Eng Ind Aerodyn 95:715-740

4. Coceal O, Dobre A, Thomas TG, Belcher SE (2007) Structure of turbulent flow over regular arrays of cubical roughness. J Fluid Mech 589:375-409

5. ESDU (1982) Strong winds in the atmospheric boundary layer. Part I: mean-hourly wind speeds. Data Item 82026 (amended 1993), Engineering Sciences Data Unit International

6. ESDU (1985) Characteristics of atmospheric turbulence near the ground. Part II: single point data for strong winds (neutral atmosphere. Data Item 852020 (amended 1993), Engineering Sciences Data Unit International

7. Grimmond CSB, Oke TR (1999) Aerodynamic properties of urban areas derived from analysis of surface form. J Appl Meteorol 38:1262-1292

8. Hagishima A, Tanimoto J, Nagayama K, Meno S (2009) Aerodynamic parameters of regular arrays of rectangular blocks with various geometries. Bound Layer Meteorol 132:315-337

9. Ho YK, Liu CH (2013) Wind tunnel modeling of flows over various urban-like surfaces using idealized roughness elements. International Workshop on Physical Modelling of Flow and Dispersion Phenomena (PHYSMOD) Sept 2013, University of Surrey, UK

10. Huq P, Franzese P (2013) Measurements of turbulence and dispersion in three idealized urban canopies with different aspect ratios and comparisons with Gaussian plume model. Bound Layer Meteorol 147:103-121

11. Kanda M, Moriwaki R, Kasamatsu F (2004) Large-eddy simulation of turbulent organized structures within and above explicitly resolved cube arrays. Bound Layer Meteorol 112:343-368

12. Kanda M (2006) Large-eddy simulations on the effects of surface geometry of building arrays on turbulent organized structures. Bound Layer Meteorol 118:151-168

13. Kang W, Sung HJ (2009) Large-scale structures of turbulent flows over an open cavity. J Fluids Struct 25:1318-1333

14. Lee JH, Sung HJ, Krogstad P (2011) Direct numerical simulation of the turbulent boundary layer over cube-roughened wall. J Fluid Mech 669:397-431

15. Lee JH, Seena A, Lee SH, Sung HJ (2012) Turbulent boundary layers over rod- and cube-roughened walls. J Turb 13:1-26

16. Liu CH, Leung DYC, Barth MC (2005) On the prediction of air and pollutant exchange rates in street canyons of different aspect ratios using large-eddy simulation. Atmos Environ 39:1567-1574

17. Macdonald RW (2000) Modelling the mean velocity profile in the urban canopy layer. Bound Layer Meteorol 97: 23-45

18. Macdonald RW, Griffiths RF, Hall DJ (1998) An improved method for the estimation of surface roughness of obstacle arrays. Atmos Environ 32:1857-1864

19. Macdonald RW, Carter Schofield S, Slawson PR (2002) Physical modeling of urban roughness using arrays of regular roughness elements. Water, Air, and Soil Pollution: Focus 2:541-554

20. Marciotto ER, Fisch G (2013) Wind tunnel study of turbulent flow past an urban canyon model. Environ Fluid Mech 13:403-416

21. Michioka T, Sato A (2012) Effect of incoming turbulent structure on pollutant removal from two-dimensional street canyon. Bound Layer Meteorol 145:469-484

22. Oke TR (1988) The urban energy balance. Prog Phys Geogr 12:471-508

23. Perret L, Savory E (2013) Large-scale structures over a single street canyon immersed in an urban-type boundary layer. Bound Layer Meteorol 148:111-131

24. Rafailidis S (1997) Influence of building areal density and roof shape on the wind characteristics above a town. Bound Layer Meteorol 85:255-271

25. Ricciardelli F, Polimeno S (2006) Some characteristics of the wind flow in the lower urban boundary layer. J Wind Eng Ind Aerodyn 94:815-832

26. Rivet C (2014) Étude en soufflerie atmosphérique des interactions entre canopée urbaine et basse atmosphère par PIV stéréoscopique. Dissertation, École Centrale de Nantes

27. Rotach MW (1995) Profiles of turbulence statistics in and above an urban street canyon. Atmos Environ 29:1473-1486

28. Salizzoni P, Marro M, Soulhac L, Grosjean N, Perkins R (2011) Turbulent transfer between street canyons and the overlying atmospheric boundary layer. Bound Layer Meteorol 141:393-414

29. Sato A, Takimoto H, Michioka T (2009) Impact of wall heating on air flow in urban street canyons. International Workshop on Physical Modelling of Flow and Dispersion Phenomena (PHYSMOD) August 2009, Brussels, Belgium

30. Savory E, Perret L, Rivet C (2013) Modelling considerations for examining the mean and unsteady flow in a simple urban-type street canyon. Meteorol Atmos Phys 121:1-16

31. Simoëns S, Ayrault M, Wallace J (2007) The flow across a street canyon of variable width – Part 1: kinematic description. Atmos Environ 41:9002-9017

32. Takimoto H, Inagaki A, Kanda M, Sato A, Michioka T (2013) Length-scale similarity of turbulent organized structures over surfaces with different roughness types. Bound Layer Meteorol 147:217-236

33. Volino RJ, Schultz MP, Flack KA (2009) Turbulence structure in a boundary layer with two-dimensional roughness. J Fluid Mech 635:75-101

Chapter 3

3   Mean turbulence statistics of idealized street canyon field experiment compared with wind tunnel model

This section provides a detailed literature review on previous urban street canyon field studies followed by an outline of the experimental details and data processing methods. Finally, the main results are discussed and conclusions are drawn.

3.1   Introduction

Wind tunnels are frequently used to model urban street canyon turbulence and ventilation dynamics [3, 13, 14]. Using simplified wind tunnel models reproduces the main features of most common street configurations, in relation to pollutant transport and air quality, but care must be taken to ensure the boundary layer is scaled correctly. As will be shown by this introductory review there have been few studies in which mean and unsteady flow dynamics from a wind tunnel and field study have been quantified and compared in order to justify the validity of the wind tunnel results. Urban areas vary drastically with geographic location, not only in regard to natural landscape but also to the style of architecture and building density. Field studies have been conducted in dense urban areas including skyscrapers in North America [1, 2, 4, 10, 11, 16, 31] and Asia [12, 13], as well as more low-rise urban areas in Europe [5, 14, 20, 22, 23, 28, 29]. In addition, some studies have opted to conduct measurements in simplified roughness arrays within the atmospheric boundary layer [12, 13, 19]. The variety of these studies makes comparison difficult because the aspect ratio (AR, the ratio of height, H, to width, W, of the canyon), packing density (λ_p, the ratio of the plan area covered by building structures to the total plan area) and ambient wind and temperature conditions differ considerably from study to study.

Much previous full-scale work has been completed to study the dispersion of pollutants in urban areas. Some major field studies, such as the Mock Urban Setting Test (MUST) [30] and a study in the Hamamatsu-cho Minato-ku area of Tokyo, Japan [27], have focused on pollutant concentration measurements, with only limited wind velocity and

turbulence measurements. While some studies, such as MUST, comprise of simplified roughness arrays, most have conducted measurements within existing urban areas, such as the study in Tokyo [27]. Other studies have also included the effects of traffic flow on the dispersion in existing urban areas, such as in Gottinger Strabe, Hanover [15, 25] and Jagtvej, Copenhagen [15, 20]. Although these concentration measurement studies are important to the understanding of the dispersion of pollutants in urban areas they will not be considered further in the present thesis since the focus is on the mean and unsteady wind flow field in urban canyons.

Table 4 summarizes the literature that includes significant flow measurements as part of their field study. The most common method for field studies are *in-situ* measurements within urban areas. In North America, the Oklahoma City Joint Urban 2003 (JU2003) [2, 10, 31] and Manhattan Midtown-2005 (MID05) [11] urban field experiments both conducted near street level and building roof level flow measurements. Similarly, a study in Columbus, Ohio included measurements above the canyon, at the height of the canyon building roofs and within the canyon [1]. Finally, *in-situ* measurements were conducted in Chicago, Illinois within the street canyon and above the building roofs [4]. In Europe major field campaigns such as the Nantes'99 experiment [14, 28, 29], the Basel UrBan Boundary Layer Experiment (BUBBLE) [23], the Zurich Urban Climate Program [22], air pollution from traffic in urban areas conducted in Jagtvej, Copenhagen [20] and a study in Goteborg, Sweden [5] included *in-situ* measurements within and above street canyons. The majority of these studies used sonic anemometers for the flow measurements within and above the canyon. However, in one case high frequency LiDAR [23] was used and, in another, helium balloons [4] were released into the canyon and cameras were used to track their trajectory. The studies were each conducted for a different purpose and, thus, the acquisition frequency of the instrumentation varied for each study with some having a low sampling frequency of 1 Hz [1, 4]. This sampling frequency may not be high enough to capture some of the turbulent dynamics of interest in the present work. The length of sampling time is also dissimilar between cases and ranges from less than one day to over one year. This is likely due to the differing purpose of each study, as some required specific ambient conditions, thus requiring longer sampling periods to filter out undesired conditions while others did not. Generally, the

averaging period for the results was between 30 – 60 min, with some studies using averaging periods as low as 5 min. This short averaging period could present issues, as statistical flow averages may not have had sufficient time to converge. Finally, when processing the data several studies used filtering methods to remove interference from instrumentation or low frequency winds while several studies did not report any filtering prior to calculating flow statistics. It is important to apply appropriate filtering techniques to remove unwanted interference from low frequency synoptic winds, as these will influence the turbulence statistics.

From the literature several conclusions can be drawn. The presence of vortices at the end of an urban canyon has been confirmed by two studies that both found horizontally rotating vortices close to the canyon edge [2, 31]. DePaul et al [4] and Klein et al. [16] show evidence of a single vortex contained within the canyon when the approach flow is perpendicular to the canyon. Arnfield and Mills [1] discuss the presence of an along-canyon wind that is proportional to the along-canyon velocity above the canyon (z/h > 1), even for cases that have a perpendicular approach flow, that has a tendency to decelerate as it approaches the mid-point along the canyon due to friction with the building walls and street. Klein et al. [16] also observed strong along-canyon channeling even in perpendicular cases while Brown et al. [2] found channeling in several cases, but it reached only approximately 25% of the canyon length at each end of the canyon. This suggests that modeling urban street canyons as two-dimensional in the wind tunnel may not be appropriate. The presence of strong along-canyon winds may be attributed to the high-sensitivity of the canyon flow to large-scale wind direction changes [16, 31]. Eliasson et al. [5] found that the along-canyon flow increases with the changing of the ambient wind direction. The ambient wind velocity magnitude also has a significant effect on the canyon flow. At low ambient wind velocities, less than 1.5 m/s, the vortex was found by DePaul et al. [4] to disappear, while for these low velocities Eliasson et al. [5] observed a secondary vortex circulation counter-rotating relative to the upper vortex for short time periods (on the order of seconds) in the lower portion of the canyon. The scaling of the vertical velocity using the streamwise ambient velocity was also found not to be applicable to cases where the ambient wind speed was less than 1 m/s [20]. This suggests that at low ambient wind speed there is a loss of consistent scalable flow

structure within the canyon. Finally, there are some discrepancies in the effect of atmospheric stability on canyon flow. Hanna et al. [10] found only small differences in the turbulence statistics due to stability when comparing daytime (slightly unstable, $0.5 < z'/L < 0.1$) and nighttime results (very slightly unstable $z'/L < 0.5$), whereas Rotach [22] found that the velocity variances were strongly related to stability with stable conditions resulting in constant velocity variance throughout the height of the canyon while unstable conditions resulted in diverse velocity variances throughout the canyon. Klein et al. [16] found that the dependence on stability varied depending on the height used for calculating statistics for normalization. When using suburban data taken 1 km upstream of the canyon at the average roof level, there was a strong influence of stability on the canyon flow statistics, although only a minor effect is seen when using a normalization height of 80 m above the canyon [16]. It was noted that in terms of mean flow there is weaker reverse flow in the lower part of the canyon for neutral ($|z'/L| < 0.1$) and unstable ($z'/L < -0.1$) cases compared to stable ($z'/L > 0.1$) cases. As well, stable conditions result in stronger downward motions at the upper and middle levels of the canyon than unstable and neutral cases. Both Hanna et al. [10] and Rotach [22] normalized the canyon flow, such as velocity variance and mean along-canyon wind velocity, using data obtained above the roof of the upstream building. It is, therefore, likely that this discrepancy is a result of differences in site characteristics as Hanna et al. [10] measured in a North American city and Rotach [22] conducted measurements in a European city.

Table 4   Field studies including significant flow measurements

Location	W/H	*In-situ* or Idealized	Terr. Rough.	Meas. Quan.	Device	Hz	Sample Length	Prefilt-ering	Author
				U V W T					Brown et al. [2]
				U V W T					Zaijic et al. [31]
				U V W T					Hanna et al. [10]
Oklahoma City, USA	0.5	*In-situ*	Urban	U V W T	SA	10	6-9 hr	Not stated	Klein et al. [16]
Goteburg, Sweden	2.1	*In-situ*	Urban	U V W T	SA	10	13 days	Yes	Eliasson et al. [5]
				U V W					Inagaki and Kanda [12]
				U V W	SA	50	~ 1 yr	Yes	Inagaki and Kanda [13]
Saitama, Japan	1	Idealized	Aligned Cubes	U V W	PIV	30	1 hr	Yes	Takimoto et al. [26]
Manhattan, NY, USA	-	*In-situ*	Dense urban	U V W T	SA	10	~ 7.5 hr	Not stated	Hanna and Zhou [11]
UK	1.43	Idealized	Rural	U V W	SA	21	5 months	Yes	Louka et al. [19]
Zurich, Switzerland	1	*In-situ*	Urban	U V W	SA	1	18 months	Yes	Rotach [22]
Columbus, Ohio, USA	0.66	*In-situ*	Urban	U W	SA	1	11 days	Not stated	Arnfield and Mills [1]
Copenhagen, Denmark	1	*In-situ*	Urban	U W	SA	Not given	185 days	Not stated	Neilsen [20]
BUBBLE Basel, Switzerland	No data	*In-situ*	Urban	U V W T CO_2 q'	LiDAR, wind profiler	5000 - 6000	~ 1 yr	Yes	Rotach et al. [23]
				U V W T CO					Vachon et al. [28]
				U V W					Kastner-Klein and Rotach [14]
Nantes, France	0.7	*In-situ*	Urban	U V W T CO	SA	4	12 hrs	Yes	Vachon et al. [29]
Chicago, USA	0.71	*In-situ*	Urban	U W	Balloons, camera	1	~ 3 days	Not stated	DePaul and Sheih [4]

As mentioned earlier the complexity of urban areas makes comparison between studies difficult and also limits the applicability of the data to other sites. Thus, some researchers have opted to use simplified roughness arrays in the atmospheric boundary layer. One notable study is the Comprehensive Outdoor Scale MOdel experiment for urban climate (COSMO) located in Saitama, Japan [12, 13, 26]. The study comprised of 512 1.5 m high cubic obstacles spanning an area of 5000 m^2 and they utilized Particle Image Velocimetry (PIV) to obtain detailed flow measurements within the cube array [12, 13, 26]. Another study used existing peaked roof barns of ridge height, h = 4.2 m, to act as a simplified canyon and included measurements within and above the canyon [19]. The focus of these papers was not specifically on canyon flow dynamics and so comparison with the present work is limited due to the analysis of their work. Inagaki et al. [12, 13] found large coherent structures elongated in the streamwise direction, which are responsible for ventilation events such as sweeps and ejections. Similarly to the literature discussed above, it was found that both wind direction [5, 12, 13, 16, 31] and stability [12, 13, 16, 22] resulted in changes to the mean flow fields within the canyon.

The majority of studies included in this review consider only field measurements. However, to better understand the wind flow dynamics of the urban environment and how to model them, one must consider comparable wind tunnel models. Of the above-mentioned studies the Nantes'99 experiment [14], BUBBLE [23] and COSMO [26] are the only ones that also included significant wind tunnel flow measurements. Therefore, these studies will be primarily used for comparison with the present work.

It is important when discussing wind tunnel studies to consider the quality of the boundary layer scaling to ensure that the results are applicable to full-scale applications. The three studies that include wind tunnel models as part of their discussion all include sufficient boundary layer development and scaling [14, 23, 26]. Vortex generators and upstream roughness were used in all three cases, as well as scaling using the d and z_o boundary layer parameters. However, Jensen number scaling was not provided by any of these studies.

Due to the focus of the studies, e.g. measurement of passive scalar concentrations, there is a limited focus on the turbulence statistics within and above the canyon. Takimoto et al. [26] measured the mean two-dimensional flow fields as well as the mean turbulent momentum flux and standard deviation of the streamwise and vertical velocity components within a cube array. The main focus of the study was to identify instantaneous sweep and ejection events [26]. Both Kastner-Klein et al. [14] and Rotach et al. [23] provide mean profiles of streamwise and vertical velocity. Rotach et al. [23] also include vertical flux, streamwise integral length scale and spectra while Kastner-Klein et al. [14] also provide other mean profiles of turbulent kinetic energy and Reynolds stress, $\overline{u'w'}$. Takimoto et al. [26] found a significant difference in the mean flow fields between the wind tunnel and field experiments. Both field and wind tunnel results showed a vortex within the canyon, but it was stronger in the field case and was located at x/H = 0.46 in the field and x/H = 0.37 in the wind tunnel. As discussed above, this is likely due to an influence of the ambient wind direction and stability in the field experiment. It was also determined that the impact of long-period, outer-layer disturbances was minor. Both the wind tunnel and field experiment showed strong, large-scale upward motions that were found to be correlated with low-speed streaks [26]. This suggests that the wind tunnel model was able to properly represent the full-scale intermittent canyon dynamics of full-scale well. Similarly, Rotach et al. [23] found good agreement between the turbulence characteristics of the *in-situ* field measurements and the reduced scale site-specific wind tunnel model up to a height of z = 2.5h. However, Kastner-Klein et al. [14] found that the site-specific wind tunnel model under-predicted the two-dimensional turbulent kinetic energy of the full-scale *in-situ* measurements. The reason for this discrepancy is unclear as both studies were conducted in European cites and used site-specific wind tunnel models.

From this present overview it may be seen that many studies have investigated the flow within urban areas using field data either *in-situ*, within an urban area, or within simplified roughness arrays set-up at a test site. However, due to the complexity of the urban environment and the challenges of conducting studies within the atmospheric

boundary layer these studies provide limited information about the flow dynamics governing street canyon ventilation. From this review an important question still remains:

- Does a properly scaled wind tunnel model reproduce the main flow features within a full-scale street canyon that govern ventilation, notably the unsteady flow dynamics?

Previous field studies, specifically those involving comparisons with wind tunnel models, have mostly focused on dispersion characteristics with only limited mean and turbulent flow analysis. The present work seeks to improve the understanding of the turbulent flow within a canyon in the atmospheric boundary layer and the differences seen in a wind tunnel model. The overall goal of the present work is to determine whether, for perpendicular approach flow conditions, the oncoming boundary layer mean flow and turbulence statistics match those of a realistic street canyon and whether the main features of the canyon mean and turbulent flow are reproduced in the wind tunnel when compared to the case of the realistic street canyon. This goal will be achieved by examining measurements taken within a full-scale single canyon at a field site along with corresponding data from a wind tunnel study of equivalent canyon configuration. The next section will discuss the site-specific experimental details of both the field study and the wind tunnel study, which will be followed by a description of the data selection and processing method and, finally, a discussion of the main results and conclusions.

3.2 Experimental details

This work consists of two phases of experimentation. The first is a field study, which will be discussed in the first section and the second is a wind tunnel study of an equivalent reduced-scale geometry.

3.2.1 Field experiment

Field data were provided from the *Influence des effets micro-météorologiques sur la propagation acoustique en milieu urbain* (EM2PAU) campaign [9], which took place in Nantes, France. The campaign took place over a two-year period and used sonic anemometers to measure the three components of velocity as well as the temperature within an idealized canyon. The canyon was made from shipping crates with aspect ratio

W/h = 0.7 and L/h = 4.6 and located in a parking lot surrounded by forest and fields with some buildings nearby, outside of the city of Nantes (Figure 25). This study will focus on flows perpendicular to the canyon. From the figure it is evident that the upstream terrain varies for each perpendicular approach flow. From the north-west (approach flow from the 313° direction) the terrain is wooded and will have a z_o of 0.3 m [6, 7]. However, from the south-east (approach flow from the 133° direction) the terrain is flat grassland and fields resulting in a z_o range of 0.03 – 0.1 m [6, 7]. From this direction there are also several large buildings at a distance of approximately 11.5h from the canyon, which will influence the flow around and within the canyon.

As previously stated, this study will focus only on those cases when the approach flow is perpendicular to the canyon. Figure 26 shows the coordinate system that is used for the data, with U perpendicular to the canyon, V along the canyon axis and W as the vertical component. During analysis the coordinate system u-component and v-component is reversed for the 133° approach direction to ensure positive oncoming streamwise velocity towards the canyon. Within the canyon there are six sonic anemometers aligned with the axis of the canyon all located 12 m from each of the canyon ends and spaced 0.8 m apart in the streamwise direction with three at a height of z/h = 0.38 (S14, S15, S16) and another three at z/h = 0.77 (S11, S12, S13) from the ground (Figure 26). A seventh sonic anemometer is located on a mast at 10 m height (S10), x/h = 1.7 and y/h = 5 away from the centre of the canyon, to determine the characteristics of the oncoming flow, and is aligned with the North direction (Figure 26). All of the sonic anemometers have an acquisition frequency of 20 Hz and measure U, V, W velocity components and temperature. The resolution of the sonic anemometers is 0.01 m/s, 0.1^o and 0.01^oC with a stated accuracy of 1.5% r.m.s. and 2° for velocity and wind direction, respectively.

From the entire two year data collection period, data of interest were selected using the following critera: direction range $133^o \pm 15^o$ or $313^o \pm 15^o$, Monin-Obukhov length absolute value > 1000 m and periods that satisfy this criteria for $\geq$ 30 min. These angles were chosen as this study is interested only in flow that is perpendicular to the canyon. The averaging period of at least 30 min is required to ensure statistical convergence and was tested using some sample data sets (see Appendix B). Finally, the Monin-Obukhov length

criterion was chosen to ensure near-neutral stability during the data period. Using these criteria 17 periods and 21 periods were found for the 133$^\mathrm{o}$ and 313$^\mathrm{o}$ wind directions, respectively.

3.2.2　Wind tunnel experiment

The wind tunnel experiment was conducted in the low-speed, suck-down boundary layer wind tunnel in the LHEEA at École Centrale de Nantes (Figure 27). Details on the wind tunnel set-up, including turbulence generation and apparatus details, can be found in Section 2.2. Flow measurements were conducted using stereoscopic PIV to record all three components of velocity (Figure 27). The upstream roughness used in the current case consisted of 50 mm cubes arranged in a staggered array with λ_p = 25%. The flow configuration investigated used a canyon of W/h = 0.7 and L/h = 4.6 to match the field experiment aspect ratio. The wind tunnel boundary layer was scaled using ESDU and was found to best match a suburban terrain with z_o = 0.2 m at a scale of 1:200 (Figure 28) [6, 7]. Since the two approach flow terrain are different in the field site this wind tunnel boundary layer is a reasonable compromise to represent both terrain types.

Figure 25 Field canyon and surrounding landscape with canyon obstacles highlighted using green arrow (Google Maps)
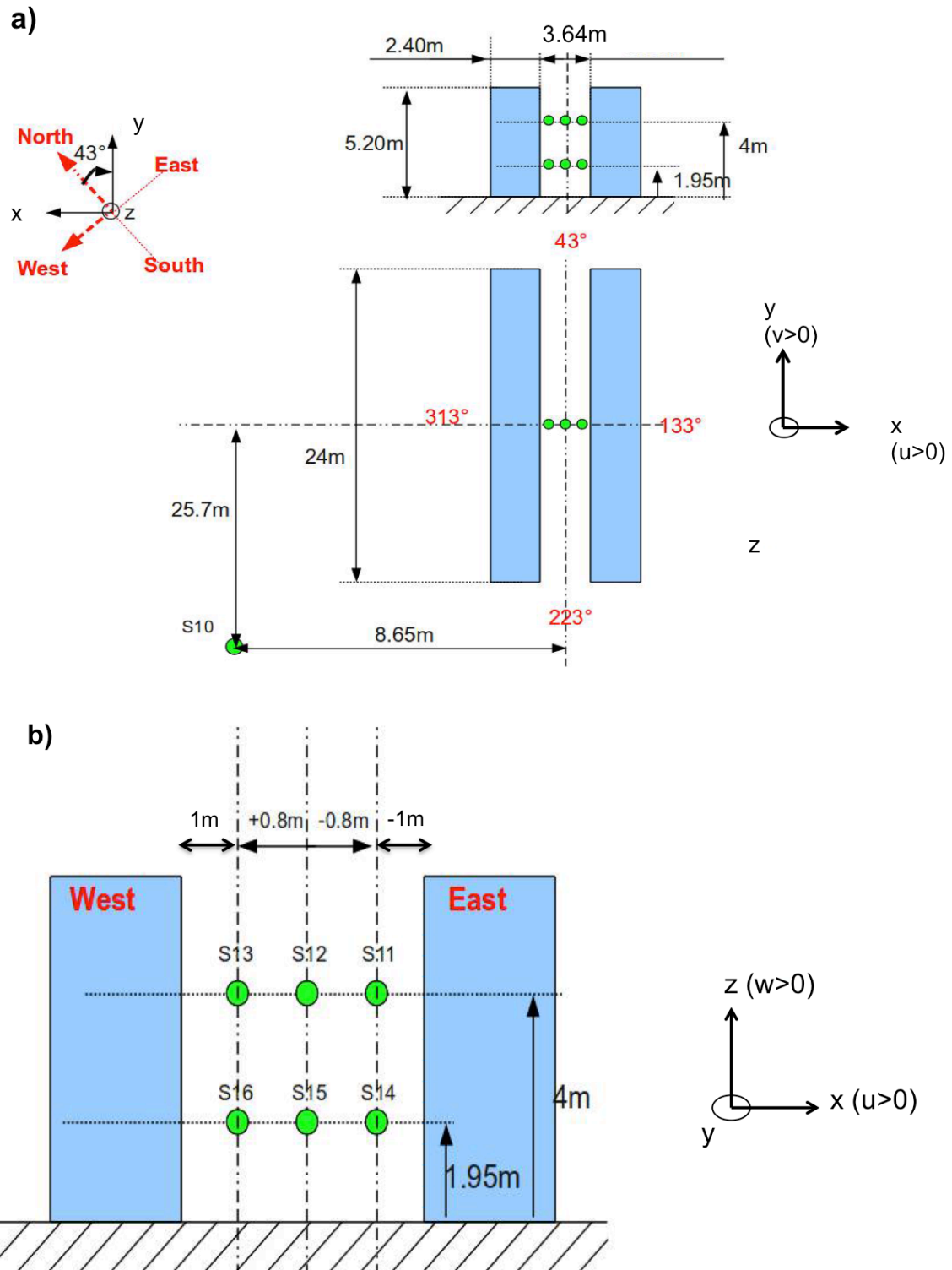
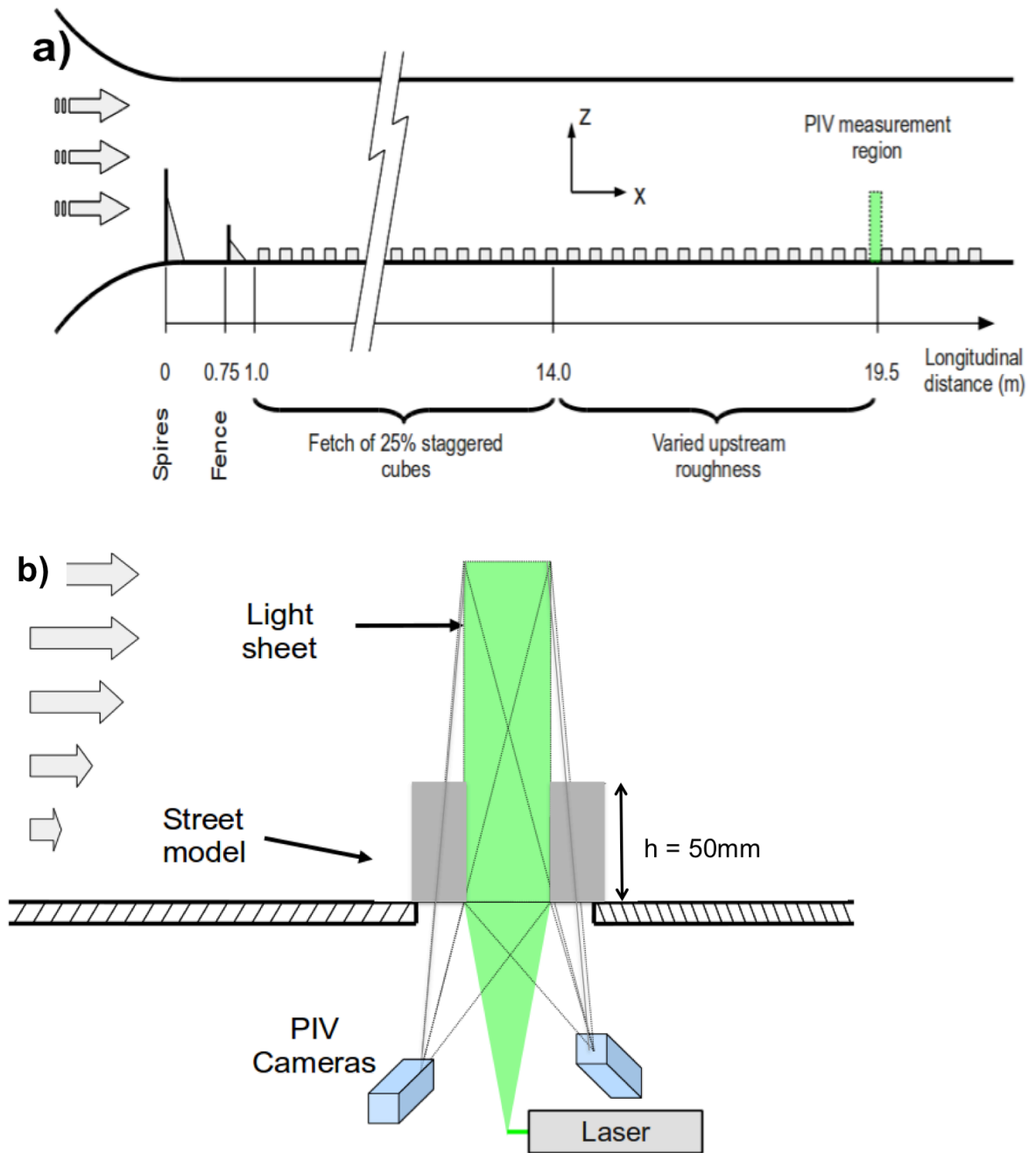**Figure 26** a) Side and aerial view of canyon and mast; b) side view of canyon with sonic anemometer spacing

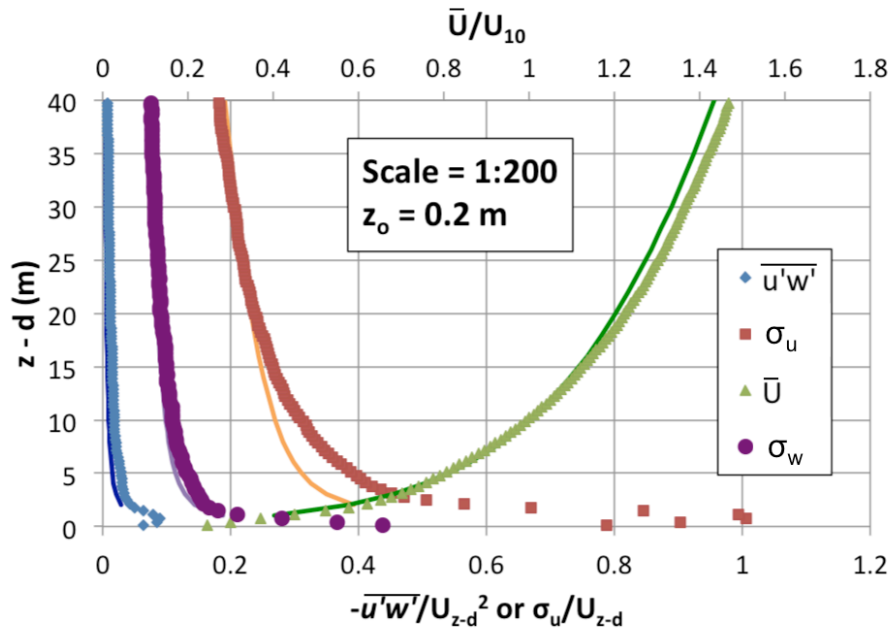**Figure 27**   a) Wind tunnel set-up; b) stereoscopic PIV set-up

Figure 28   Wind tunnel scaling with ESDU profiles [6, 7]

3.3   Data selection and processing

As the data collection periods that were saved in continuous intervals of 15 minutes ran over the course of two years (2011-12), a data selection criteria was determined to include only those periods appropriate for comparison with the wind tunnel experiment. To understand the fundamental physics involved in canyon ventilation we are interested only in flow that is perpendicular to the canyon. Thus, 15 minute periods where the flow direction was $133^{o} \pm 15^{o}$ and $313^{o} \pm 15^{o}$ were selected. This allowed sufficient periods for averaging of data with ambient flow conditions perpendicular to the canyon. The Monin-Obukhov length was required to be a minimum of 1000 m to ensure neutral stability [3]. For a sufficient data set to achieve reliable averages these criteria had to be satisfied for a period of at least 30 minutes.

Once appropriate data periods were collected the data were processed to determine characteristic statistical averages. The first stage of the processing is to convert the S10 data to the coordinate system of the canyon over the period. The following trigonometric equations yield the streamwise (U) and spanwise (V) velocity.

Equation 7   Trigonometric equation for streamwise velocity

$$U = U_W \cos(\alpha) + U_N \sin(\alpha)$$

Equation 8   Trigonometric equation for spanwise velocity

$$V = U_N \cos(\alpha) - U_W \sin(\alpha)$$

where α is the angle between the North axis and the axis perpendicular to the canyon. Since the sonic anemometers within the canyon were already aligned with the canyon axis no direction correction was required.

Since this study is concerned with the turbulence characteristics of the canyon flow care must be taken to remove the low frequency synoptic-scale fluctuations caused by the natural variability of the atmospheric boundary layer (ABL). Liu et al. [18] outline a method that can be used to filter out the synoptic-scale fluctuations. The filter time scale is chosen as the spectral gap between the low frequency and the higher, turbulent, frequencies and is usually on the order of 150-500s [18]. This time scale is then used in a low-pass filter to leave only those frequencies within the synoptic-scale. Synoptic-scale winds are large-scale weather systems ranging from several hundred to several thousand kilometres in length and do not contribute to the intermittent turbulence associated with ventilation events [3]. These signals are then subtracted from the raw signals to leave only the turbulence fluctuations required. This procedure is applied to both the mast (S10) and canyon sonic anemometers. When applied to the mast (S10) and canyon sonic anemometers (Figure 29) it is evident that the low frequency synoptic-scale winds are not captured. This is a result of the shorter time intervals, as low as 30 minutes, used for the spectra calculation. Thus, no filtering was applied to remove the synoptic-scale winds.
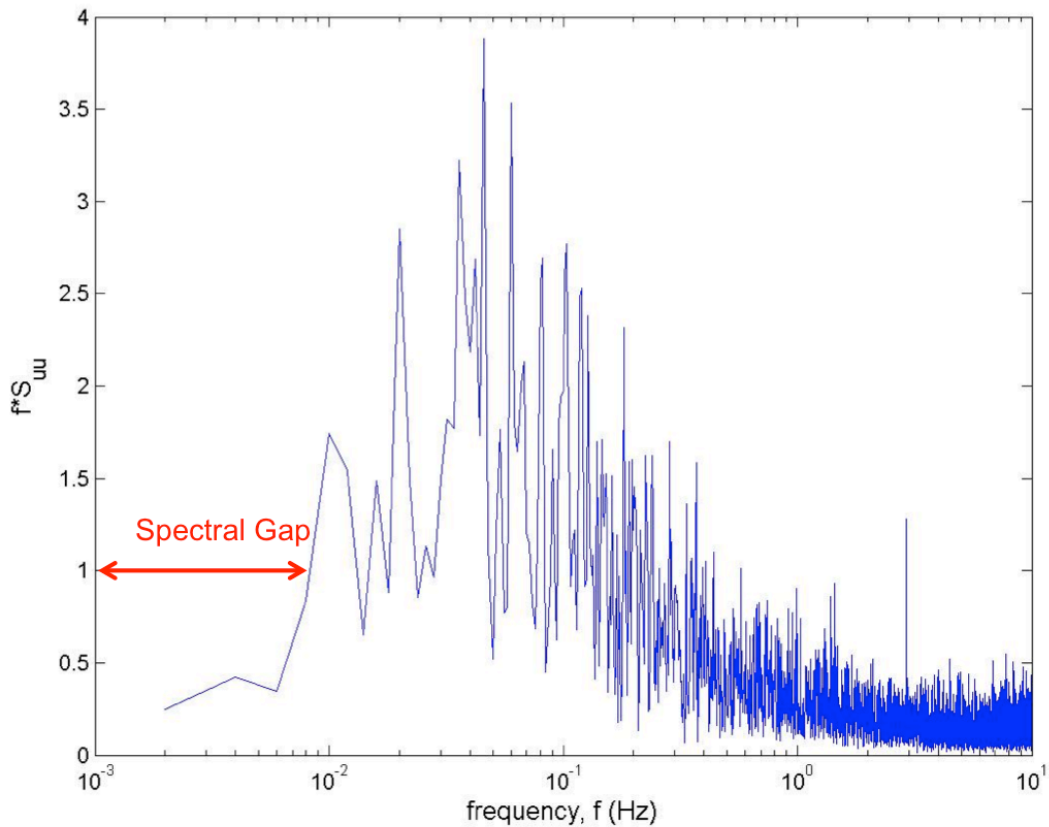
Figure 29 Example of turbulence spectra for one 30 minute period showing spectral gap

After processing a test for stationarity is used to determine whether the statistical parameters vary in time [17]. The test used in this case utilizes the covariance and compares the covariance for the averaging period and for short intervals within this period. The averaging period of 30 minutes was split into M = 6 intervals of 5 minutes. The covariance is then calculated using Equation 9 and Equation 10 where N is the number of measuring points of the short interval (N = 3000).

Equation 9 Stationarity covariance

$$(\overline{x'w'})_i = \frac{1}{1-N}\left[\sum_j x_j w_j - \frac{1}{N}\sum_j x_j \sum_j w_j\right]$$

Equation 10   Stationarity mean covariance

$$\overline{x'w'} = \frac{1}{M} \sum_i \overline{(x'w')}_i$$

This value is then compared to the covariance of the entire averaging period given by Equation 11.

Equation 11   Stationarity entire averaging period covariance

$$(\overline{x'w'})_o = \frac{1}{M(N-1)} \left[\sum_i \sum_j (x_j w_j)_i - \frac{1}{MN} \sum_i \left(\sum_j x_j \sum_j w_j \right)_i \right]$$

If the difference between the covariances, defined by Equation 12, is less than 30% then the averaging period is deemed stationary. Any periods that fail this test are removed and not considered in the ensemble averaging.

Equation 12   Stationarity covariance magnitude difference

$$RN_{cov} = \left| \frac{(\overline{x'w'}) - (\overline{x'w'})_o}{(\overline{x'w'})_o} \right|$$

Within the field the varying ambient wind conditions make comparison with controlled wind tunnel simulations difficult. In particular, a strong along-canyon flow is observed in the field (up to 67% of the streamwise velocity measured at the mast for the 133° approach direction). To reduce the influence of this along-canyon wind on the mean statistics a new criterion is applied to the processed data. If the along canyon wind averaged across the canyon is greater than 10% of the mean streamwise velocity at the mast for the corresponding period then that period is removed from the ensemble averaging. Finally, the mean velocity vectors within the canyon were examined to ensure that the mean flow is consistent with a mean centre vortex as seen in the wind tunnel (Figure 30). The reference velocity (U_{ref}) was used to scale the in canyon velocities where U_{ref} is the velocity taken at the mast ($x/h = 1.7$, $y/h = 5$ and $z/h = 1.92$) and $x/W = -0.52$ and $z/h = 1.9$ for the field and wind tunnel data, respectively. Using this selection criteria

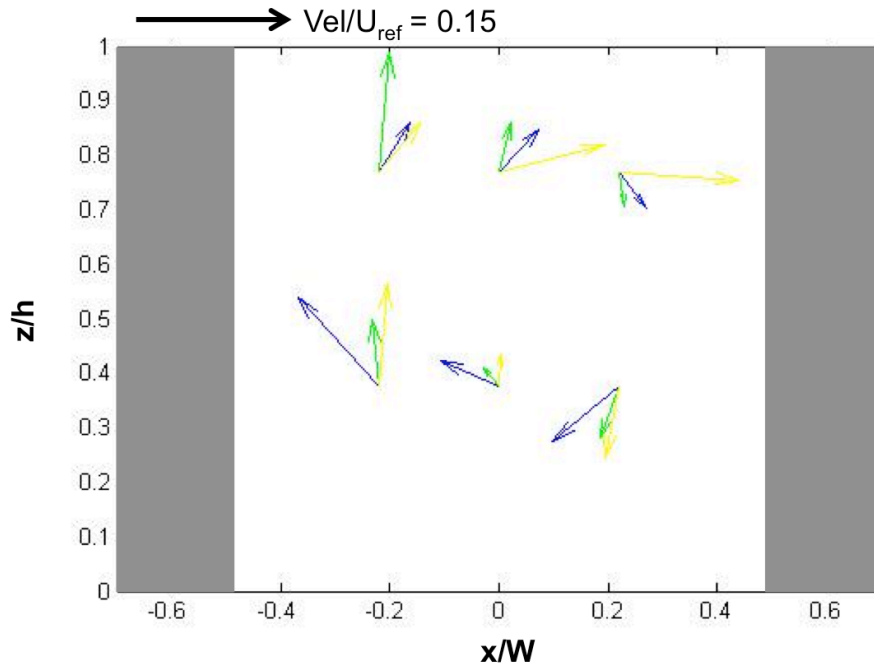12 and 5 instances of 30 minute periods were obtained for the 133° and 313° approach directions, respectively.

Figure 30   Example of mean velocity vectors using one 30-min period of flow within the canyon for 133° approach direction (blue), 313° approach direction (green) and wind tunnel PIV (yellow)

3.4   Results and discussion

3.4.1   Statistical averaging method

All of the canyon flow statistics were calculated using the raw data processed as outlined above. In order to average statistics from various periods with varying ambient conditions the statistics were averaged using the following procedure.

Let $\bar{k}$ be the time average of any quantity k(t) over a 30 min period and $\langle \bar{k} \rangle$ be the ensemble average of $\bar{k}$ obtained over all the periods. For each period an average streamwise wind velocity U_{mast} and friction velocity u_* is defined from the S10 mast data. The time averaged $\bar{k}$ for each period is then normalized by either U_{mast} or u_* depending on the quantity for the corresponding period $\dfrac{\bar{k}}{U_{mast} \; or \; u_*}$. Finally, the normalized statistics

from each period are ensemble averaged $\langle \frac{\bar{k}}{U_{mast}\ or\ u_*} \rangle$. This averaging was used for all of the statistics and periods deemed acceptable using the criteria outlined above. However, the statistics were not averaged between the two different approach flow directions, 133° and 313°, perpendicular to the canyon due to the varying terrain from wooded with westerly winds (approach flow from 313°) to open fields and isolated buildings with easterly winds (approach flow from 133°).

3.4.2   Scaling of the approaching boundary layers

The terrain of the site varies in each direction perpendicular to the canyon. To determine the terrain characteristics of the site in each direction a method outlined by Graf et al. [8] was employed. Using this method the d values for the approach flow directions 133° and 313° were found to be approximately 2.4 m and 5 m, respectively. The corresponding z_o values were determined to be 0.46 m and 0.68 m for 133° and 313°, respectively. The displacement height and roughness length can also be approximated based on 70% of the obstacle height and the terrain using ESDU [7]. Using this approximation the displacement height for 133° and 313° should be between 0-2 m and 5-7 m, respectively. In addition, from the terrain z_o is expected to be between 0.03-0.1 m and 0.3 m for the 133° and 313° approach flow directions, respectively. It is therefore concluded that the method employed by Graf et al. [8] does not provide reliable estimates for these parameters. This is, perhaps, a result of the location and height of the mast. The mast is located upstream of the canyon for the 313° approach flow direction, but downstream of the canyon for the 133° approach flow direction which may result in influences from the canyon as well as from the upstream isolated building. Furthermore, the height of the mast is 10 m above ground, which is at the height of the trees, 7-10 m, in the 313° approach flow direction. The terrain parameters estimated using ESDU will, therefore, be used.

With an estimate of terrain parameters a comparison with ESDU profiles is possible. A z_o = 0.3 m has been used for the comparisons with both upstream terrain. This roughness length was chosen, as it matches the roughness length of the wooded terrain, which is approximately uniform, whereas in the direction of the field terrain there is an isolated

building close to the canyon. As well, the mast used to record boundary layer characteristics is located upstream of the canyon in the wooded terrain direction and downstream in the field terrain direction. Finally, this roughness length was chosen as it resulted in the best agreement with the ESDU profiles for both terrains and is similar to the value obtained from the wind tunnel study (z_o = 0.2 m). The streamwise turbulence spectra is shown with the corresponding ESDU profile for z_o = 0.3 m and the wind tunnel results (Figure 31) [6, 7]. The spectra were calculated for each continuous time period of data by a fast Fourier transform (FFT) with each of these periods being separated into blocks of length, FFT = 12^{12} with 50% overlap. The frequency axis was normalized using the mean streamwise velocity at the mast and the streamwise integral length scale. The integral length scale was calculated by first finding the integral time scale using the auto-correlation of the streamwise velocity at the mast and then using Taylor's Hypothesis of frozen turbulence to determine the integral length scale. The spectra for both approach directions result in good agreement, less than 25% difference, with ESDU and the wind tunnel study. Figure 32 shows the ensemble-averaged turbulence statistics for each direction and the corresponding ESDU profile for a suburban terrain with z_o = 0.3 m. As well, d values were selected based on which value from the range provided by ESDU resulted in the best agreement with the ESDU profiles. The resulting d values are 2 m and 7 m for the 133° and 313° approach flow directions, respectively. The figures show that although the spanwise turbulence intensity is over-estimated by approximately 20%, the remaining profiles match well with ESDU. The wind tunnel study has also been scaled with ESDU and is shown in Figure 28 [6, 7]. In the case of the wind tunnel study the streamwise turbulence intensity is over-estimated below a full-scale equivalent height of z - d = 15m by up to approximately 25% compared with ESDU. These results show that both the wind tunnel and field data scale well with ESDU and have similar terrain characteristics.
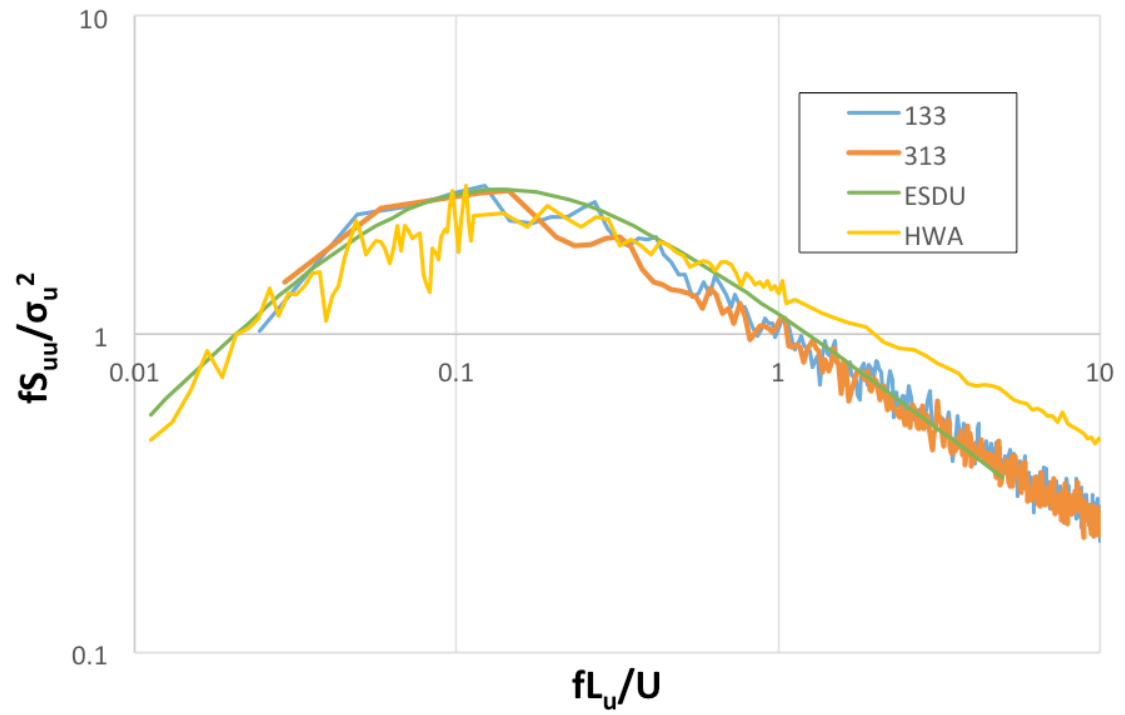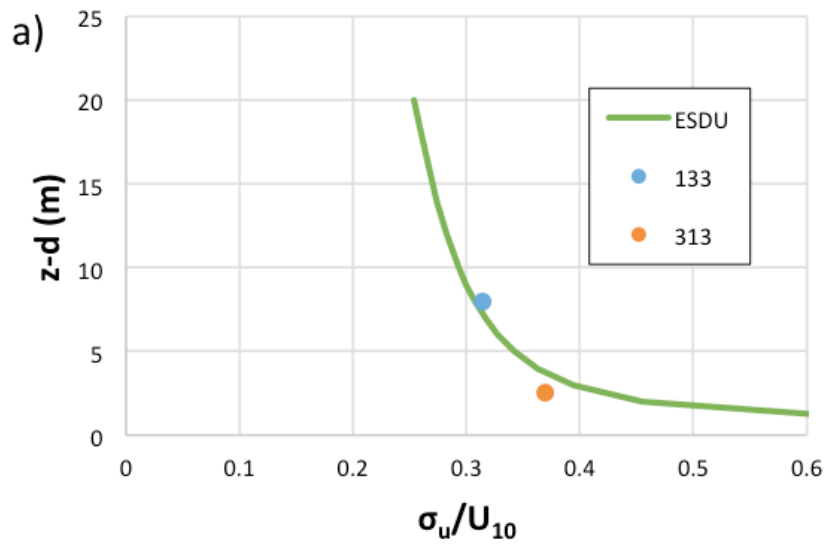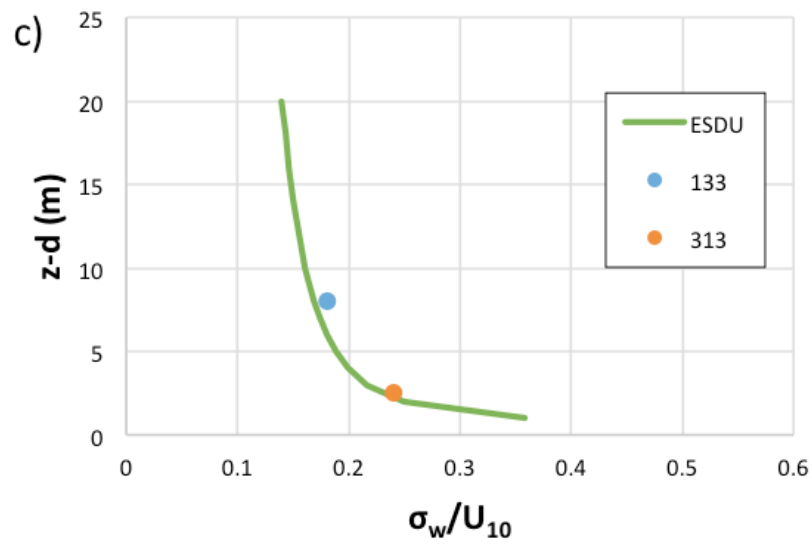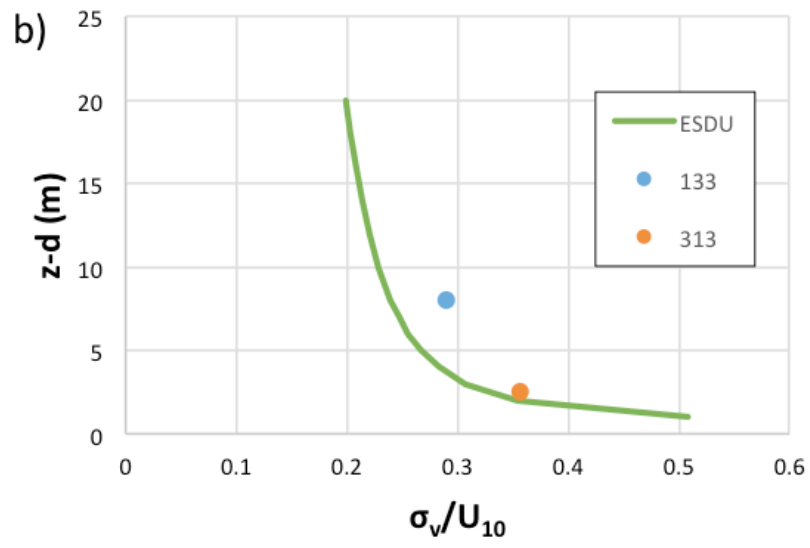
Figure 31 Streamwise turbulence spectra of the field data compared with ESDU [6, 7] and wind tunnel HWA data
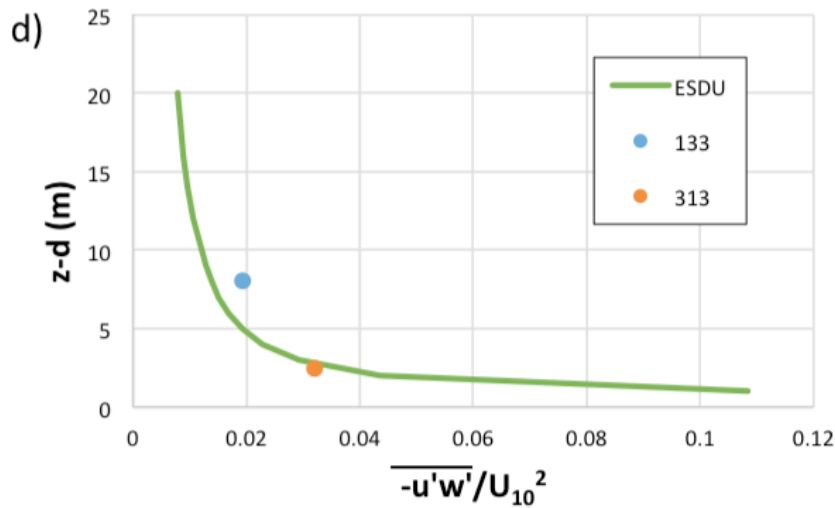
b)

c)

Figure 32   ESDU profile with field data for each approach direction a) streamwise turbulence intensity; b) spanwise turbulence intensity; c) vertical turbulence intensity; d) Reynolds shear stress [6, 7]

3.4.3   Comparison between field and wind tunnel results

The following section includes an analysis to determine whether for low wind speeds the turbulence statistics are independent of Reynolds number, followed by a comparison of the mean velocity and turbulence statistics of the field and wind tunnel data.

3.4.3.1   Influence of Reynolds number

Before comparison with the wind tunnel model, the effect of ambient streamwise velocity, where streamwise is perpendicular to the canyon axis, on the turbulence intensities within the canyon is examined. Relatively low wind speeds are experienced at the site, which may influence the canyon flow. To determine whether the normalized turbulence intensities are independent of Reynolds number even at low wind speeds two normalization parameters are investigated, the ambient streamwise velocity and friction velocity, u_*. Using the ambient streamwise velocity the variance, $R^2 = 0.003$, 0.002, 0.002, 0.042 and $R^2 = 0.009$, 0.019, 0.024, 0.002 for the streamwise, spanwise, vertical and shear stress components from the 133° and 313° approach direction, respectively (Figure 33), where a variance of 0 is a perfect fit to the data. Similarly, using friction

velocity for normalization results in coefficients of determination on same order of magnitude, $R^2 = 0.003, 0.009, 0.002, 0.001$ and $R^2 = 0.008, 0.020, 0.028, 0.002$ for the streamwise, spanwise, vertical and shear stress components from the 133° and 313° approach direction, respectively (Figure 34). This demonstrates that the turbulence intensities are independent of Reynolds number when using either of these normalization parameters.
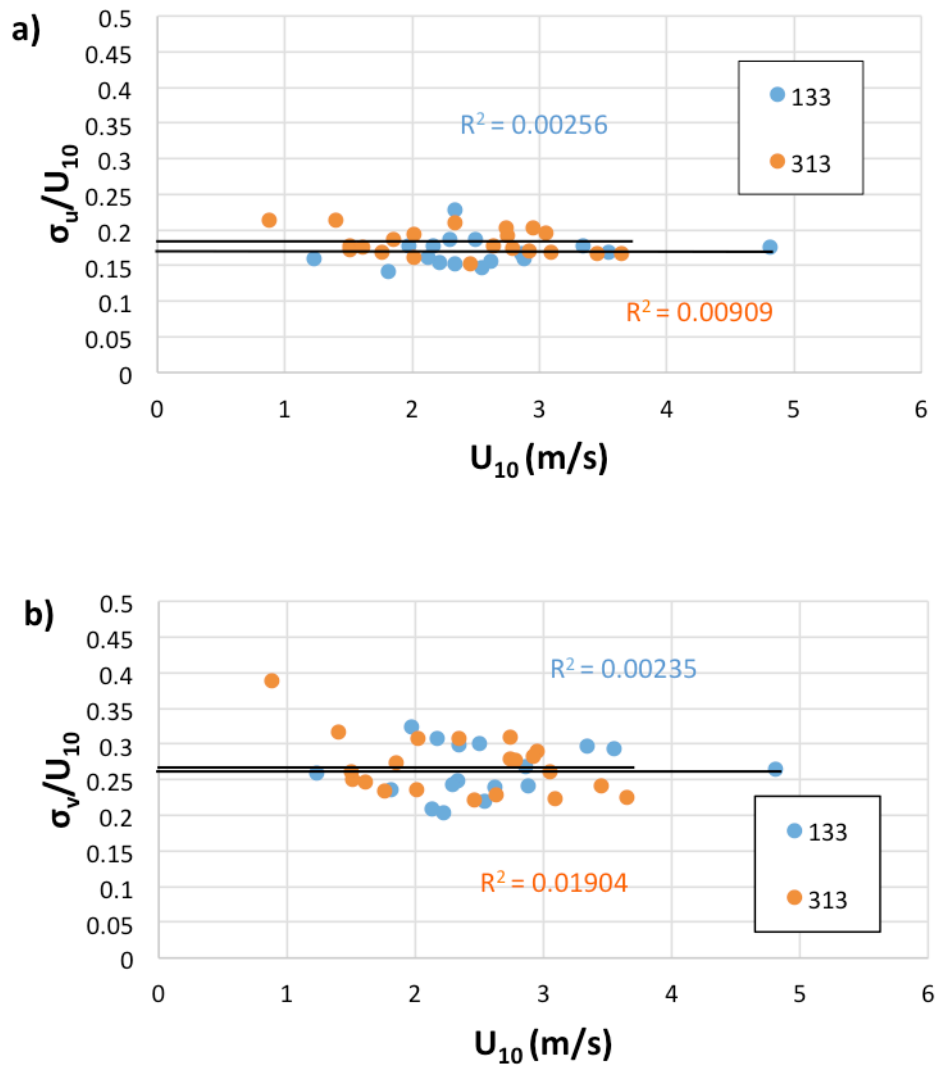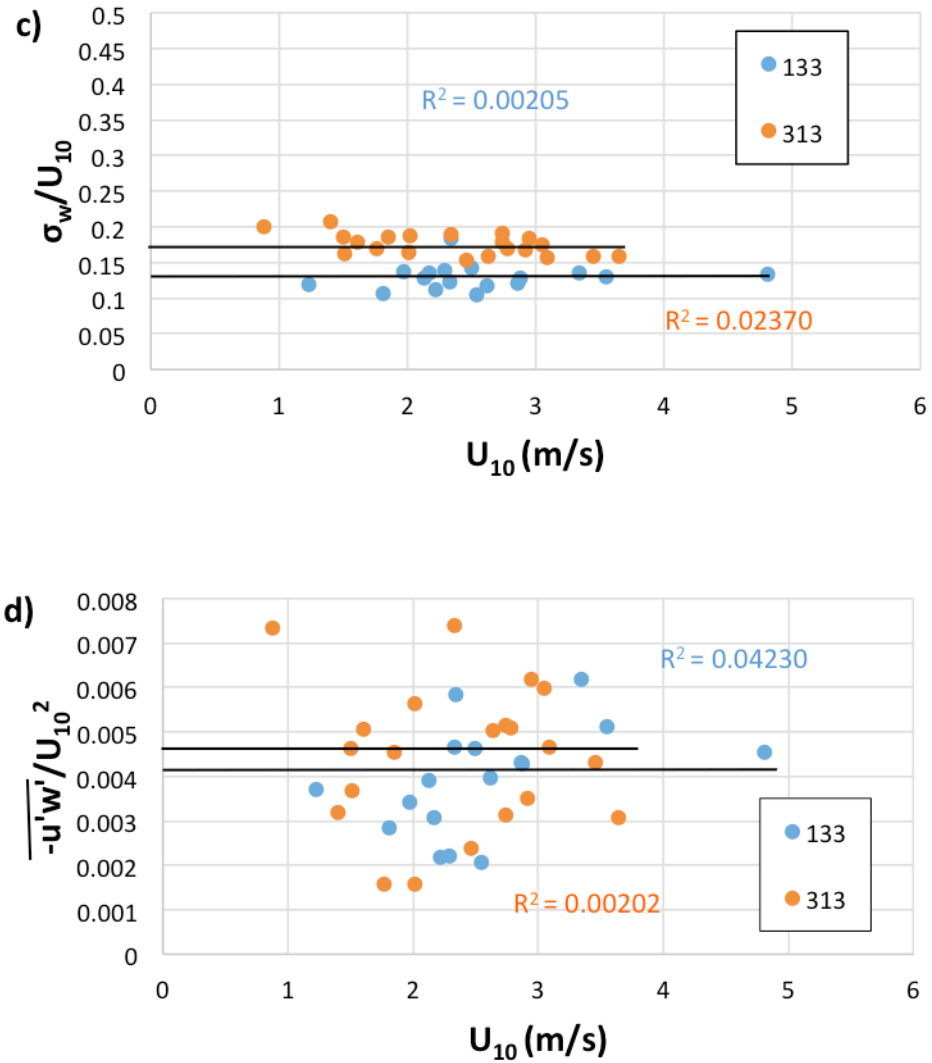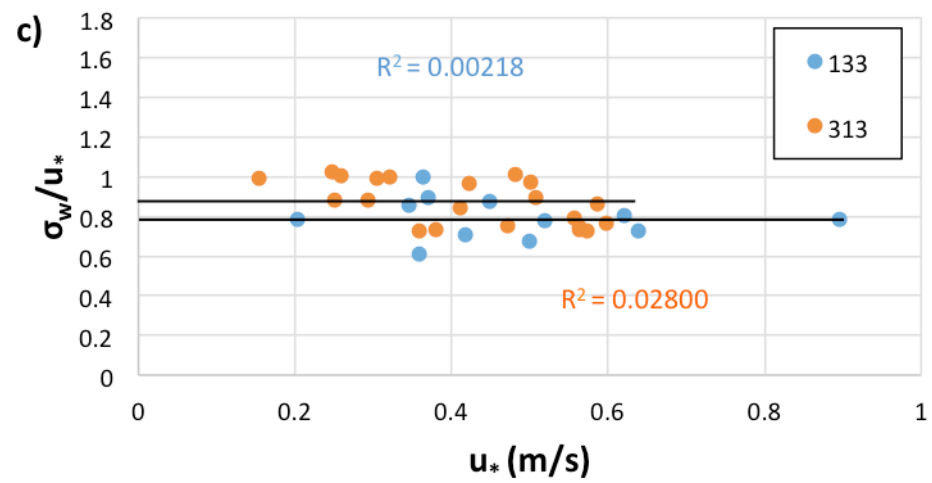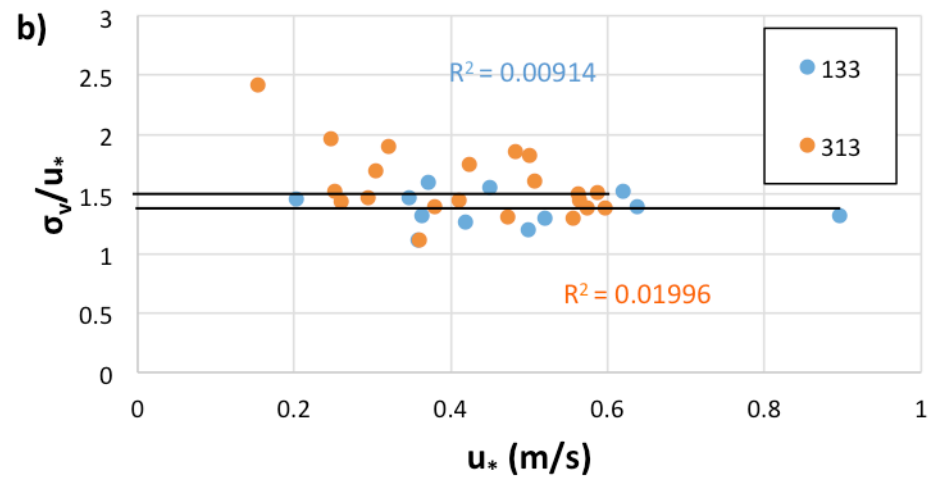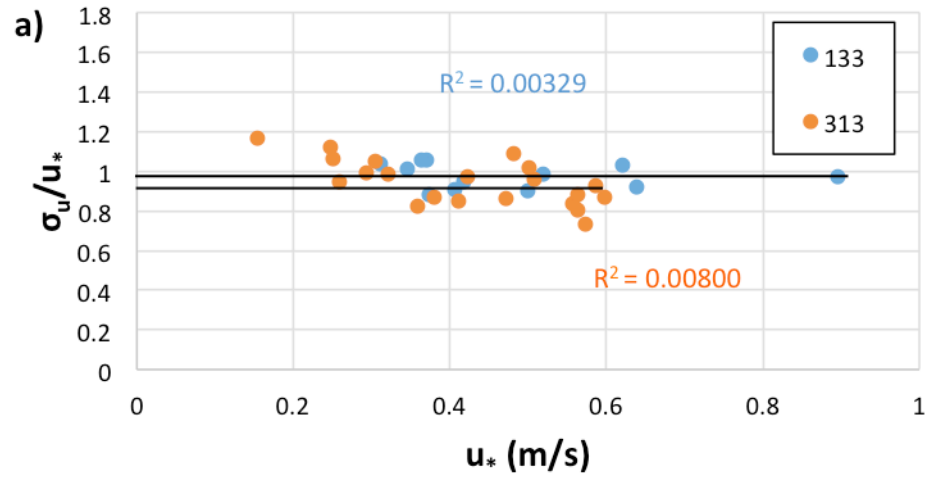
Figure 33 Variation with ambient streamwise mean velocity of a) streamwise; b) spanwise; c) vertical turbulence intensities; d) Reynolds shear stress normalized by ambient streamwise velocity, U_{10}, showing example using S12 ($x/W = 0$ and $z/h = 0.77$)
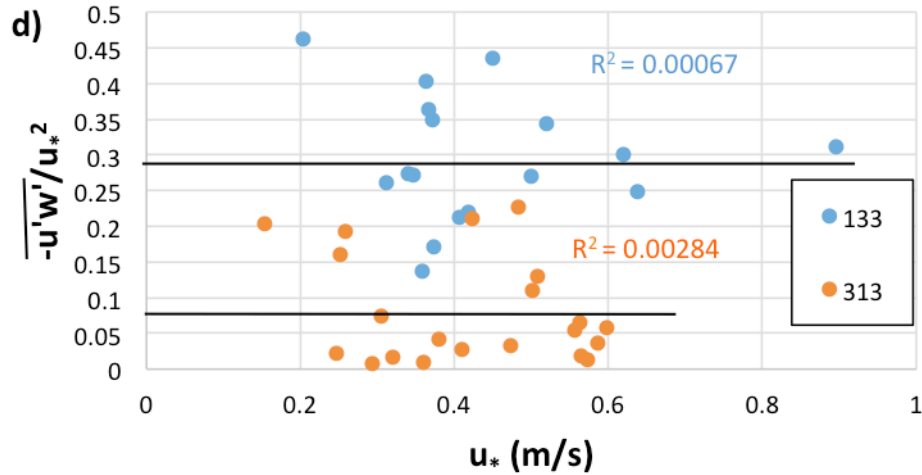
Figure 34 Variation with ambient friction velocity of a) streamwise; b) spanwise; c) vertical turbulence intensities; d) Reynolds shear stress normalized by friction velocity, u_*, showing example using S12 (x/W = 0 and z/h = 0.77)

3.4.3.2 Mean turbulence statistics

The canyon statistics from the field data are compared to the profiles obtained from the wind tunnel PIV results. The mean velocities are normalized using the mean streamwise velocity measured at the mast and the turbulence intensities are normalized by friction velocity estimated as $u_* = \sqrt{\overline{u'w'}}$ at the mast. Figure 35 shows the profiles along the centre axis of the canyon. The error bars represent the maximum and minimum mean values in the data set. There is consistency between the wind tunnel and field data for the streamwise velocity, which shows reversed flow in both cases, whilst the vertical turbulence intensity and shear stress are also in good agreement, less than 10% and 15% difference, respectively, where percent difference $= \frac{field-WT}{WT} * 100$. The vertical velocity from the PIV is within 5% of the sonic anemometers located at z/h = 0.77, but there is some overestimation, approximately 60%, in the wind tunnel for the remaining sonic anemometers located at z/h = 0.38. There is also some underestimation, approximately 20%, of the streamwise turbulence intensity, σ_u, in the wind tunnel data compared with the field data, but the largest underestimation is present in the spanwise turbulence intensity, σ_v, which shows a discrepancy of approximately 100%. This pattern is also

evident in the upstream and downstream profiles within the canyon (Figure 36, Figure 37). This disparity may be a result of the large inconsistencies, up to a factor of 100, in the mean spanwise velocity between the field and wind tunnel. The field study has a stronger mean spanwise velocity in the centre, upstream and downstream profiles with the upstream profile exhibiting the largest difference, a factor of 100, and the centre exhibiting the smallest difference, a factor of 10. Significant spanwise velocity has been noted in several other studies in the literature as discussed in Section 3.1 [1, 2, 16]. It has previously been attributed to the high-sensitivity of canyon flow to large-scale wind direction changes [5, 16, 31]. In the current study the strong spanwise velocity could also be influenced by the changing wind direction, as exactly perpendicular and constant wind directions are not present in the atmospheric boundary layer.

In general, both approach flow directions result in similar profiles with neither direction resulting in a much better fit with the wind tunnel data. The differences in the profiles between the field and wind tunnel data may be a result of the different approach flow terrain conditions as the field data ranges from $z_o = 0.1$ to 0.3 m whereas the wind tunnel is $z_o = 0.2$ m. However, since this distinction is small it is more likely that these differences are a result of inhomogeneity of the upstream terrain or the variations of the wind direction. As well, the location of the mast and the presence of the isolated building upstream of the canyon from the 133° direction will affect the profiles.

e)

f)
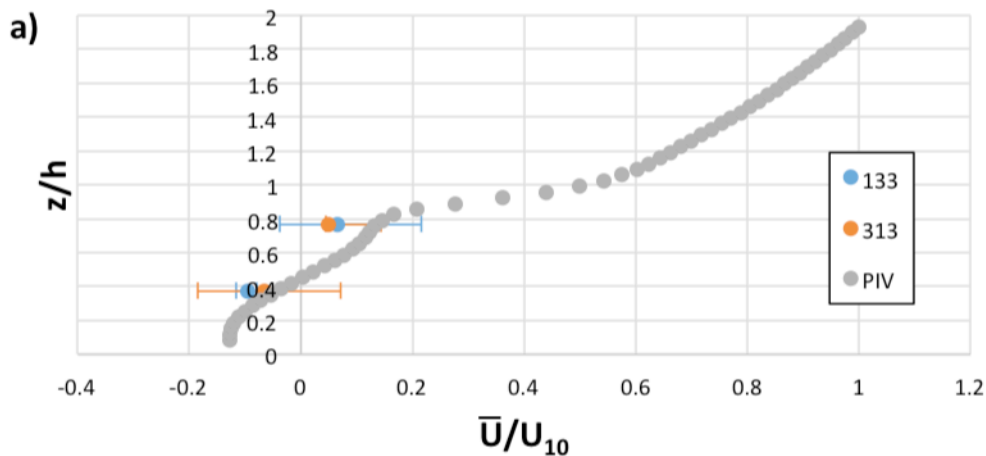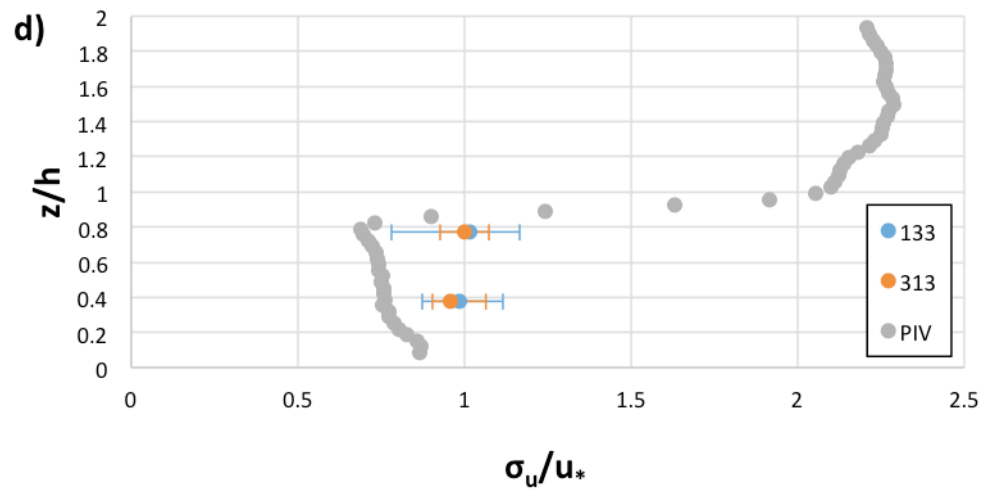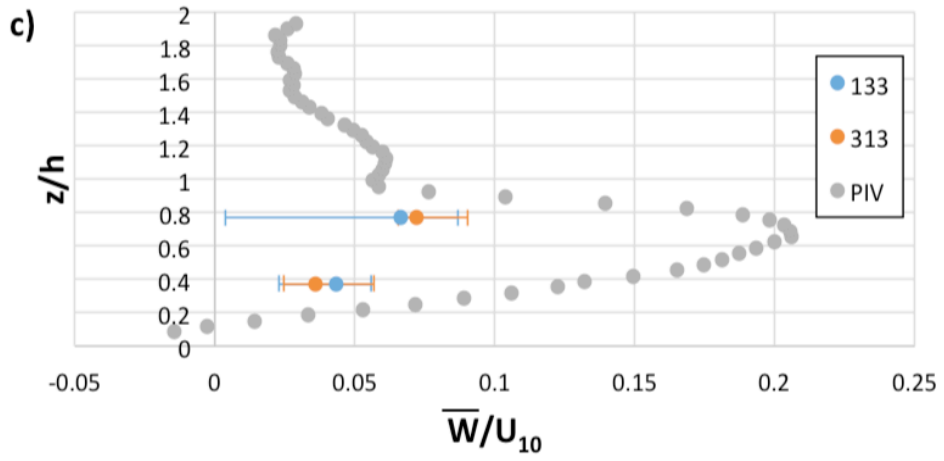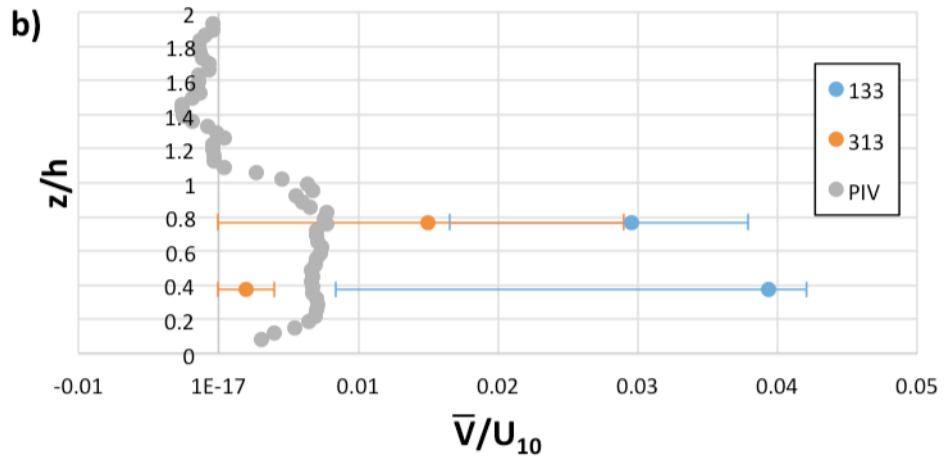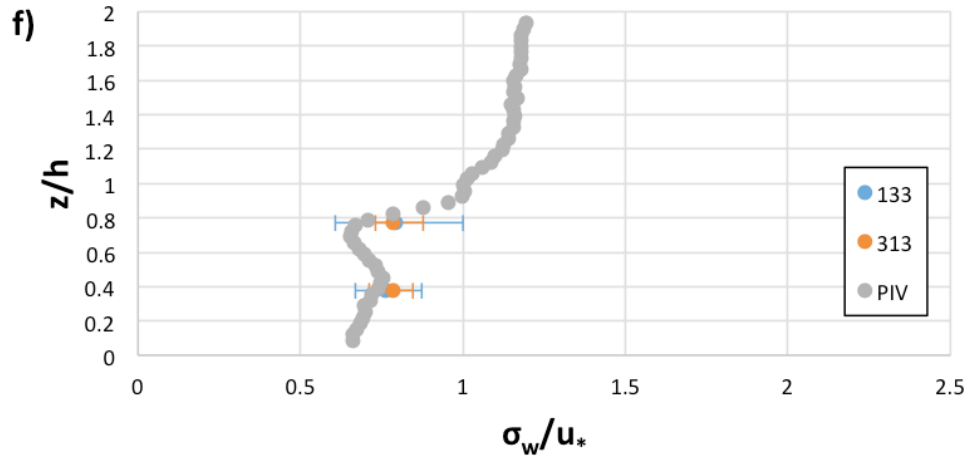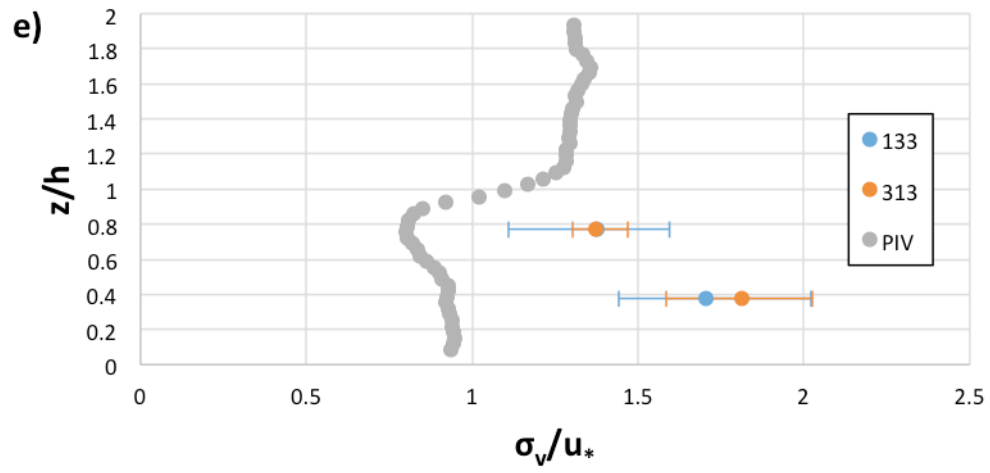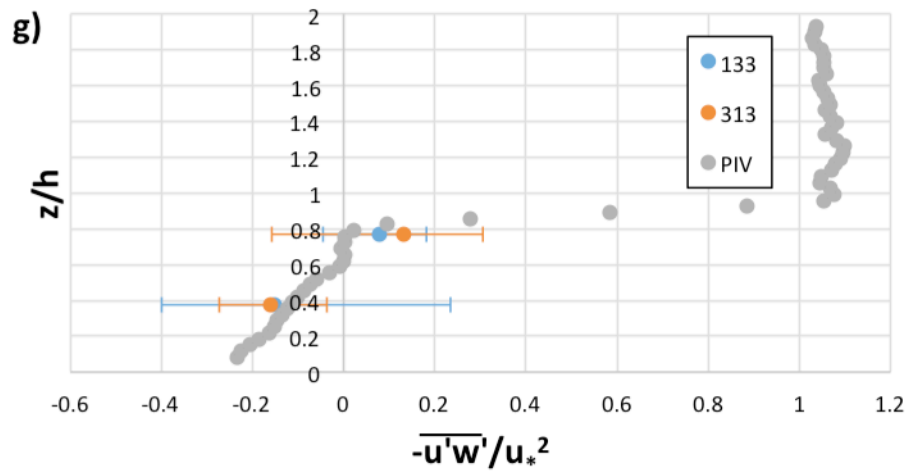
Figure 35   Field data and wind tunnel PIV profiles at centre (y/h = 0) of canyon at x/W = 0 a) streamwise velocity; b) spanwise velocity; c) vertical velocity d) streamwise turbulence intensity; e) spanwise turbulence intensity; f) vertical turbulence intensity; g) Reynolds shear stress
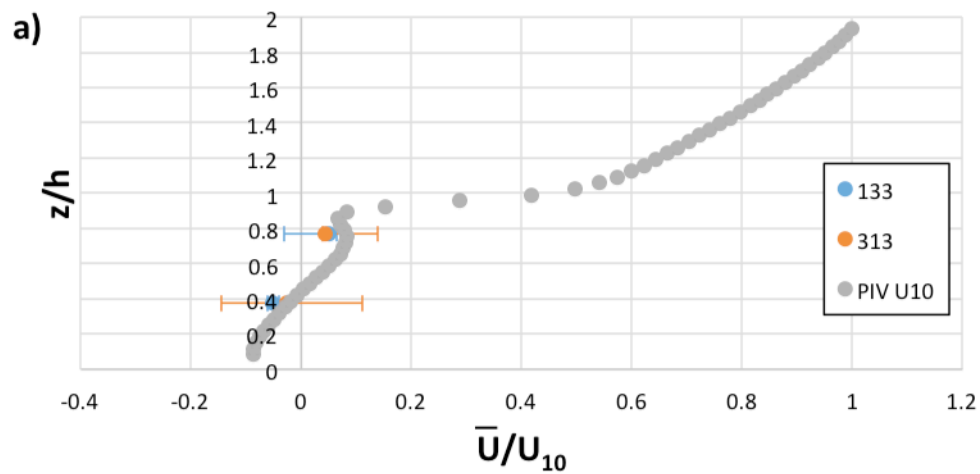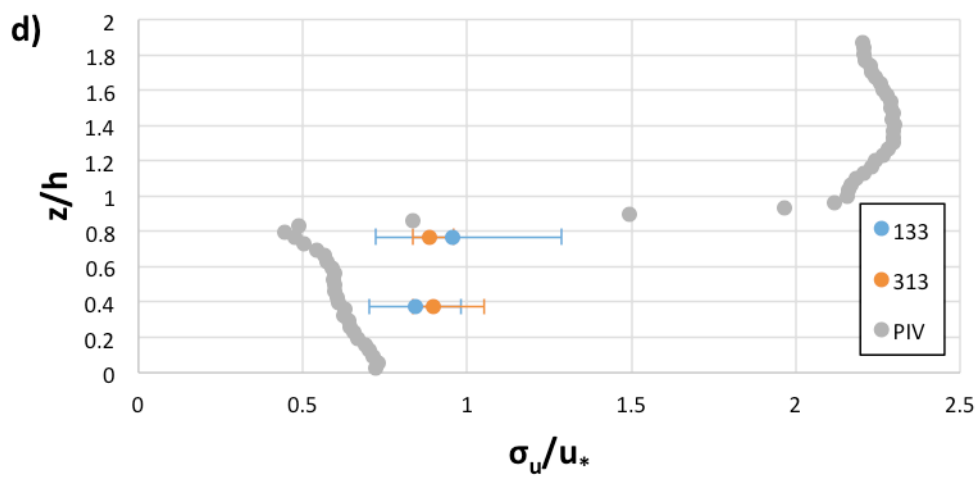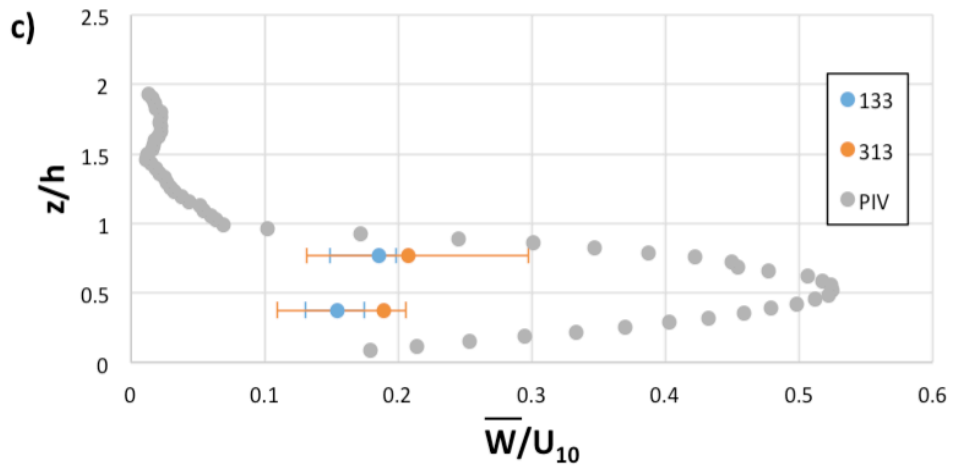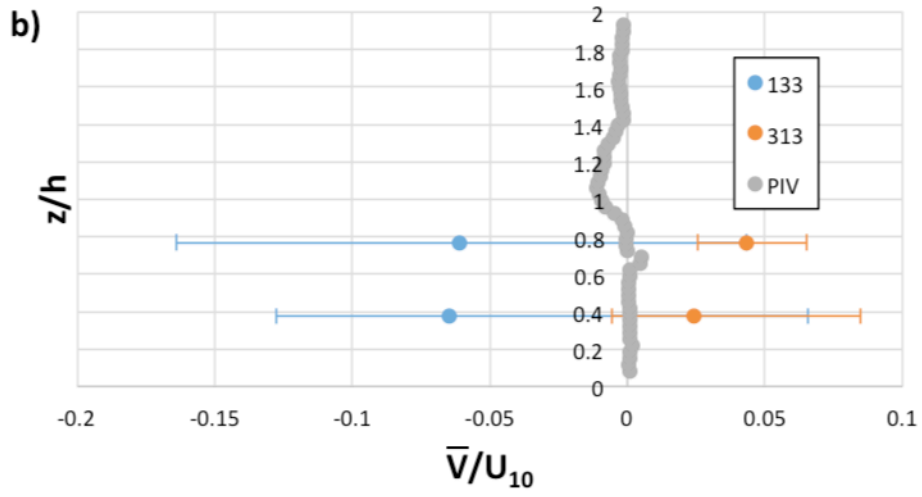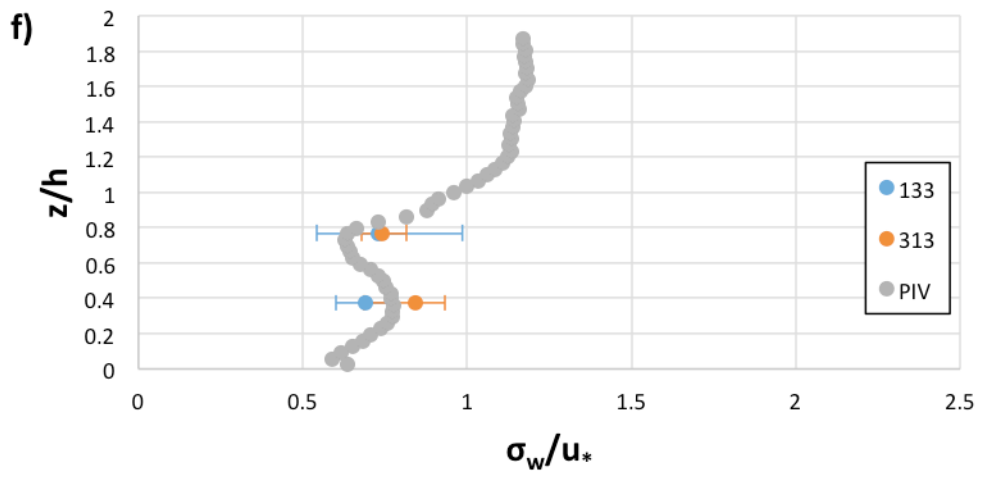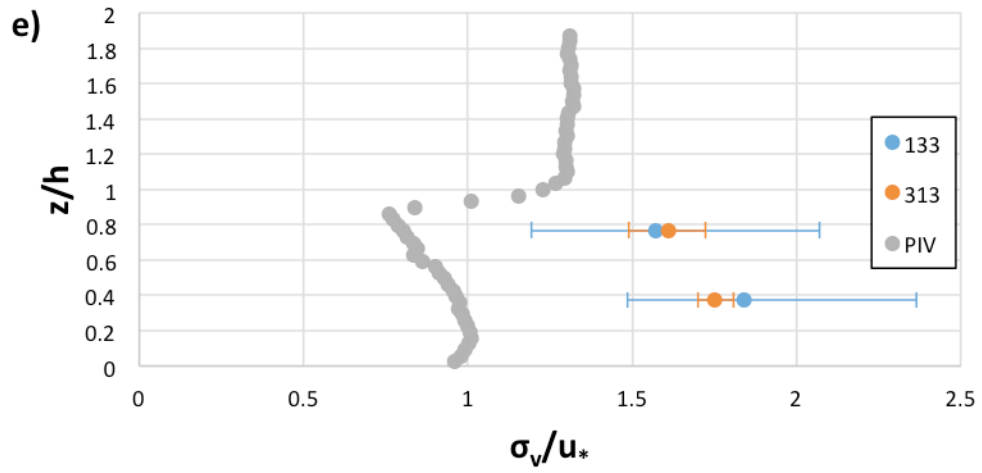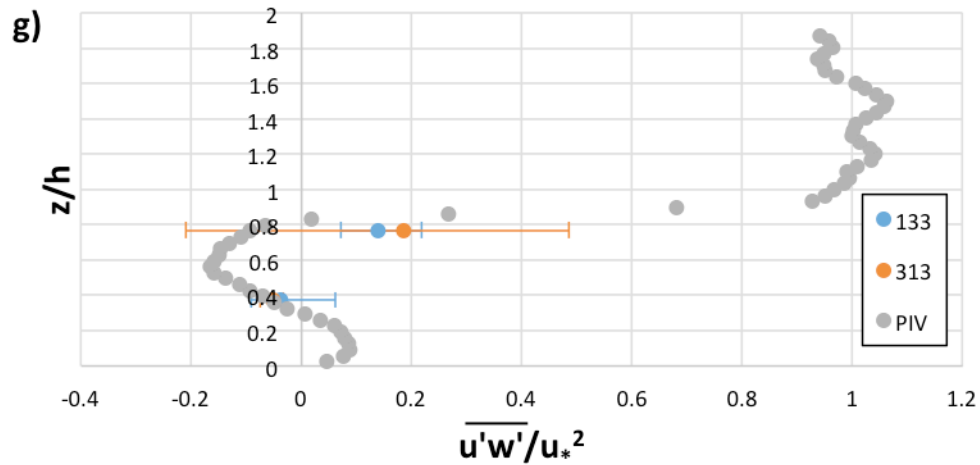
Figure 36 Field data and wind tunnel PIV profiles at centre (y/h = 0) of canyon at x/W = -0.22 a) streamwise velocity; b) spanwise velocity; c) vertical velocity d) streamwise turbulence intensity; e) spanwise turbulence intensity; f) vertical turbulence intensity; g) Reynolds shear stress

b)

c)

d)

e)
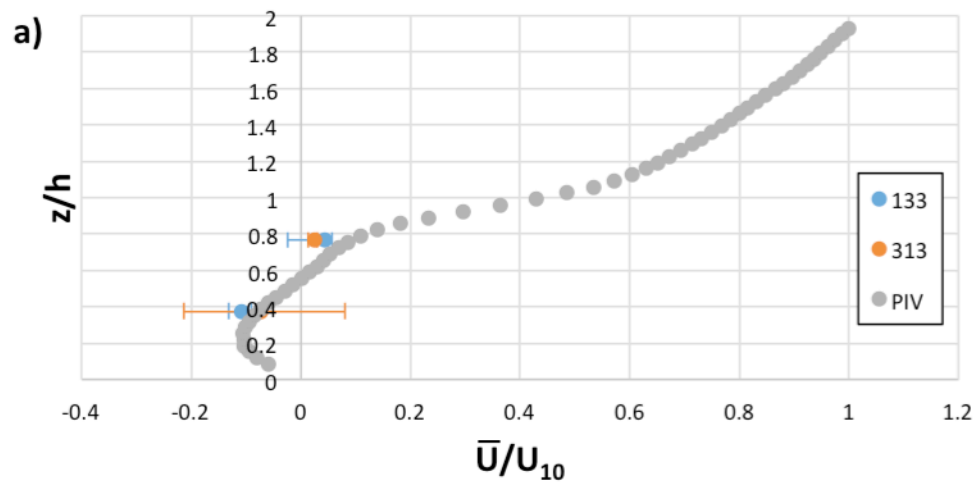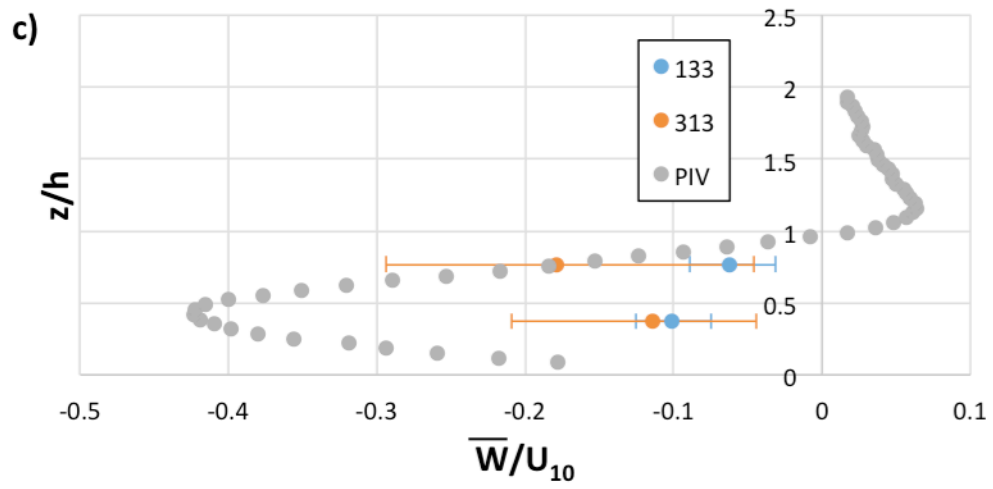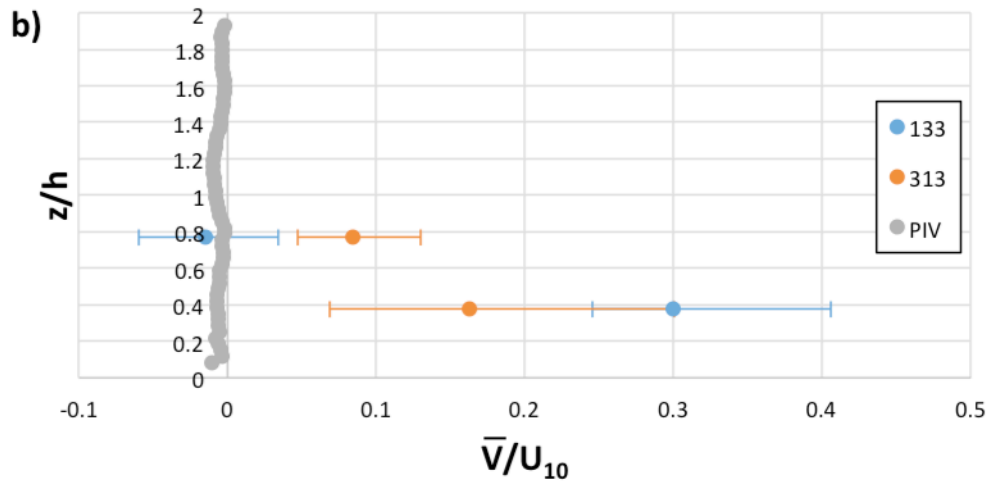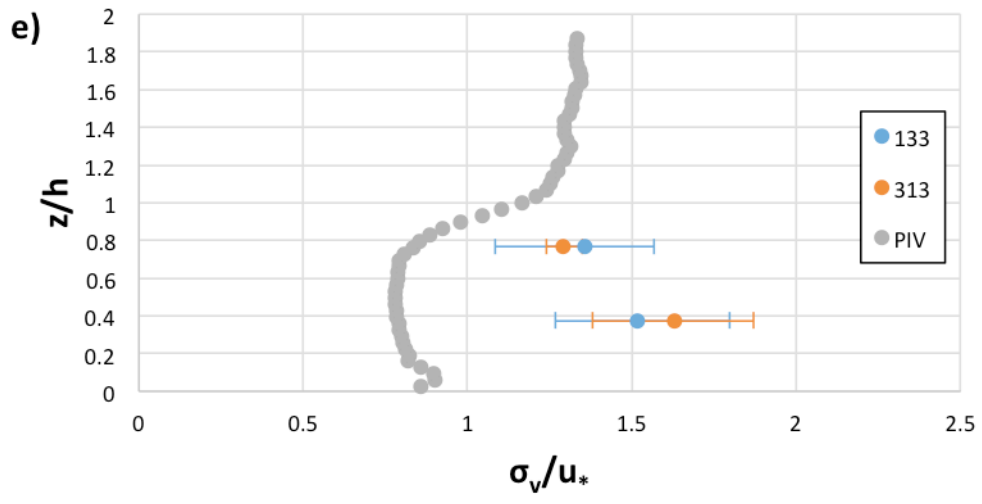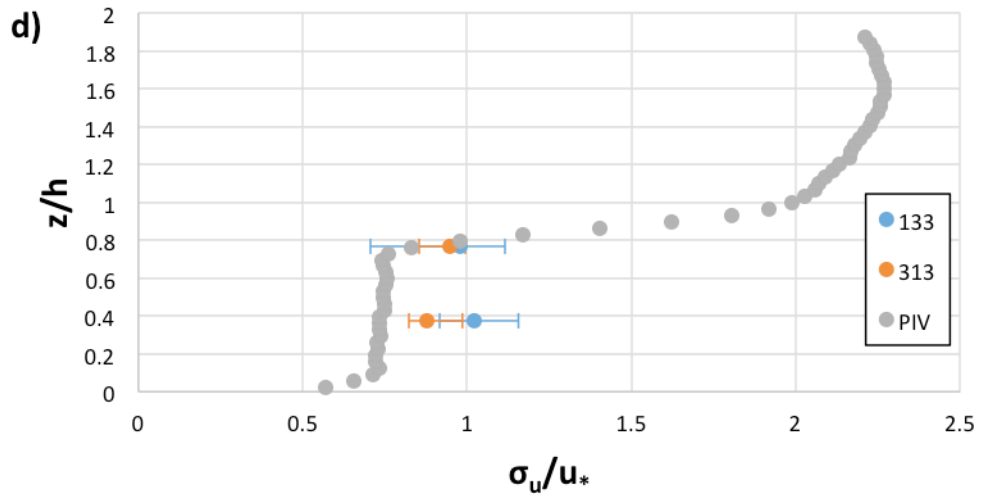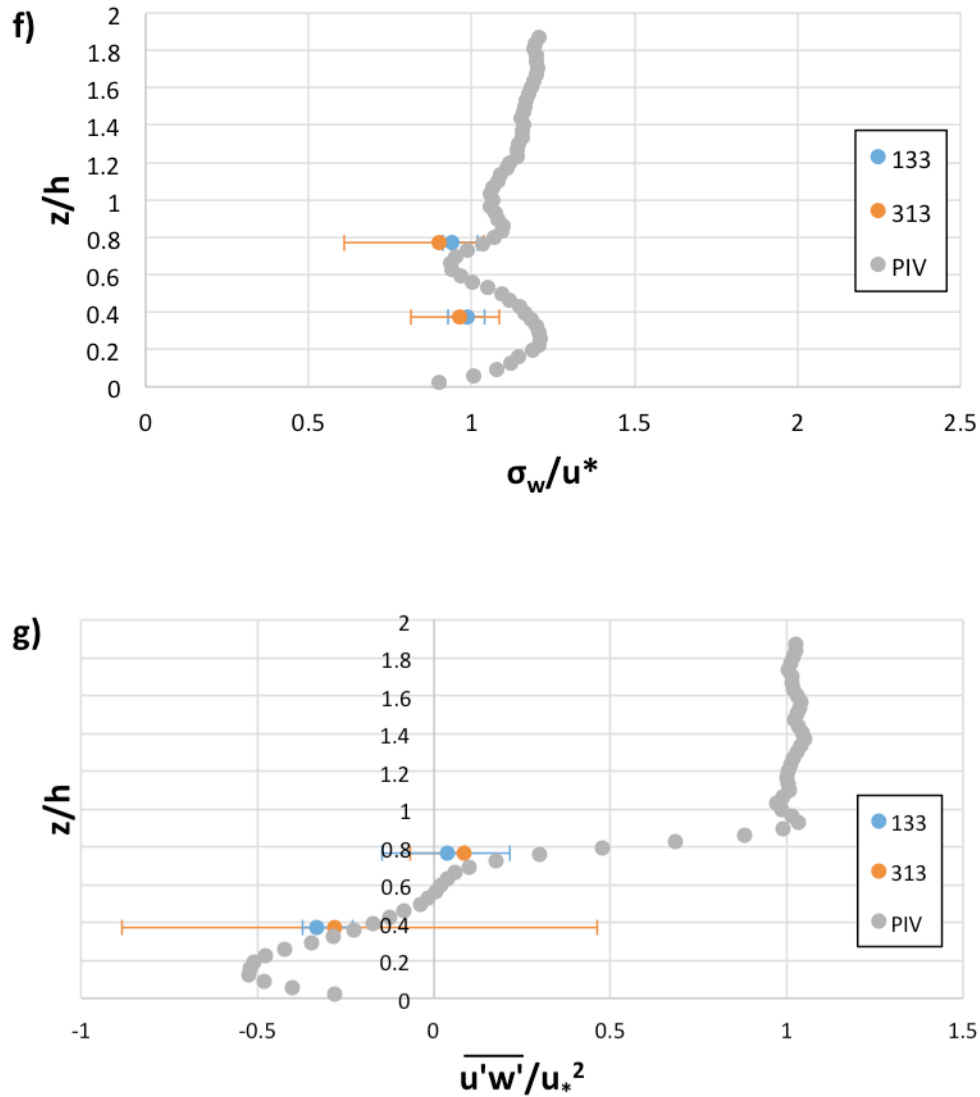
Figure 37 Field data and wind tunnel PIV profiles at centre (y/h = 0) of canyon at x/W = 0.22 a) streamwise velocity; b) spanwise velocity; c) vertical velocity d) streamwise turbulence intensity; e) spanwise turbulence intensity; f) vertical turbulence intensity; g) Reynolds shear stress

3.4.4 Influence of ambient conditions on canyon statistics

The following section is an investigation and discussion of the influence of ambient conditions on the canyon statistics including the influence of the low frequency variations of wind direction.

3.4.4.1 Ambient wind direction

The changing of the approach flow wind direction is thought to have a direct influence on the mean spanwise velocity and turbulence intensity within the canyon [5]. In the present work the influence of the changing wind direction has been investigated by comparing the mean spanwise statistics of two 30 minute periods for each approach wind direction. The two periods were chosen to have one with high and one with low standard deviation of the ambient wind direction. The periods chosen have a standard deviation of 7.8^o and 0.2^o for the 133° approach flow direction and 8.6^o and 0.8^o for the 313° approach flow direction. From Figure 38 it is apparent, specifically for the centre (x/W = 0) and downstream (x/W = 0.22) profiles, that the lower standard deviation of the ambient wind direction results in better agreement, up to a factor of 6, in mean spanwise velocity with the wind tunnel results for both approach flow directions. However, there is some discrepancy in the upstream (x/W = -0.22) profile within the canyon for the 133° approach flow direction for the sonic anemometer located at z/h = 0.77. All three profiles still show large discrepancy between the wind tunnel and field results suggesting that large mean spanwise velocity is present even for cases where wind direction changes are small. Figure 39 shows the mean spanwise turbulence intensity, which demonstrates that the low standard deviation cases result in good agreement, within 30%, with the wind tunnel results at all sonic locations. It can therefore be concluded that large wind direction changes result in both an increase in mean spanwise velocity and turbulence intensity.

a)

b)
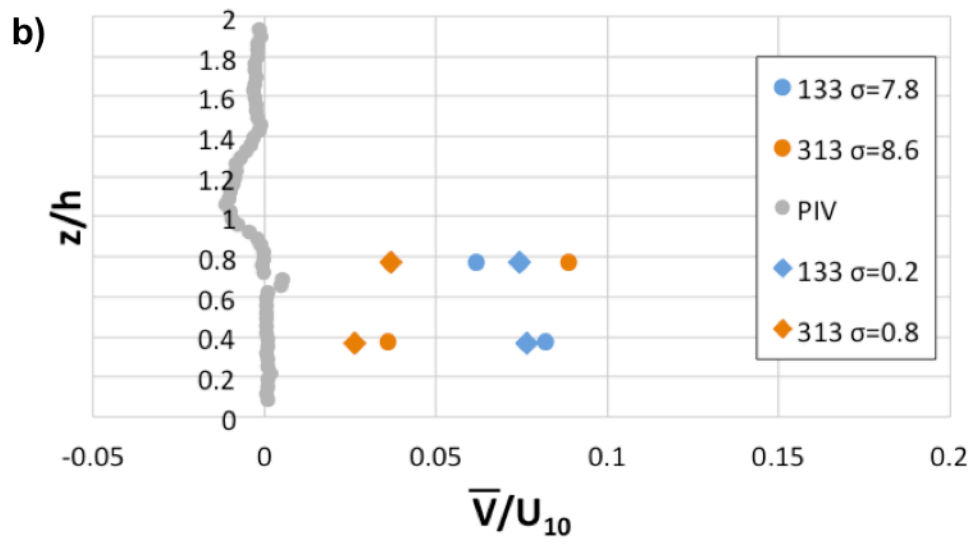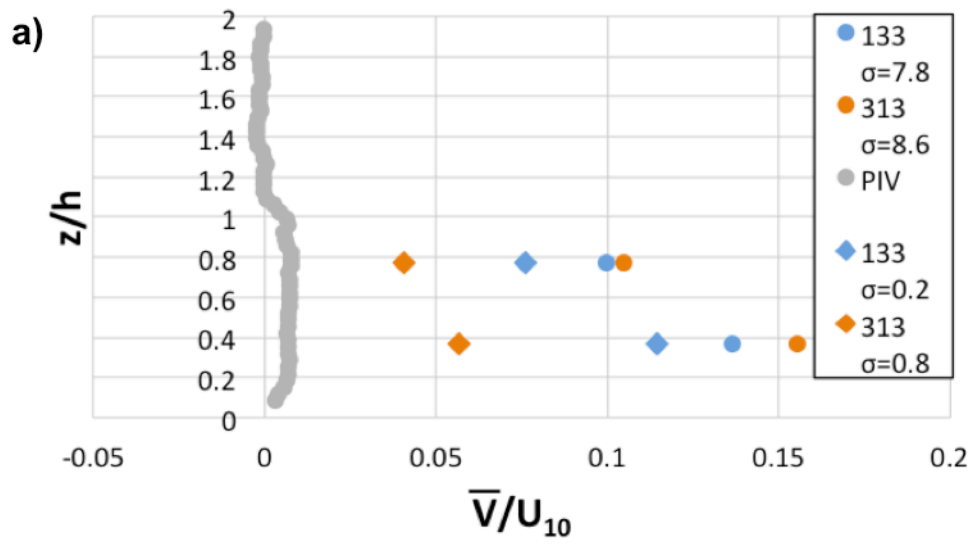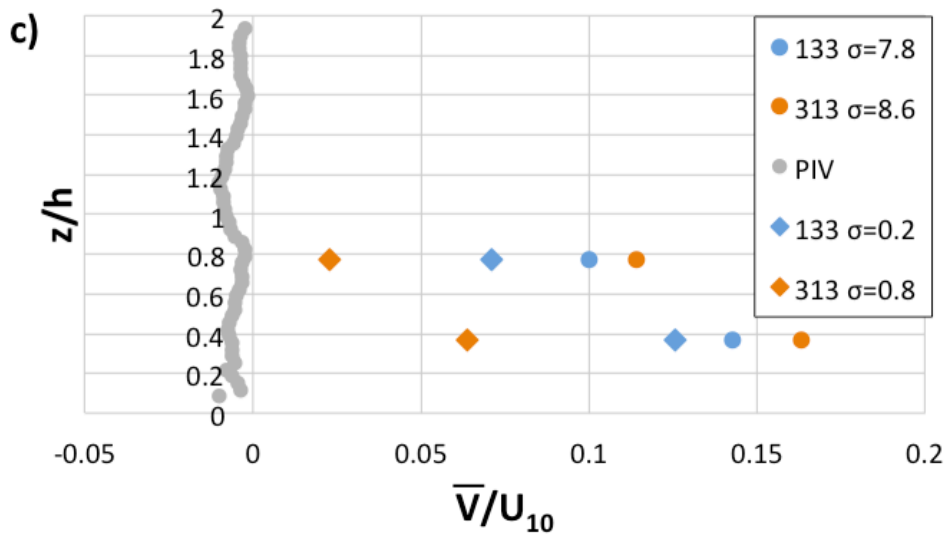
Figure 38 Time averaged mean spanwsie velocity at centre (y/h = 0) of canyon compared with wind tunnel PIV results with high and low standard deviation of ambient wind direction at a) x/W = 0; b) x/W = -0.22; c) x/W = 0.22
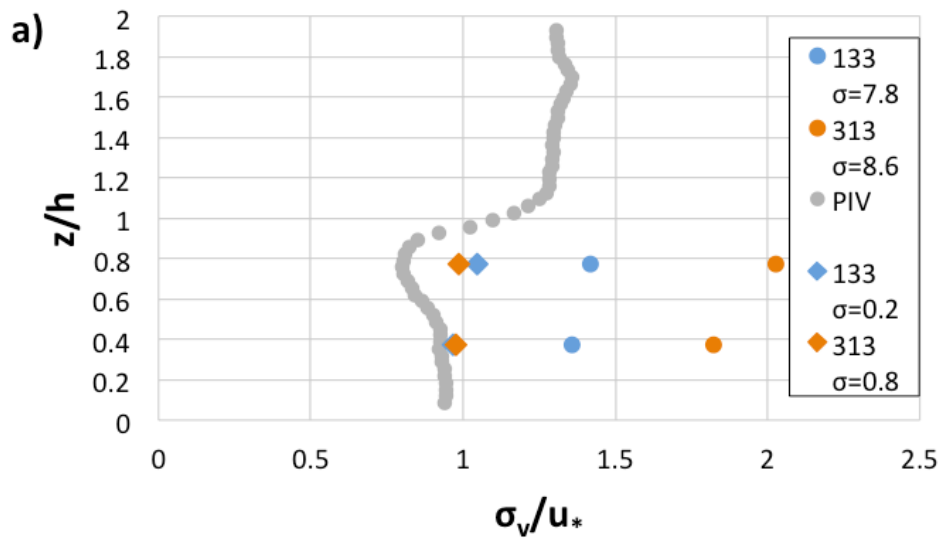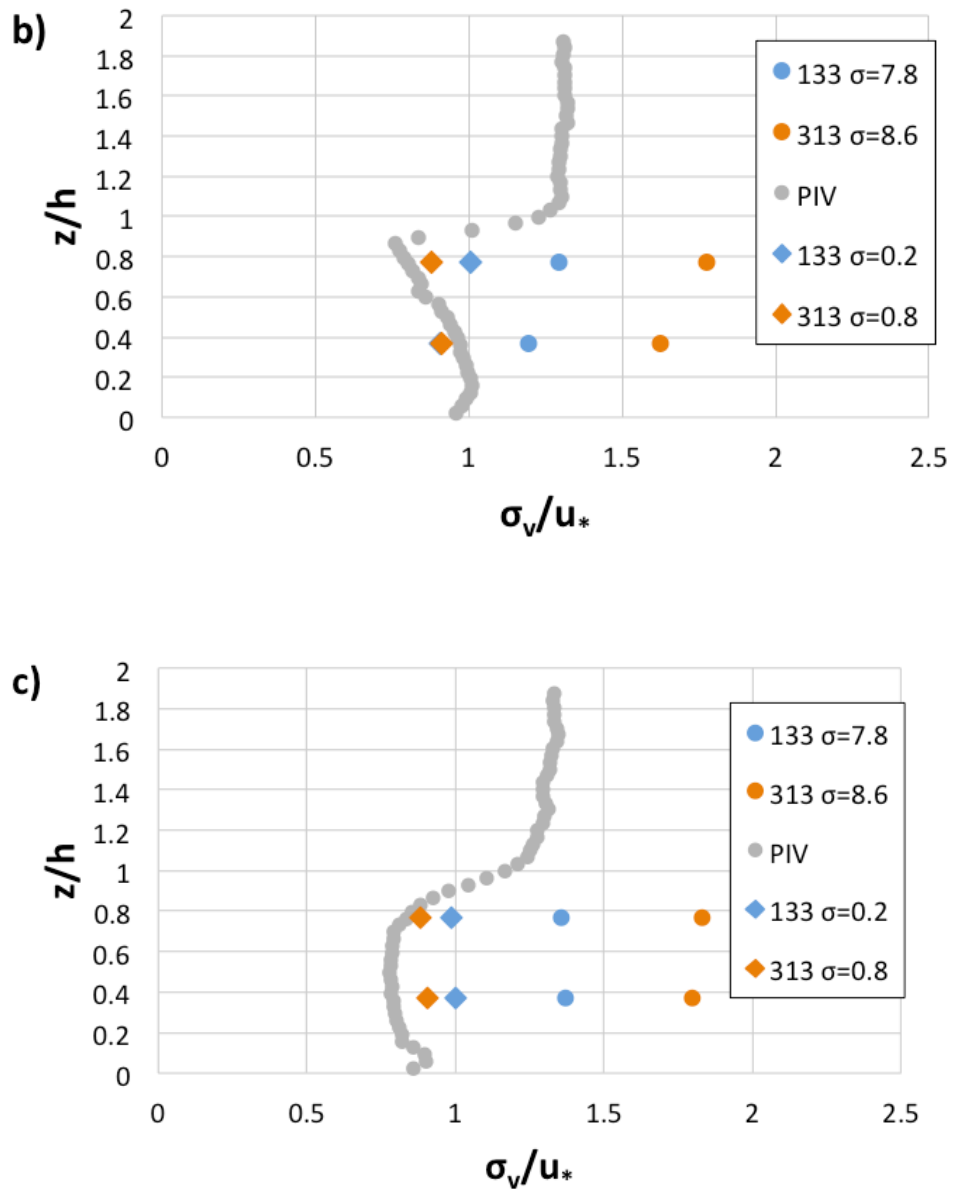
Figure 39 Time averaged mean spanwsie turbulence intensity at centre (y/h = 0) of canyon compared with wind tunnel PIV results with high and low standard deviation of ambient wind direction at a) x/W = 0; b) x/W = -0.22; c) x/W = 0.22

3.4.4.2 Low frequency motion

To further clarify the causes of the discrepancies between the wind tunnel and field study turbulence intensities within the canyon, the turbulence spectra within the canyon of the field study are examined. The spectra were calculated for each continuous time period of

data by fast Fourier transform (FFT) with each of these periods being separated into blocks of length FFT = 2^{12} with 50% overlap. The spectra were then averaged over all periods that passed the selection criteria. The results show significant low-frequency, large-scale motion in the spanwise direction. This spanwise motion is present with both approach wind directions and is particularly evident in the lower sonic anemometers (z/h = 0.38) and the upstream higher sonic (x/W = -0.22, z/h = 0.77) of the canyon (Figure 40, Figure 41b, Figure 42b). This spanwise low-frequency motion is also present in the centre and downstream higher sonic anemometers but is less pronounced (Figure 41a, Figure 42a). Inagaki and Kanda [12] computed the turbulence spectra for all three velocity components at a height of z/h = 2 over a 25% aligned cube array. Their results show an influence of low-frequency motion in both the streamwise and spanwise turbulence spectra. This motion is more pronounced in the spanwise velocity as is the case in the present study. In their study the low-frequency motion in the streamwise direction was attributed to outer-layer disturbances, which in the atmospheric boundary layer are mainly a result of convective motions [12].

There is good agreement for all spectra components (streamwise, spanwise and vertical) between the different approach flow directions. However, in the sonic located at z/h = 0.77 and x/W = 0 there is some disagreement between the streamwise component spectra of the different approach flow directions (Figure 41a). In conclusion, these results show that even with spectral gap filtering and stringent selection criteria there is still a low frequency influence in the spanwise direction that causes the spanwise turbulence intensity to be underestimated in the wind tunnel model.
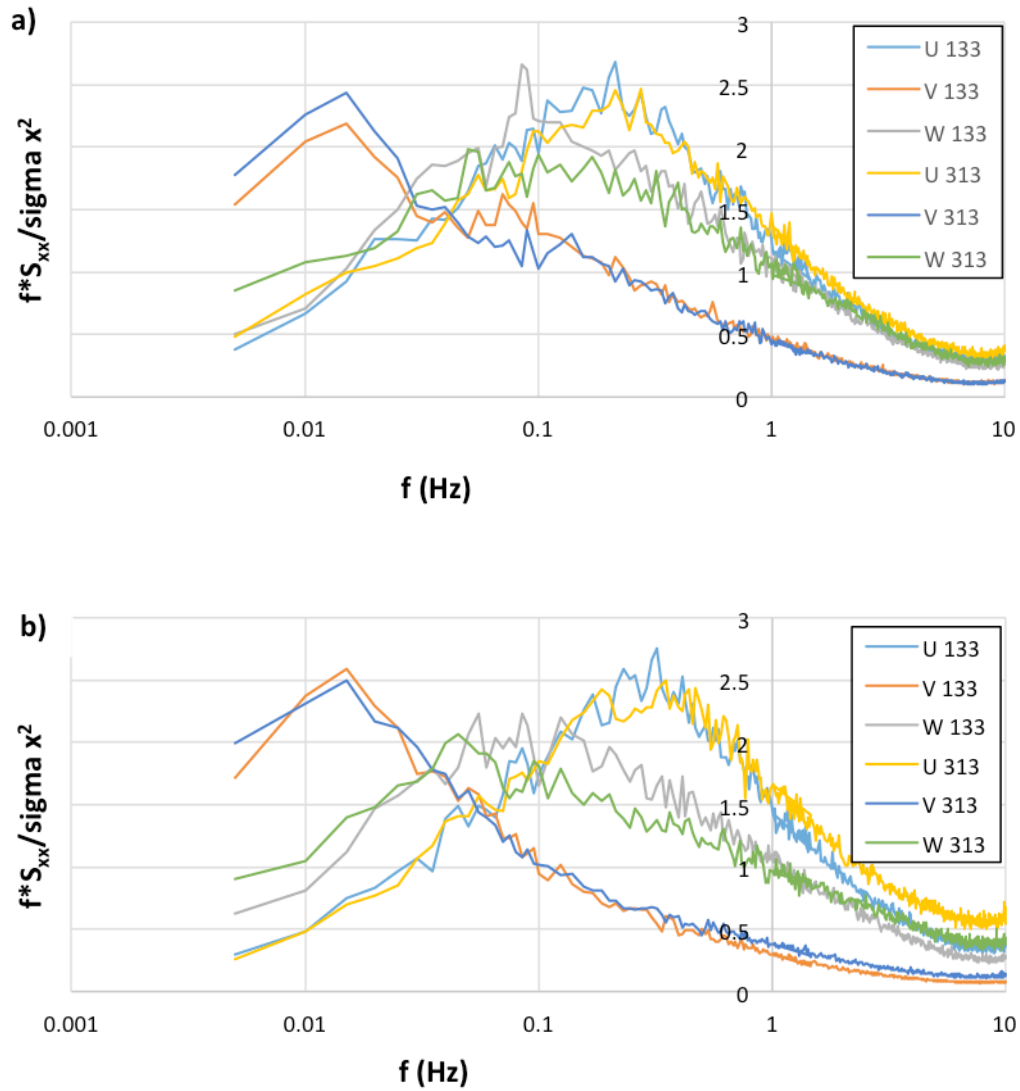
Figure 40 Ensemble averaged turbulence spectra showing both ambient wind directions and all three turbulence components at centre (y/h = 0) of canyon at x/W = -0.22 and a) z/h = 0.38; b) z/h = 0.77
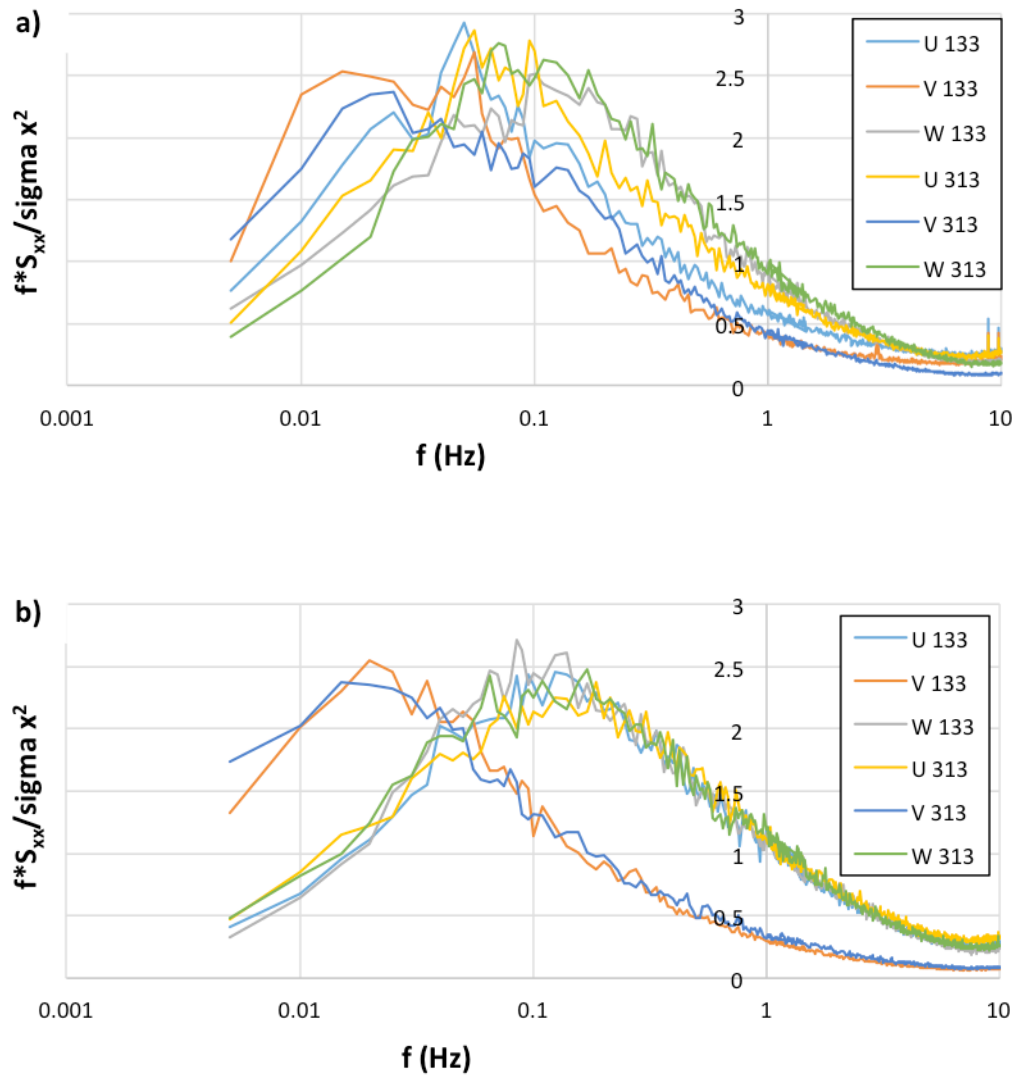
Figure 41 Ensemble averaged turbulence spectra showing both ambient wind directions and all three turbulence components at centre (y/h = 0) of canyon at x/W = 0 a) z/h = 0.38; b) z/h = 0.77
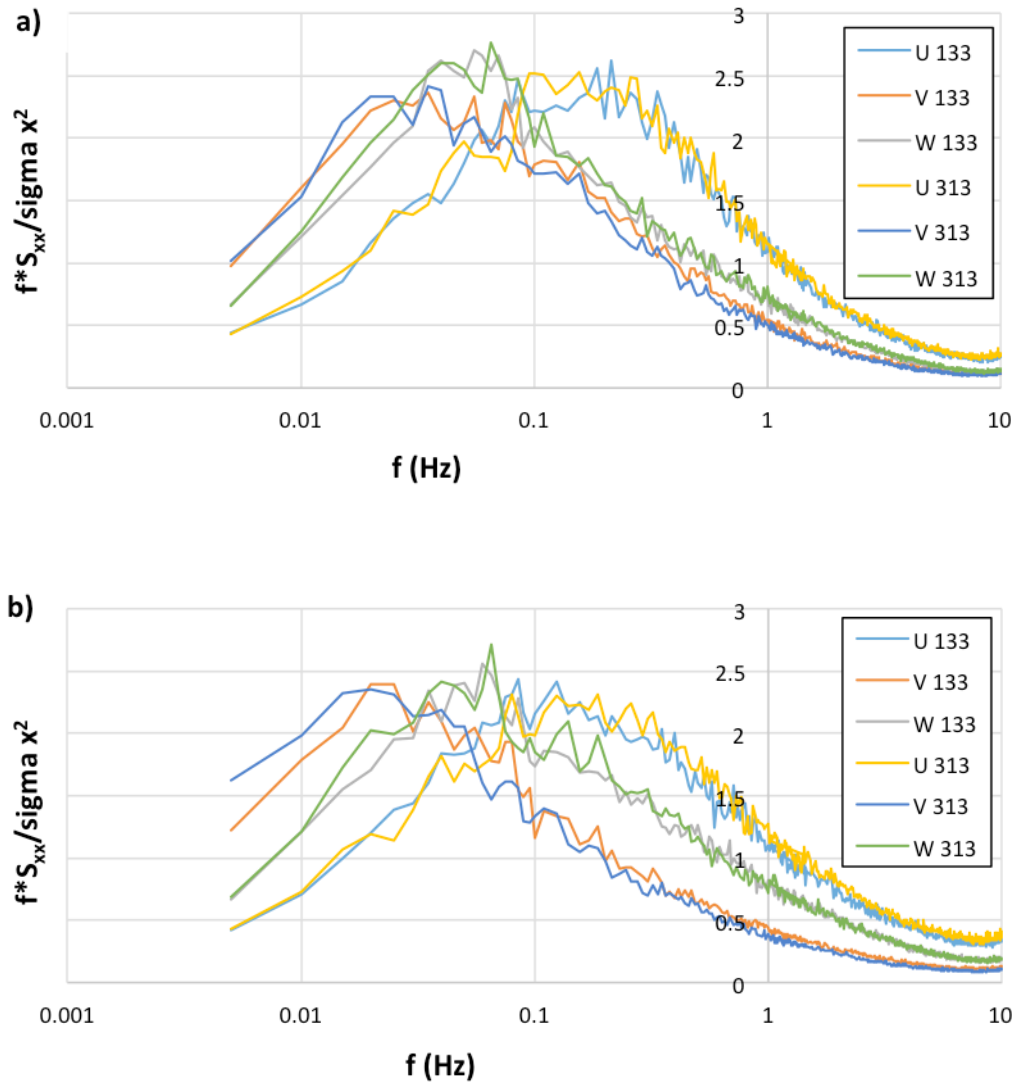
Figure 42   Ensemble averaged turbulence spectra showing both ambient wind directions and all three turbulence components at centre (y/h = 0) of canyon at x/W = 0.22 a) z/h = 0.38; b) z/h = 0.77

3.4.5   Canyon flow dynamics

The following section is a comparison of the field and wind tunnel turbulence dynamics including two-point spatial correlation and canyon ventilation flow rate.

3.4.5.1   Two-point spatial correlation

The size of the turbulent structures in the streamwise, spanwise and vertical directions can be assessed by two-point spatial correlations. The correlation was performed for each 30 minute time period that passed the post-processing selection criteria outlined in Section 3.3. For comparison purposes the two-point spatial correlation was calculated using the PIV wind tunnel data for three velocity components (U, V and W). An example of the equation used to calculate the two-point spatial correlation is shown in Equation 13 for the streamwise velocity.

Equation 13   Two-point spatial correlation coefficient for streamwise velocity

$$R_{uu}\left(x_{ref}, z_{ref}, x, z\right) = \frac{\overline{u'\left(x_{ref}, z_{ref}\right)u'(x,z)}}{\sqrt{\overline{u'^2(x_{ref}, z_{ref})}}\sqrt{\overline{u'^2(x,z)}}}$$

The location of the mast in the field is x/h = 1.7, y/h = 5 and z/h = 1.9. The equivalent location of the upstream mast of the field is not encompassed by the PIV measurements in the wind tunnel so the nearest equivalent point was selected to be the furthest upstream PIV measurement position at a height of z/h = 1.9, which is approximately x/W = -0.52. Figure 43 shows the two-point spatial correlation coefficients for the wind tunnel and field results for the streamwise, spanwise and vertical velocity components averaged over all 30 minute periods. As well, Figure 44, Figure 45, and Figure 46 show the two-point spatial correlation results of the wind tunnel data with the positions of the field sonic anemometers labeled.
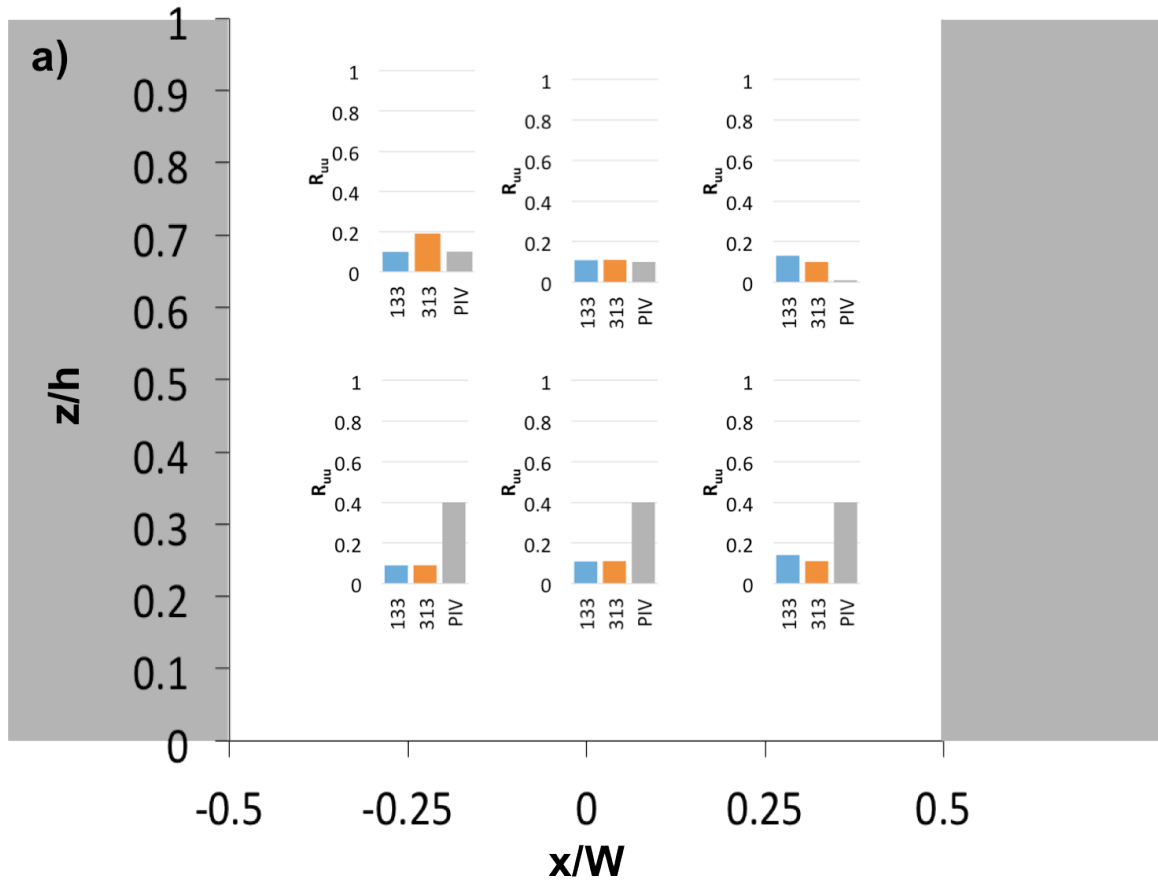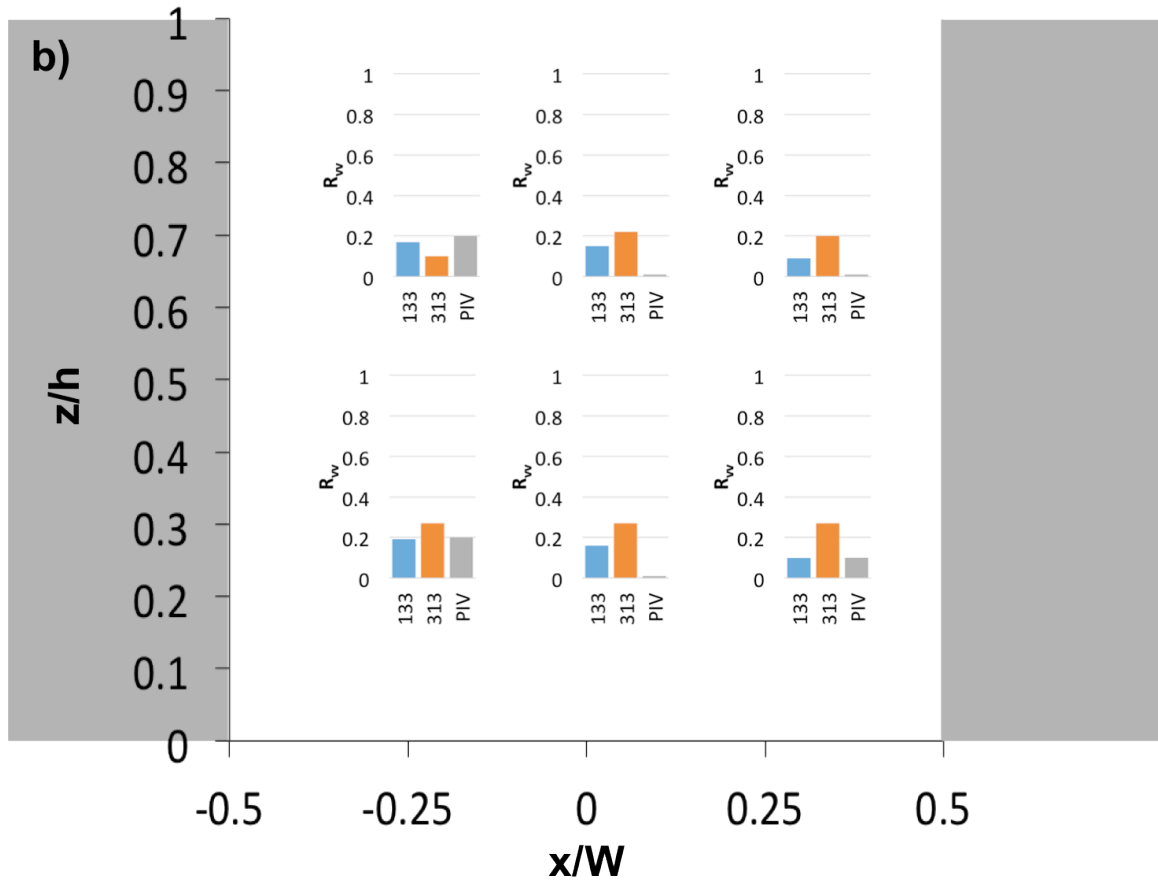
Figure 43 Two-point spatial correlation coefficient magnitudes of sonic anemometers and mast along with wind tunnel PIV with reference point $(x_{ref}/W, z_{ref}/h) = (-0.52, 1.9)$ for a) streamwise velocity component (U); b) spanwise velocity component (V); c) vertical velocity component (W). Canyon is shown (grey) with charts located where sonic anemometer are located

From these results it is evident that the wind tunnel results of the streamwise component overestimate the coefficients at locations of $z/h = 0.38$ (Figure 43a). Dissimilarly, the spanwise velocity component is underestimated, up to a factor of 20, at the downstream and centre sonic anemometer locations in the wind tunnel (Figure 43b). The vertical velocity components shows good agreement except in the case of the upstream and centre sonic anemometers located at $z/h = 0.38$ which are underestimated by a factor of 10 (Figure 43c). The discrepancy between the results of the field experiment and wind tunnel model is likely a result of the difference in reference location. The reference

location in the field experiment is located at x/h = 5 and y/h = 1.7 from the canyon centre (x/W = 0, y/h = 0) whereas in the wind tunnel the reference location is at x/W = -0.52 and y/h = 0. This will significantly effect the spatial correlation of the spanwise velocity component, as the spanwise scale of eddies within the field, approximately 2.5-4.5h, are not large enough to encompass both the mast and the canyon sonic anemometers [6, 7]. The spanwise length scales within the wind tunnel are approximately 2h, which is significantly smaller than those found in full-scale boundary layers [21]. Furthermore, as shown in section 3.4.4.1, there is a contribution to the spanwise turbulence intensity by the variation of the approaching wind direction. Therefore, these values are not based on equivalent geometry and the flow characteristics are not representative.

The position of the mast in the field experiment should provide sufficient data to classify the ambient conditions for both approach directions. However, from this analysis it is evident that the streamwise and spanwise correlation coefficients are not equivalent or symmetric for the upstream and downstream positions for each approach direction. In the streamwise velocity correlation the discrepancy is most notable in the sonic located at x/W = -.022 and z/h = 0.77 with a difference of 53% between the two directions, where percent difference is defined as $\frac{field-wind\ tunnel}{wind\ tunnel} * 100$. A difference of approximately 30-60% is evident in the spanwise upstream and downstream sonic locations. This suggests that there is some effect from either the ambient wind direction changes or the position of the mast and makes comparison with the wind tunnel results difficult for the 133° approach direction.

Figure 44 Streamwise velocity component (U) two-point correlation of wind tunnel PIV with reference point $(x_{ref}/W, z_{ref}/h) = (-0.52, 1.9)$ ($\bullet$) showing field sonic anemometers ($\bullet$)

Figure 45   Spanwise velocity component (V) two-point correlation of wind tunnel PIV with reference point $(x_{ref}/W, z_{ref}/h) = (-0.52, 1.9)$ (•) showing field sonic anemometers (•)
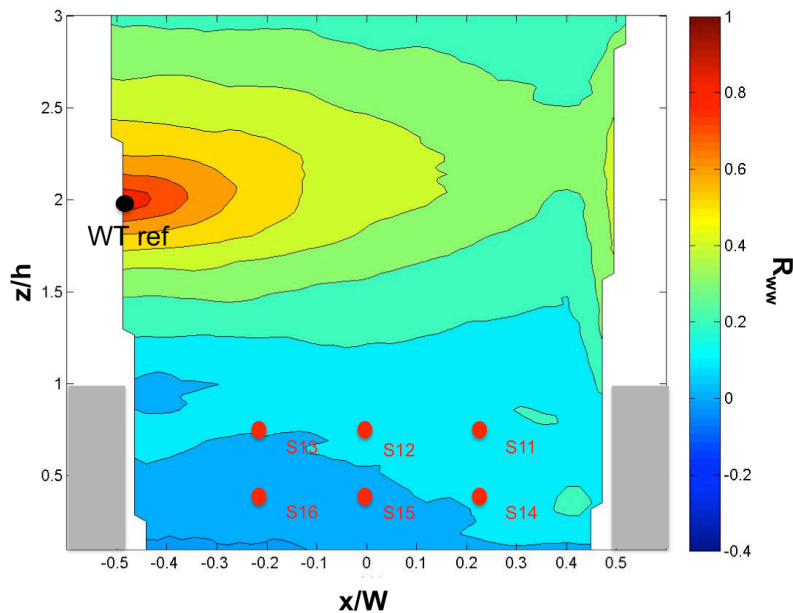
Figure 46   Vertical velocity component (W) two-point correlation of wind tunnel PIV with reference point $(x_{ref}/W, z_{ref}/h) = (-0.52, 1.9)$ (•) showing field sonic anemometers (•)

To improve the two-point spatial correlation estimates for the field data and wind tunnel data the correlation was performed using the sonic anemometer S12, located at $z/h = 0.77$ and $x/W = 0$, as the reference point (Figure 47). The correlation coefficient of the streamwise velocity component averaged over all 30 minute periods shows significantly better agreement with the wind tunnel results (Figure 47). However, the spanwise velocity correlation is overestimated by up to 50% by the wind tunnel results at the upstream ($x/W = -0.22$) sonic anemometers (Figure 49). Dissimilarly, the vertical velocity correlation is generally underestimated at all sonic positions by between 15-55% in the wind tunnel results when compared with both field approach directions (Figure 50). This discrepancy is likely a result of the differences in sizes of structures within the atmospheric boundary layer and the boundary layer produced in the wind tunnel. As seen previously, the field results display large, low-frequency spanwise motion that is not present in the wind tunnel.

There is also an effect from the upstream roughness in the field data. In the spanwise and vertical velocity correlations there is a significant difference (up to 50% for the spanwise and up to 55% for the vertical velocity) between the two approach flow directions in the upstream ($x/W = -0.22$) sonic anemometers. As well, when each approach flow direction is compared with the wind tunnel results the 313° approach direction results in a better agreement. This may be a result of difference in upstream roughness. The 313° direction has an approximately uniform upstream roughness consisting of a wooded area with $z_o = 0.3$ m, while the 133° direction has fields along with an isolated building close to the canyon obstacles with $z_o = 0.03\text{-}0.1$ m. This isolated building will influence the turbulence and size of structures within the canyon. As the flow approaches the canyon from the east the wind must move around the upstream isolated building resulting in a wake and causing increased spanwise velocity. This method of comparison between wind tunnel and field results has not been previously applied in previous work and, therefore, no comparison with the literature can be made.
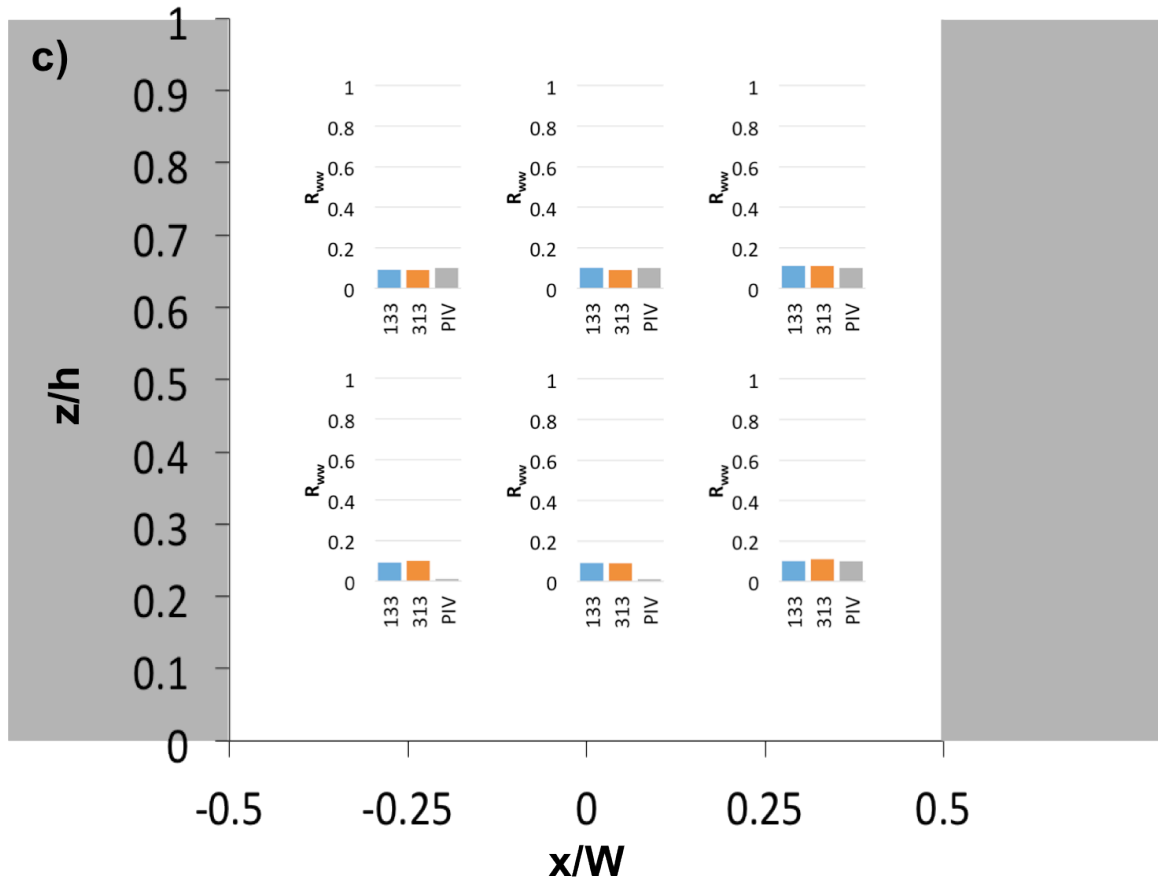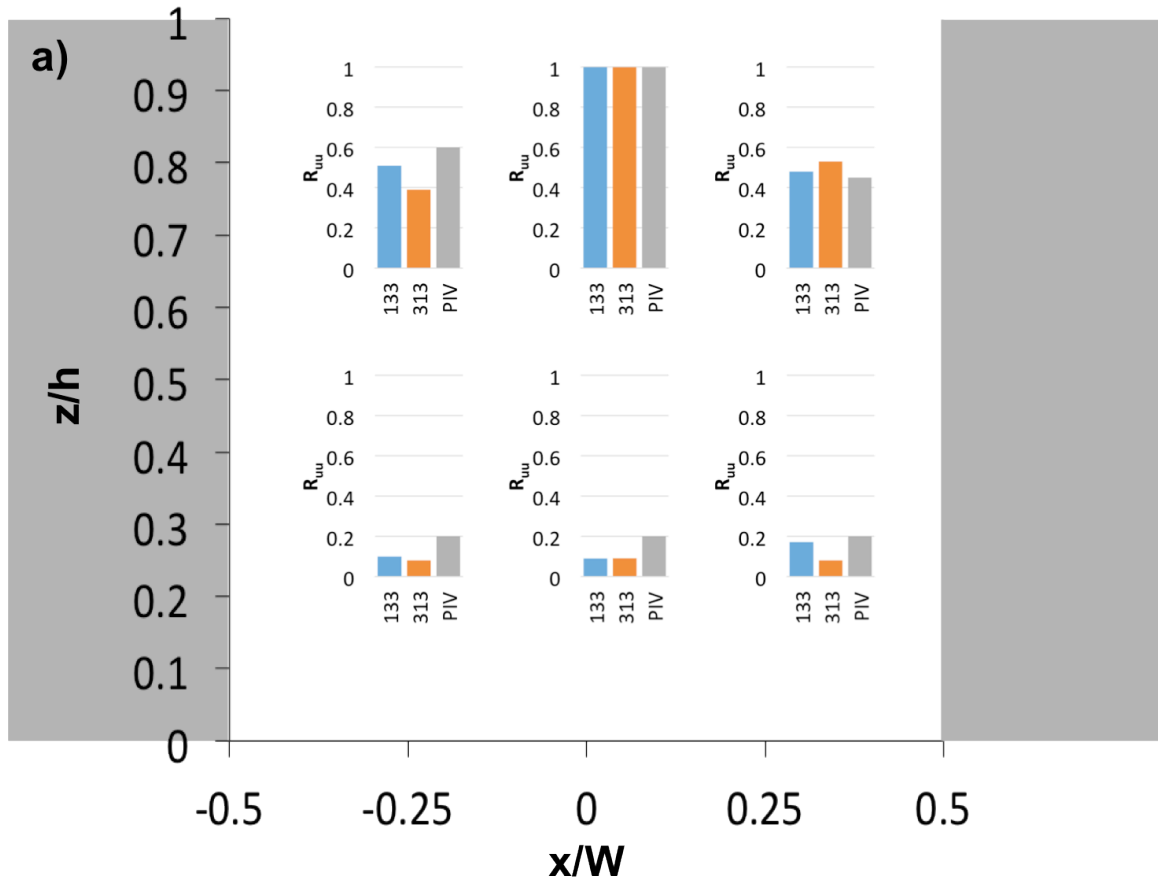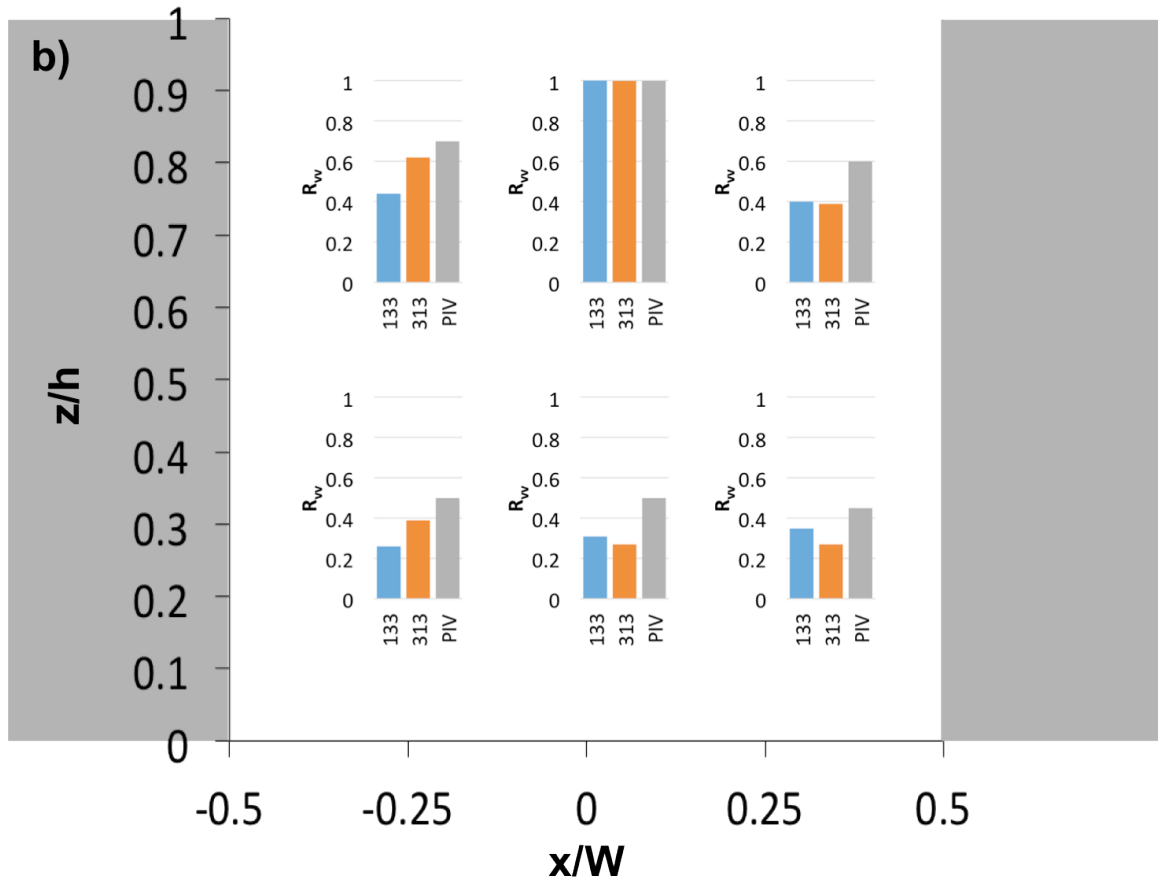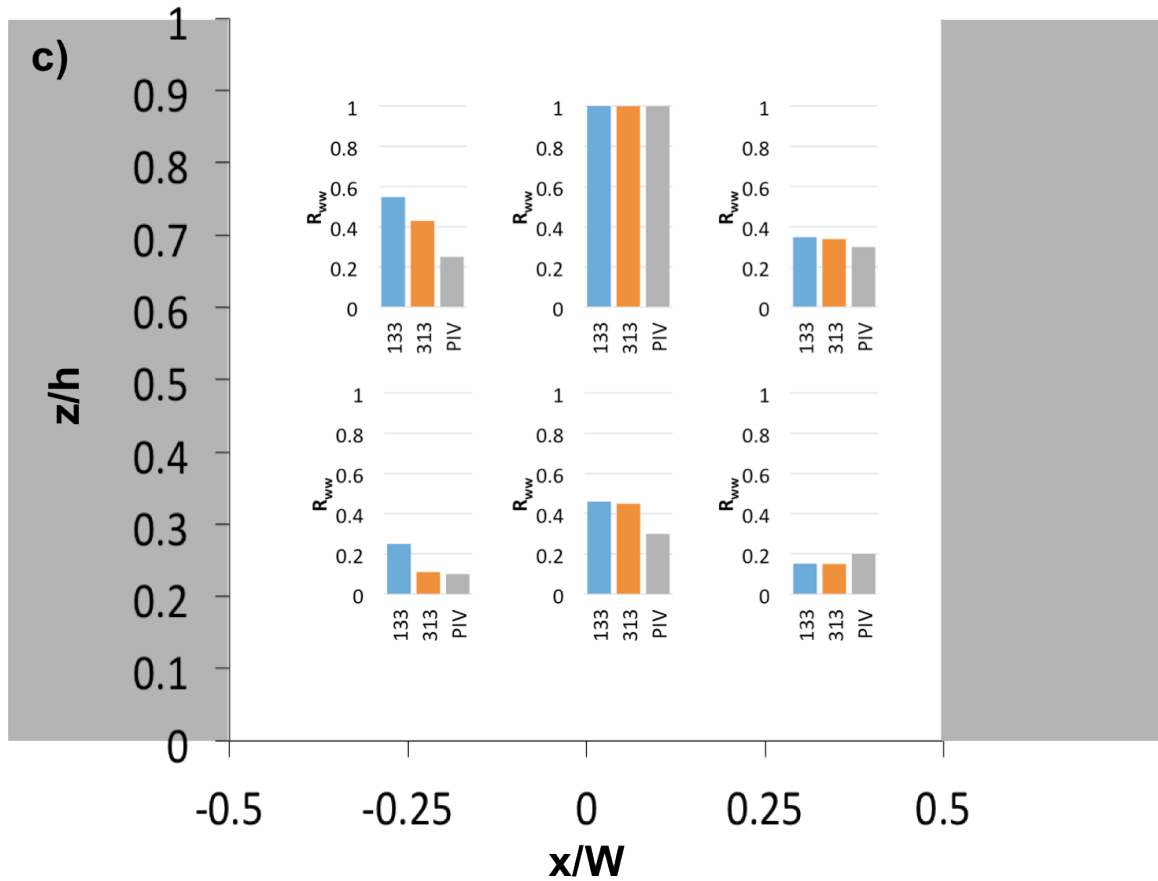
Figure 47 Two-point spatial correlation coefficient magnitudes of sonic anemometers along with wind tunnel PIV with reference point $(x_{ref}/W, z_{ref}/h) = (0, 0.77)$ for a) streamwise velocity component (U); b) spanwise velocity component (V); c) vertical velocity component (W). Canyon is shown (grey) with charts located where sonic anemometer are located
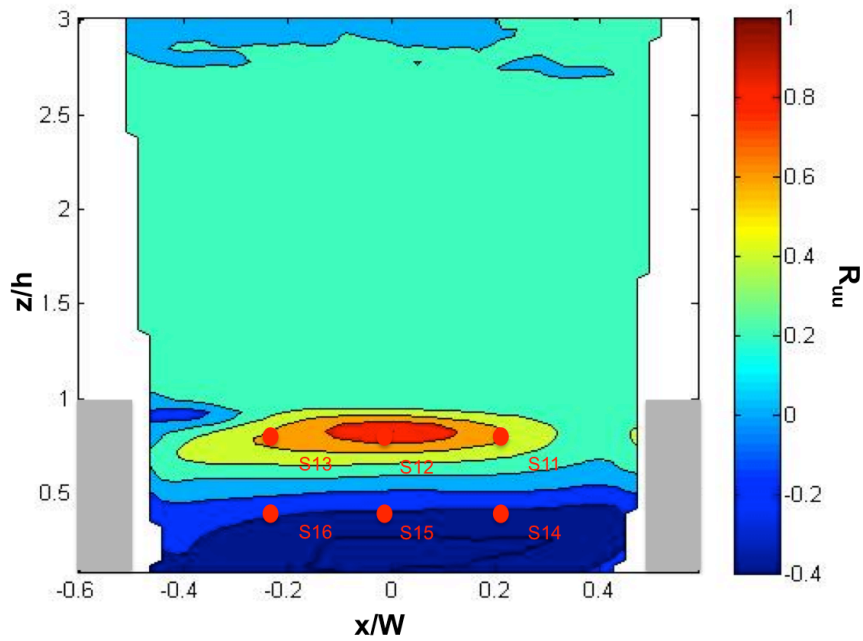
Figure 48   Streamwise velocity component (U) two-point correlation of wind tunnel PIV with reference point $(x_{ref}/W, z_{ref}/h) = (0, 0.77)$ showing field sonic anemometers (•)
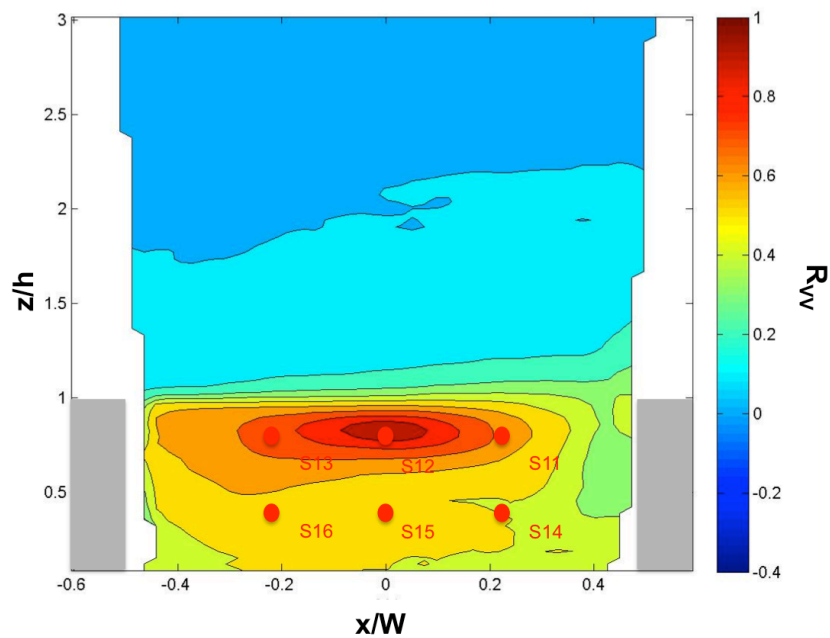
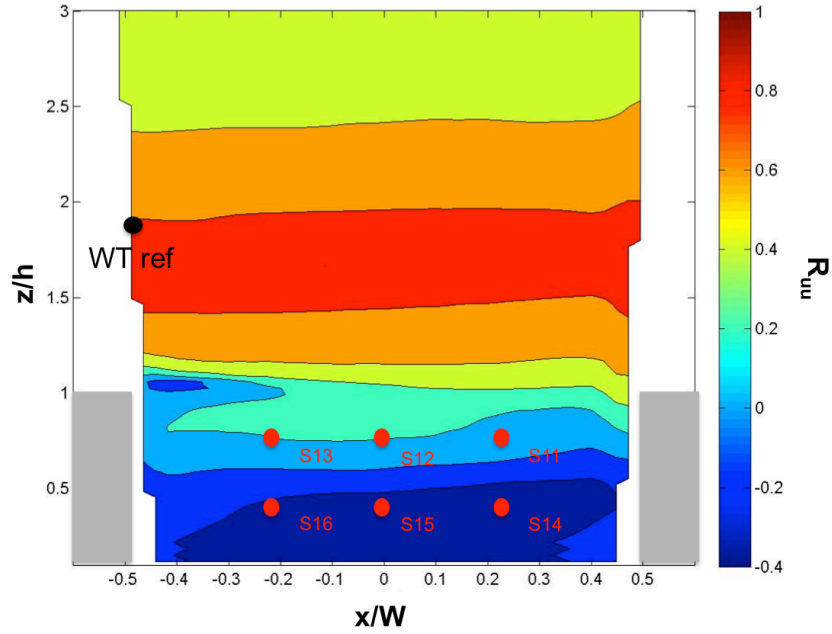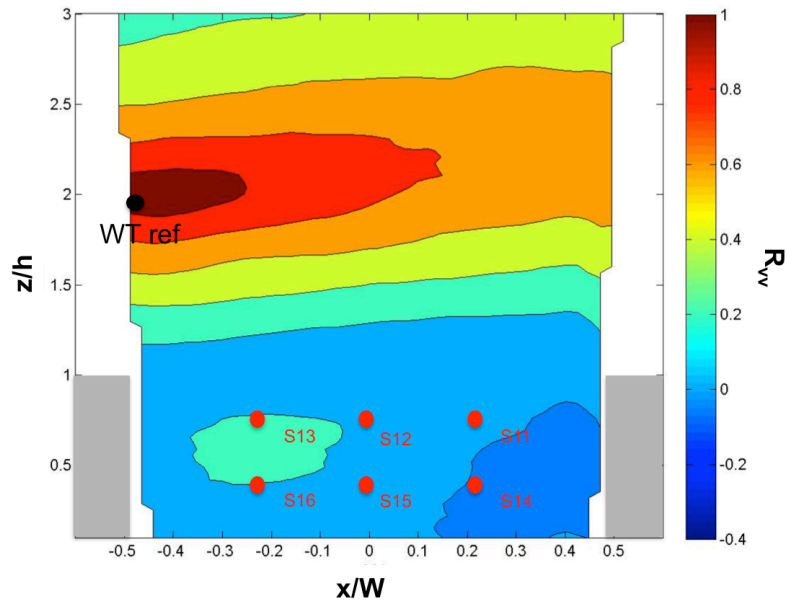**Figure 49**   Spanwise velocity component (V) two-point correlation of wind tunnel PIV with reference point $(x_{ref}/W, z_{ref}/h) = (0, 0.77)$ showing field sonic anemometers (•)
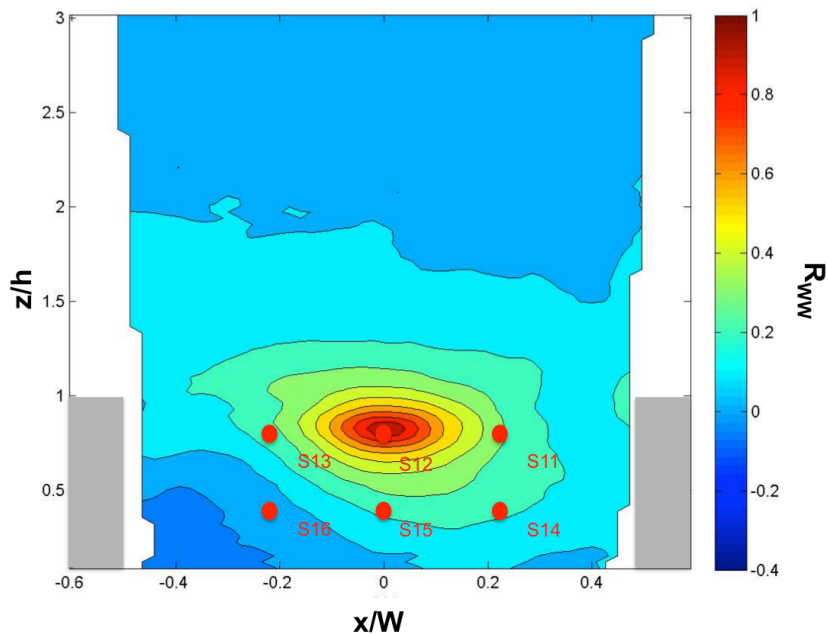
Figure 50 Vertical velocity component (W) two-point correlation of wind tunnel PIV with reference point $(x_{ref}/W, z_{ref}/h) = (0, 0.77)$ showing field sonic anemometers (•)

### 3.4.5.2 Canyon ventilation

The mean canyon ventilation flow rate can be assessed by first comparing the mean vertical velocity and turbulence intensity in both the positive and negative directions for each of the sonic anemometer locations and their respective wind tunnel PIV results. Refer to section 2.3.3 in the previous chapter for further details on this analysis technique. The field results were ensemble averaged for all periods that met the selection criteria. Both the mean vertical velocity and turbulence intensity of the field results are in good agreement with the wind tunnel results (Figure 51). The maximum percent difference is 30% and 40% for the positive vertical velocity and negative vertical velocity, respectively and 35% for both the positive and negative vertical turbulence intensity.

a)

z/h

1
0.9
0.8
0.7
0.6
0.5
0.4
0.3
0.2
0.1
0

133 313 PIV

W/U_{10}

0.25
0.15
0.05
-0.05
-0.15
-0.25

133 313 PIV

W/U_{10}

0.25
0.15
0.05
-0.05
-0.15
-0.25

133 313 PIV

W/U_{10}

0.25
0.15
0.05
-0.05
-0.15
-0.25

133 313 PIV

W/U_{10}

0.25
0.15
0.05
-0.05
-0.15
-0.25

133 313 PIV

W/U_{10}

0.25
0.15
0.05
-0.05
-0.15
-0.25

133 313 PIV

W/U_{10}

0.25
0.15
0.05
-0.05
-0.15
-0.25

-0.5   -0.25   0   0.25   0.5

x/W
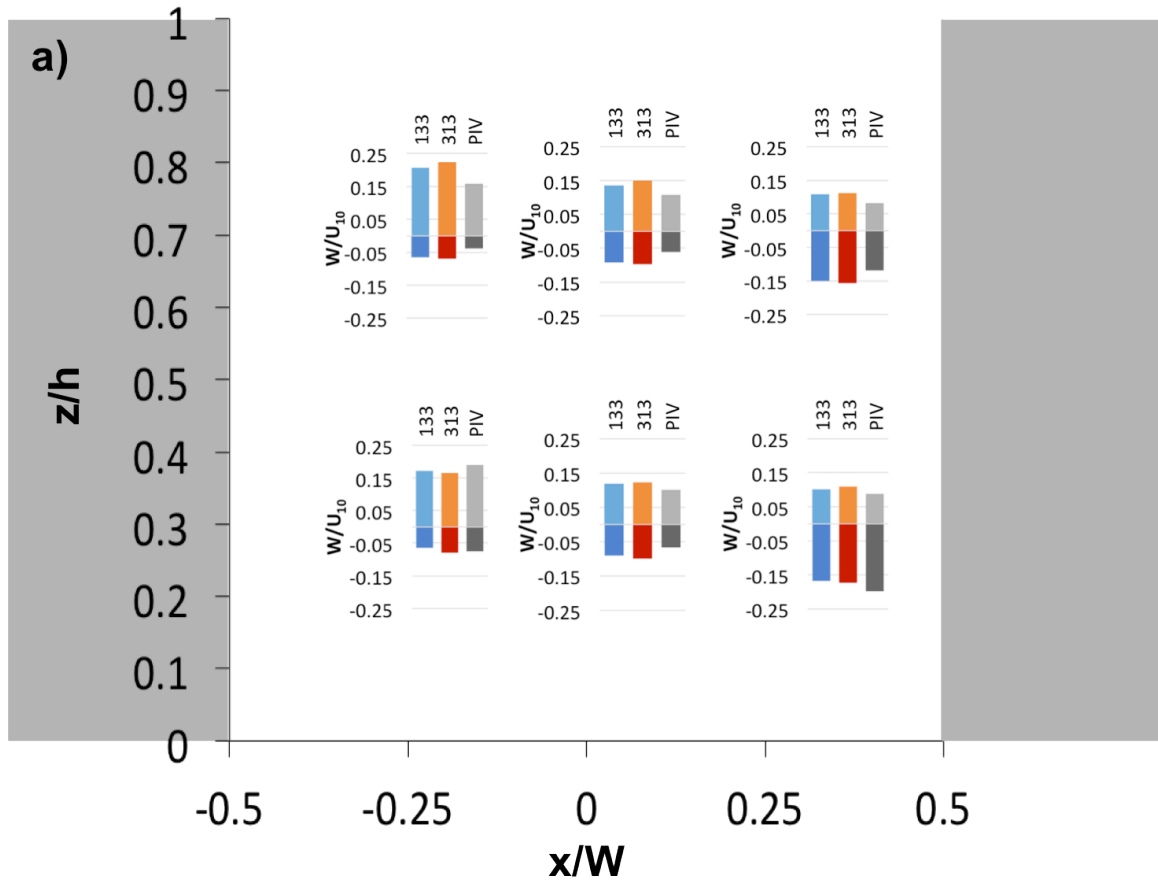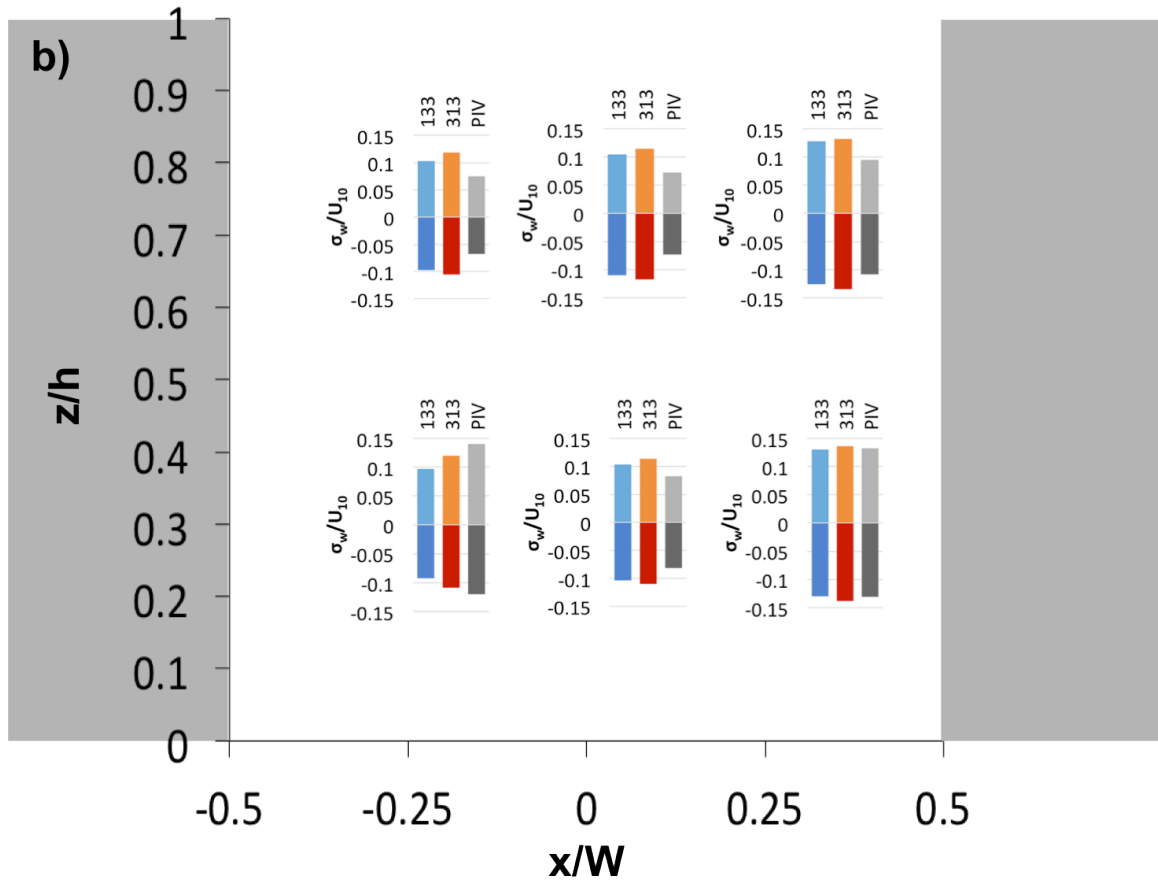
Figure 51 Positive and negative vertical flow rate of sonic anemometers and wind tunnel PIV represented as a) mean vertical velocity; b) turbulence intensity. Canyon is shown with charts located where sonic anemometers are located

Due to the location of the sonic anemometers in the field a direct calculation of the ventilation rate across the canyon opening cannot be performed. However, since good agreement was found between the wind tunnel and field results for the vertical velocity and turbulence intensity an estimation of the ventilation can be made using wind tunnel data alone. The ventilation flow rate is compared to wind tunnel configurations from Chapter 2 (Figure 52). As shown, both the mean and total flow rates are smaller in both the positive and negative directions when compared with the configuration of a canyon with AR = 1h and upstream roughness of a λ_p = 25% cube array. This upstream roughness is the same as used in the current wind tunnel model used for comparison with

the field data. Thus, it is clear that the small AR (0.7) of the present canyon restricts the ventilation flow rate.
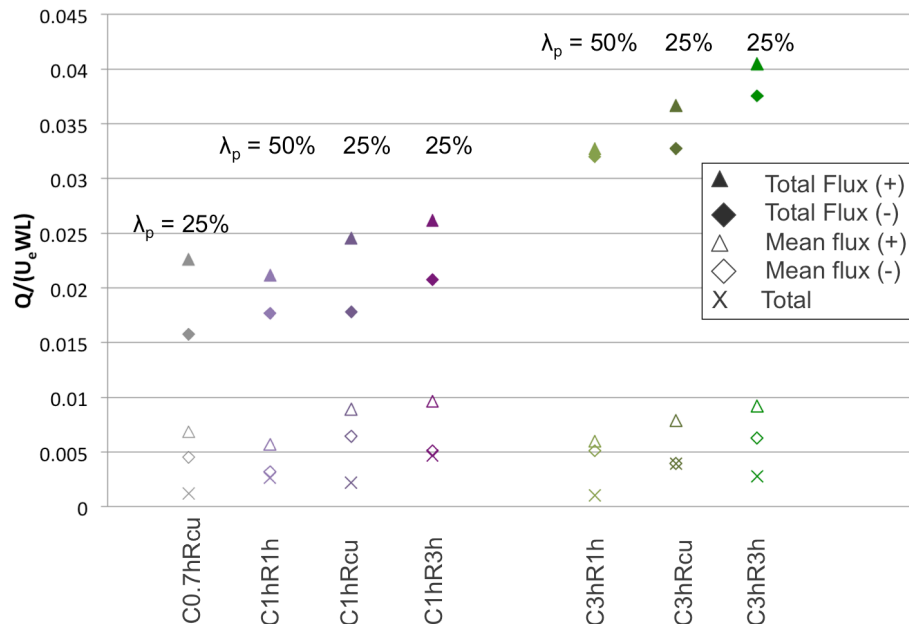
Figure 52   Positive vertical flow rate across the canyon opening (▲), negative flow rate across the canyon (♦) and total flow rate across the canyon (×) for the 6 different configurations (W = canyon streamwise width, L = canyon lateral length); open symbols: contribution of the mean flow to the flow rate; filled symbols: contribution of both the mean flow and fluctuation to the flow rate

3.5   Conclusions

The turbulence statistics of the *Influence des effets micro-météorologiques sur la propagation acoustique en milieu urbain* (EM2PAU) campaign [9], which took place in Nantes, France, and a wind tunnel model of equivalent geometry were investigated. The field experiment was found to scale with the Engineering Sciences Data Unit (ESDU) profiles as a wooded terrain boundary layer (z_o = 0.3 m) and a field terrain boundary layer (z_o = 0.03-0.1 m), while the wind tunnel model represented a suburban boundary layer (z_o = 0.2 m). However, these values are within the acceptable factor range of 2-3 of each other.

Friction velocity was found to provide adequate scaling for Reynolds number independence of the mean turbulence statistics, which were well predicted within the canyon by the wind tunnel model except in the case of the mean spanwise velocity and spanwise turbulence intensity. This discrepancy was found to be a result of the changing approach flow wind direction. As the wind shifts direction over time the effect is a channeling of flow through the canyon. This phenomena was also found in many studies from the literature [2, 5, 16, 31]. The wind tunnel model, although of equivalent geometry, produces nominally two-dimensional flow and, therefore, cannot accurately represent the spanwise flow phenomena of channeling. Its presence was further confirmed by an analysis of spectra that showed low frequency motion in the spanwise direction. Finally, the turbulence dynamics were investigated through two-point spatial correlation of the streamwise, spanwise and vertical velocity components and ventilation flow rate. It was determined that when a reference point within the canyon is chosen the streamwise, spanwise and vertical velocity correlation show good agreement between the field and wind tunnel results excepting the upstream sonic locations which show 55% and 52% discrepancy for the spanwise and vertical velocity components, respectively. Good agreement was also shown when investigating the vertical mean and instantaneous flow rate of the field and wind tunnel results. It is, therefore, expected that the field study will have similar canyon ventilation to that of the wind tunnel model. The wind tunnel model shows restricted ventilation due to the narrow AR of the canyon.

Current knowledge of canyon flow in field studies is limited, as most previous work has been focused on dispersion [15, 20, 25, 27, 30]. The present work is a significant contribution to the field of environmental fluid mechanics as it provides a detailed scaling analysis of the approaching boundary layer [24], a comparison with a wind tunnel model of equivalent geometry [14, 23, 26] and detailed analysis of turbulence statistics within the canyon, all of which are not commonly done for canyon flow studies. Finally, the present work has confirmed that the large spanwise velocity and turbulence intensity within a street canyon is a result of the changing of the ambient wind direction.

3.6 Summary

Idealized canyons within the wind tunnel are able to reproduce the main flow features of idealized field canyon of equivalent geometry except in the case of spanwise velocity and turbulence intensity. The following chapter is a discussion and comparison of the main results from Chapter 2 and Chapter 3.

3.7 References

1. Arnfield AJ, Mills GM (1994) An analysis of the circulation characteristics and energy budget of a dry, asymmetric, east-west urban canyon. I. Circulation characteristics. Int J Climatol 14:119-134

2. Brown MJ, Khalsa H, Nelson M, Boswell D (2004) Street canyon flow patterns in a horizontal plane: measurements from the joint urban 2003 field experiment. Proceedings of the 5th Symposium on the Urban Environment 2004, Tokyo, Japan

3. Cook NJ (1985) The designer's guide to wind loading of building structures: Part 1. The University Press, Cambridge

4. DePaul FT, Sheih CM (1986) Measurements of wind velocities in a street canyon. Atmos Environ 20:455-459

5. Eliasson I, Offerle B, Grimmond CSB, Lindqvist S (2006) Wind fields and turbulence statistics in an urban street canyon. Atmos Environ 40:1-16

6. ESDU (1982) Strong winds in the atmospheric boundary layer. Part I: mean-hourly wind speeds. Data Item 82026 (amended 1993), Engineering Sciences Data Unit International

7. ESDU (1985) Characteristics of atmospheric turbulence near the ground. Part II: single point data for strong winds (neutral atmosphere. Data Item 852020 (amended 1993), Engineering Sciences Data Unit International

8. Graf A, van de Boer A, Moene A, Vereecken H (2014) Intercomparison of methods for the simultaneous estimation of zero-plane displacement and aerodynamic roughness length from single-level eddy-covariance data. Bound Layer Meteorol 151:373-387

9. Guillaume G, Ayrault C, Berengier M, Calmet I, Gary V, Gaudin D, Gauvreau B, L'hermite Ph, Lihoreau B, Perret L, Picaut J, Piquet T, Rosant JM, Sini JF (2012)

Micrometeoriological effects on urban sound propagation: a numerical and experimental study. All Glo Sus 19:109-119

10. Hanna S, White J, Zhou Y (2007) Observed winds, turbulence, and dispersion in built-up downtown areas of Oklahoma City and Manhattan. Bound Layer Meteorol 125:441-468

11. Hanna S, Zhou Y (2009) Space and time variations in turbulence during the Manhattan Midtown 2005 field experiment. Amer Meteorol Soc 48:2295-2304

12. Inagaki A, Kanda M (2008) Turbulent flow similarity over an array of cubes in near-neutrally stratified atmospheric flow. J Fluid Mech 615:101-120

13. Inagaki A, Kanda M (2010) Organized structure of active turbulence over an array of cubes within the logarithmic layer of atmospheric flow. Bound Layer Meteorol 135:209-228

14. Kastner-Klein P, Rotach MW (2004) Mean flow and turbulence characteristics in an urban roughness sublayer. Bound Layer Meteorol 111:55-84

15. Ketzel M, Berowicz R, Lohmeyer A (2000) Comparison of numerical street dispersion models with results from wind tunnel and field measurements. Environ Monit Assess 65:363-370

16. Klein P, Clark JV (2007) Flow variability in a North American downtown street canyon. Amer Meteorol Soc 46:851-877

17. Lee X, Massman WJ, Law B (2004) Handbook of micrometeorology: a guide for surface flux measurements and analysis. Kluwer Academic Publishers, The Netherlands pp. 181-208

18. Liu HY, Bo TL, Wang GH, Zheng XJ (2014) The analysis of turbulence intensity and Reynolds shear stress in wall-bounded turbulence flows at high Reynolds numbers. Bound Layer Meteorol 150:33-47

19. Louka P, Belcher SE, Harrison RG (2000) Coupling between air flow in streets and the well-developed boundary layer aloft. Atmos Environ 34:2613-2621

20. Nielsen M (2000) Turbulent ventilation of a street canyon. Environ Monit Assess 65:389-396

21. Rivet C (2014) Étude en soufflerie atmosphérique des interactions entre canopée urbaine et basse atmosphère par PIV stéréoscopique. Dissertation, École Centrale de Nantes

22. Rotach MW (1995) Profiles of turbulence statistics in and above an urban street canyon. Atmos Environ 29:1473-1486

23. Rotach MW, Vogt R, Bernhofer C, Batchvarova E, Christen A et al. (2005) BUBBLE – an urban boundary layer meteorology project. Theor Appl Climatol 81:231-261

24. Savory E, Perret L, Rivet C (2013) Modelling considerations for examining the mean and unsteady flow in a simple urban-type street canyon. Meteorol Atmos Phys 121:1-16

25. Schatzmann M, Leitl B, Liedtke J (2000) Dispersion in urban environments comparison of field measurements with wind tunnel results. Environ Monit Assess 65:249-257

26. Takimoto H, Sato A, Barlow JF, Moriwaki R, Inagaki A, Onomura S, Kanda M (2011) Particle image velocimetry measurements of turbulence flow within outdoor and indoor urban scale models and flushing motions in urban canopy layers. Bound Layer Meteorol 140:295-314

27. Tominaga Y, Iizuka S, Imano M, Kataoka H, Mochida A, Nozu T, Ono Y, Shirasawa T, Tsuchiya N, Yoshie R (2013) Cross comparisons of CFD results of wind and dispersion field for MUST experiment: evaluation exercises by AIJ. J Asian Arch Build Eng 12:117-124

28. Vachon G, Rosant JM, Mestayer PG, Sini JF (1999) Measurements of dynamic and thermal field in a street canon. URBCAP Nantes'99. Proceedings of the 6th International Conference on Harmonisation within Atmospheric Dispersion Modeling for Regulatory Purposes October 1999, Rouen, France

29. Vachon G, Louka P, Rosant JM, Meystayer PG, Sini JF (2002) Measurements of traffic-induced turbulence within a street canyon during the Nantes'99 experiment. Water Air Soil Poll 2:127-140

30. Yassin MF, Kato S, Ooka R, Takahashi T, Kouno R (2005) Field and wind-tunnel study of pollutant dispersion in a built-up area under various meteorological conditions. J Wind Eng Ind Aerodyn 93:361-382

31. Zajic D, Fernando HJS, Calhoun R, Princevac M, Brown MJ, Pardyjak ER (2011) Flow and turbulence in an urban canyon. Amer Meterol Soc 50:203-223

Chapter 4

4   Discussion

The following section is a discussion of the relevant conclusions drawn from the results of Chapter 2 and Chapter 3. A discussion of the significance of the research to the field of environmental fluid mechanics is also included followed by recommendations and final conclusions.

4.1   Modeling urban boundary layers in the wind tunnel

When conducting wind tunnel studies for the purpose of pollutant transport and canyon ventilation one must always ensure that the model reproduces the main features of interest of the full-scale case. To ensure this one must consider the scaling of the upstream boundary layer, comparison of the mean turbulence statistics and an investigation of the instantaneous turbulence dynamics.

It is well established that atmospheric boundary layers can be simulated using roughness, barriers and turbulence generators to produce specific aerodynamic roughness lengths, length scales and other important boundary layer parameters within the wind tunnel [4, 5]. However, this method is not commonly employed when investigating the flow in urban street canyons [10]. Using scaling methods described by ESDU the idealized wind tunnel models from the present research reproduced boundary layers ranging from rural to urban demonstrating the ability to use idealized roughness arrays to investigate multiple full-scale urban street canyon cases. This scaling method was also applied to a full-scale case and determined that this case is also well represented by ESDU profiles.

A comparison between wind tunnel and field data of equivalent geometry has shown that the wind tunnel model is able to reproduce the mean turbulence statistics of the full-scale case with the exception of the mean spanwise velocity and turbulence intensity. Both of these are under-estimated by the wind tunnel model. The strong spanwise velocity is likely a result of the constant variation of the upstream wind direction causing channeling within the canyon. This is a common issue as several other field studies in the literature

have noted the phenomena [1, 2, 6]. The influence of the spanwise velocity within the canyon also results in a discrepancy between the wind tunnel and field results of two-point spatial correlations between the sonic anemometers within the canyon. The presence of strong spanwise velocity within the canyon suggests that modeling a canyon within the wind tunnel as two-dimensional may not be appropriate for the full-scale case. The effect of atmospheric stability has been investigated in the literature and has shown that stability influences the velocity variances within the canyon [6, 9]. Since wind tunnel models are generally subjected to atmospheric boundary layers of neutral stability (except in specialized stratified flow wind tunnels) this could limit their applicability to many full-scale cases. It has been suggested by Takimoto et al. [11] that a cube array of equivalent geometry can reproduce the intermittent sweep and ejection events of the full-scale case along with the large-scale coherent structures in the overlying boundary layer. The present study does not include any analysis of the intermittent canyon dynamics and, therefore, cannot confirm this statement.

Overall, idealized wind tunnel roughness arrays and canyon models reproduce the main features of full-scale cases. However, there is some question on whether wind tunnel models using two-dimensional canyons can duplicate the large spanwise velocity present in the field and whether neutral stability is appropriate.

4.2 Influence of approach flow conditions

The influence of the upstream boundary layer has been investigated for several wind tunnel configurations and in the field study. Three different roughness arrays were used in the wind tunnel to include both two-dimensional and three-dimensional roughness as well as different plan area packing densities. The results show that above the canyon the mean turbulence statistics such as mean streamwise velocity and Reynolds shear stress are directly influenced by the upstream roughness and show little influence from the canyon aspect ratio, AR. However, within the canyon there is negligible influence from the upstream roughness on the mean streamwise velocity or the streamwise turbulence intensity. This is in agreement with the field study data as within the canyon the mean turbulence statistic profiles including mean streamwise, Reynolds shear stress and all three components of turbulence intensity, show that the different upstream terrain types

result in only small differences in the profiles. However, it should be noted that the two terrain types studied in the field were of similar roughness length and only small differences in the profiles are, therefore, to be expected. From the wind tunnel study it can also be seen that the size of the shear layer above the canyon is mainly influenced by the canyon AR with little impact from the upstream roughness. However, the across canyon opening vertical fluxes, that influence canyon ventilation, are influenced by both the upstream roughness and canyon AR. The wind tunnel model using the field study configuration further confirms this as the reduced AR results in reduced vertical fluxes compared with the case of AR = 1 and 25% staggered cube array (Rcu). From the field study, it can be seen that the turbulence spectra for all three components of velocity are similar for both upstream roughnesses, as are the vertical fluxes from both the mean and instantaneous velocity. The two-point spatial correlation between the mast and the canyon show some differences between the approach flow directions, but this is likely a result of the location of the mast, which is upstream for one case and downstream for the other. The influence of the upstream roughness in the field study is possibly limited due to the similar values of roughness length from the two terrain types (z_o = 0.1 m and 0.3 m), whereas in the wind tunnel the roughness lengths vary greatly from 0.03 m to 0.7 m.

The influence of the wind direction is not commonly studied within the wind tunnel and in the present case only perpendicular flow was studied. Although care was taken to select only cases that have approximately perpendicular flow in the field study there is a significant increase of the spanwise turbulence intensity and mean velocity when compared with wind tunnel data. From the investigation in Chapter 3 and as previously mentioned this has been found to be a result of large-scale changes in approach wind direction [3, 6, 12].

Overall, the upstream roughness is an important influence on the characteristics of the flow within and above the canyon. When modeling street canyon configurations in the wind tunnel care must be taken to select the appropriate upstream roughness configuration to achieve the desired boundary layer characteristics.

4.3 Significance and application

The present study is a significant contribution to the field of environmental fluid mechanics. It is one of the only wind tunnel studies to have encompassed both two-dimensional and three-dimensional roughness configurations and different plan area packing densities. These geometries were chosen to ensure both skimming and wake interference flow regimes were modeled. As well, it includes detailed scaling of the upstream boundary layer, which is commonly overlooked in the literature relating to street canyon flow modelling. The present research is also one of the first studies to have compared field data with wind tunnel data in terms of canyon flow and turbulence statistics. Previous literature in this area has focused on dispersion characteristics with little attention given to flow measurements. The present work provides sufficient measurements to describe the mean turbulence statistics within the canyon.

Poor air quality is significant concern for human health, particularly in urban areas. The transport of momentum, heat and pollutants in urban areas is a result of the intermittent interaction between the highly-sheared atmospheric boundary layer and the individual street canyons. The present work provides a basis for understanding the flow structures that govern these processes. The analysis of the wind tunnel study provides important information relating to boundary layer characteristics that can then be used to classify the approach flow regime. Future analysis of the intermittent flow structures governing street canyon ventilation will include classification of the dynamical structures in terms of the approaching boundary layer flow regime. The future work will aim to identify and quantify the frequency and strength of these flow structures that play a key role in the transport of momentum and pollutants in urban areas.

The overall goal of the present research program is to develop methodologies and models able to reproduce both the dynamical and the thermo-dynamical interactions between atmospheric boundary layer flows and urban areas. This will be done from the city scale, with the Large Eddy Simulation atmospheric model ARPS/SUBMESO [8], to the street scale, with Computational Fluid Dynamics (CFD) models using Reynolds-Averaged Navier-Stokes (RANS) approaches within the code CHENSI [7].

With current public interest in air quality and air contaminants increasing this research is significant as it can be used to further understand the mechanisms behind car and building exhaust recirculation and re-entrainment in urban street canyons. Furthermore, with an understanding of the turbulent flow mechanisms involved, future urban planning can prevent negative air quality issues from arising in the urban environment.

4.4 Recommendations

From the present work several recommendations can be made. First, it is evident that scaling of the approaching boundary layer is particularly important to defining the upstream roughness. Knowing which full-scale case (urban, suburban or rural) is being modeled will help determine whether the configuration is applicable to urban street canyon ventilation. Furthermore, the 2D roughness configuration with AR = 1 (R1h) represents a rural boundary layer and is, therefore, not applicable to urban areas. Although this is one of the most often used wind tunnel configurations when investigating urban canyon ventilation it is recommended that it is not used in future studies. It is also recommended that the geometry of the configuration be chosen carefully because cases with equal plan area packing density, but different geometry, have been shown to exhibit different flow characteristics.

Modeling this problem in the wind tunnel has been shown to underestimate the spanwise velocity and turbulence intensity of the full-scale case. This large discrepancy is postulated to be a result of the changing of the wind direction. As such, it is recommended that wind tunnel modeling be undertaken to investigate the effect of changing wind direction within the wind tunnel on the spanwise statistics. The low frequency, large-scale wind changes could be investigated using slow rotations of the canyon model on a turntable. As well, the influence of atmospheric stability should be investigated in the present work to compare with results found in the literature.

Finally, it is recommended that further analysis be conducted on the results from the present wind tunnel configurations, as well as other configurations varying in plan area packing density. This analysis would investigate the spatio-temporal dynamics of the complex flow that exists in the canyon and that is believed to be responsible for the

pollution ventilation mechanisms. It would provide a quantification of both frequency and strength of the flow mechanisms very close to that encountered in real cities.

4.5 Conclusion

The present work has been a significant contribution to the field of environmental fluid mechanics. It furthers the understanding of urban street canyon flow in terms of modeling the urban boundary layer in the wind tunnel and the influence of the approaching flow conditions on the canyon flow. This work provides a basis for future work in analyzing the spatio-temporal dynamics of the mechanisms responsible for the transport of pollutants in urban areas.

4.6 References

1. Arnfield AJ, Mills GM (1994) An analysis of the circulation characteristics and energy budget of dry, asymmetric, east-west urban canyon. I. Circulation characteristics. Int J Climatol 14:119-134

2. Brown MJ, Khalsa H, Nelson M, Boswell D (2004) Street canyon flow patterns in a horizontal plane: measurements from the joint urban 2003 field experiment. Proceedings of the 5th Symposium on the Urban Environment 2004, Tokyo, Japan

3. Eliasson I, Offerle B, Grimmond CSB, Lindqvist S (2006) Wind fields and turbulence statistics in an urban street canyon. Atmos Environ 40:1-16

4. ESDU (1982) Strong winds in the atmospheric boundary layer. Part I: mean-hourly wind speeds. Data Item 82026 (amended 1993), Engineering Sciences Data Unit International

5. ESDU (1985) Characteristics of atmospheric turbulence near the ground. Part II: single point data for strong winds (neutral atmosphere. Data Item 852020 (amended 1993), Engineering Sciences Data Unit International

6. Klein P, Clark JV (2007) Flow variability in a North American downtown street canyon. Amer Meteorol Soc 46:851-877

7. Lakehal D, Mestayer PG, Edson JB, Anquetin S, Sini JF (1995) Eulero-Lagrangian simulation of raindrop trajectories and impacts within the urban canopy. Atmos Environ 29: 3501-3517

8. Leroyer S (2006) Simulations numeriques de l'atmosphere urbaine avec le modele SUBMESO: application a la champagne CLU-ESCOMPTE sur l'agglomeration de Marseille. Dissertation, École Centrale de Nantes

9. Rotach MW (1995) Profiles of turbulence statistics in and above an urban street canyon. Atmos Environ 29:1473-1486

10. Savory E, Perret L, Rivet C (2013) Modelling considerations for examining the mean and unsteady flow in a simple urban-type street canyon. Meteorol Atmos Phys 121:1-16

11. Takimoto H, Sato A, Barlow JF, Moriwaki R, Inagaki A, Onomura S, Kanda M (2011) Particle image velocimetry measurements of turbulence flow within outdoor and indoor urban scale models and flushing motions in urban canopy layers. Bound Layer Meteorol 140:295-314

12. Zajic D, Fernando HJS, Calhoun R, Princevac M, Brown MJ, Pardyjak ER (2011) Flow and turbulence in an urban canyon. Amer Meterol Soc 50:203-223

Appendices

The following appendices provide additional figures supplementary to those provided in the thesis text.

Appendix A: Boundary layer characteristics using the Log Law

The boundary layer characteristics, roughness length (z_o), displacement height (d) and friction velocity (u_*), were calculated for each upstream boundary layer using the log law (Equation 14). The following appendix describes the procedure for calculating these parameters using the 2D bar with $\lambda_p = 25\%$ configuration (R3h) as an example.

Equation 14 Log law

$$u_z = \frac{u_*}{k}\left[\ln\left(\frac{z-d}{z_o}\right)\right]$$

u_* is determined from the region of constant stress in the shear stress profile using Equation 15 (Figure 53). Within the wind tunnel a region of constant stress is not typically observed so the shear stress must be approximated by an average of the shear stress over some region, in the current example this region is from z = 0.1 – 0.2 m. This region is selected based on a combination of the flattest region of the profile and the expected value for this configuration from the literature. The resulting u_* for the R3h configuration is 0.42 m/s.

Equation 15 Friction velocity
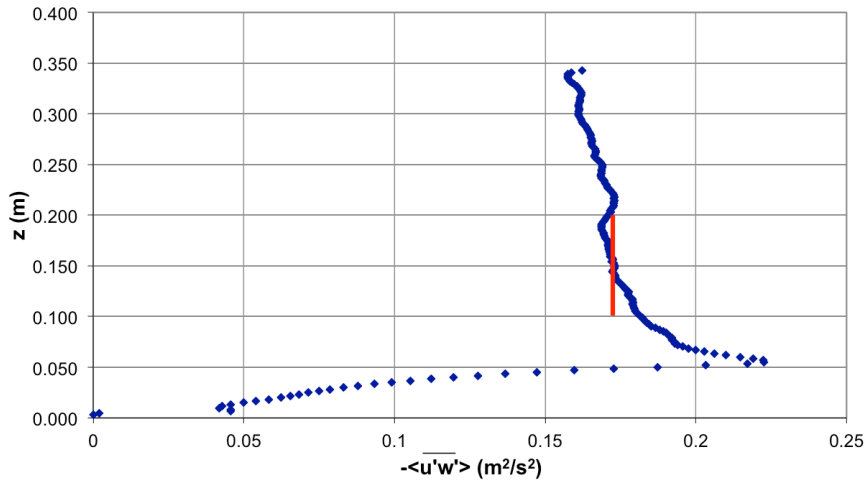
$$u_* = \sqrt{-u'w'}$$

Figure 53   R3h spatially averaged profile of shear stress with constant shear stress region shown with red line

A plot of streamwise velocity, U, as a function of height, z, is then used to determine z_o and d (Figure 54). The streamwise velocity is plotted as $\exp(Uk/u_*)$ where k is the Von Karman constant equal to 0.4. The parameters are found using the slope and intercept of the linear region of this plot (Equation 16). The parameters are highly dependent on the selection of the linear region, consequently results from the literature were used to verify the selection. Using this procedure for the R3h configuration z_o and d were found to be 0.006 m and 0.036 m, respectively.

Equation 16   Slope and intercept for z_o and d

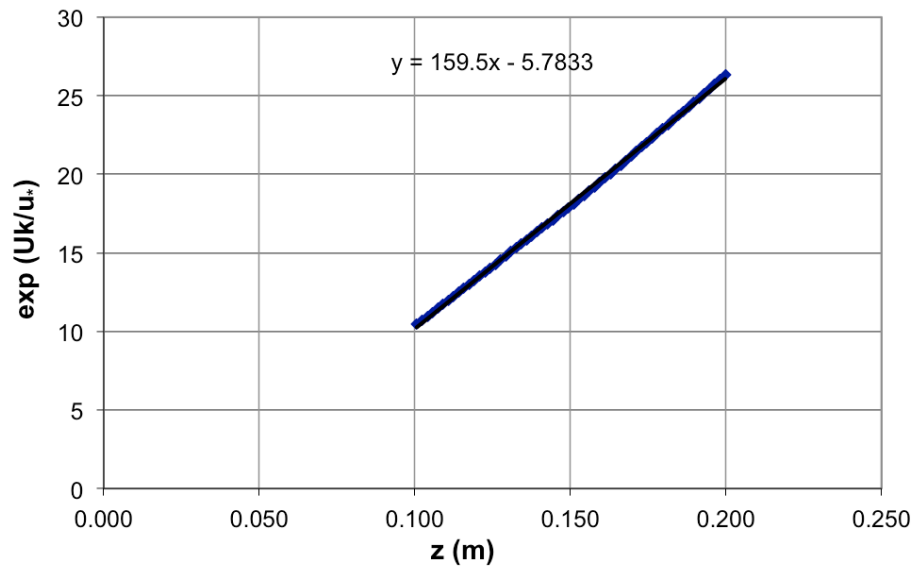$$Slope = \frac{1}{z_o} \qquad Intercept = \frac{d}{z_o}$$

Figure 54 Spatially averaged streamwise velocity showing linear region

Appendix B: Internal boundary layer development

The wind tunnel experiments of the present work employed an initial fetch of $\lambda_p = 25\%$ staggered cube array to initiate the development of a turbulent boundary layer. This results in the development of an internal boundary layer for both the R1h and R3h upstream roughness cases. The following section is an investigation of the development of the IBL.
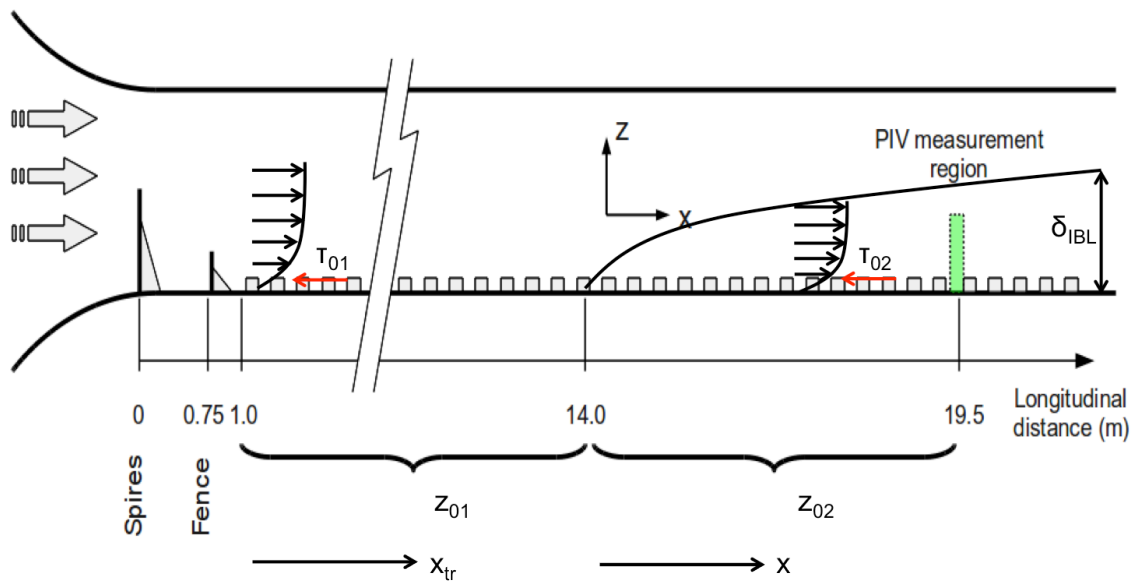

Figure 55 Wind tunnel experimental set-up showing internal boundary layer characteristics
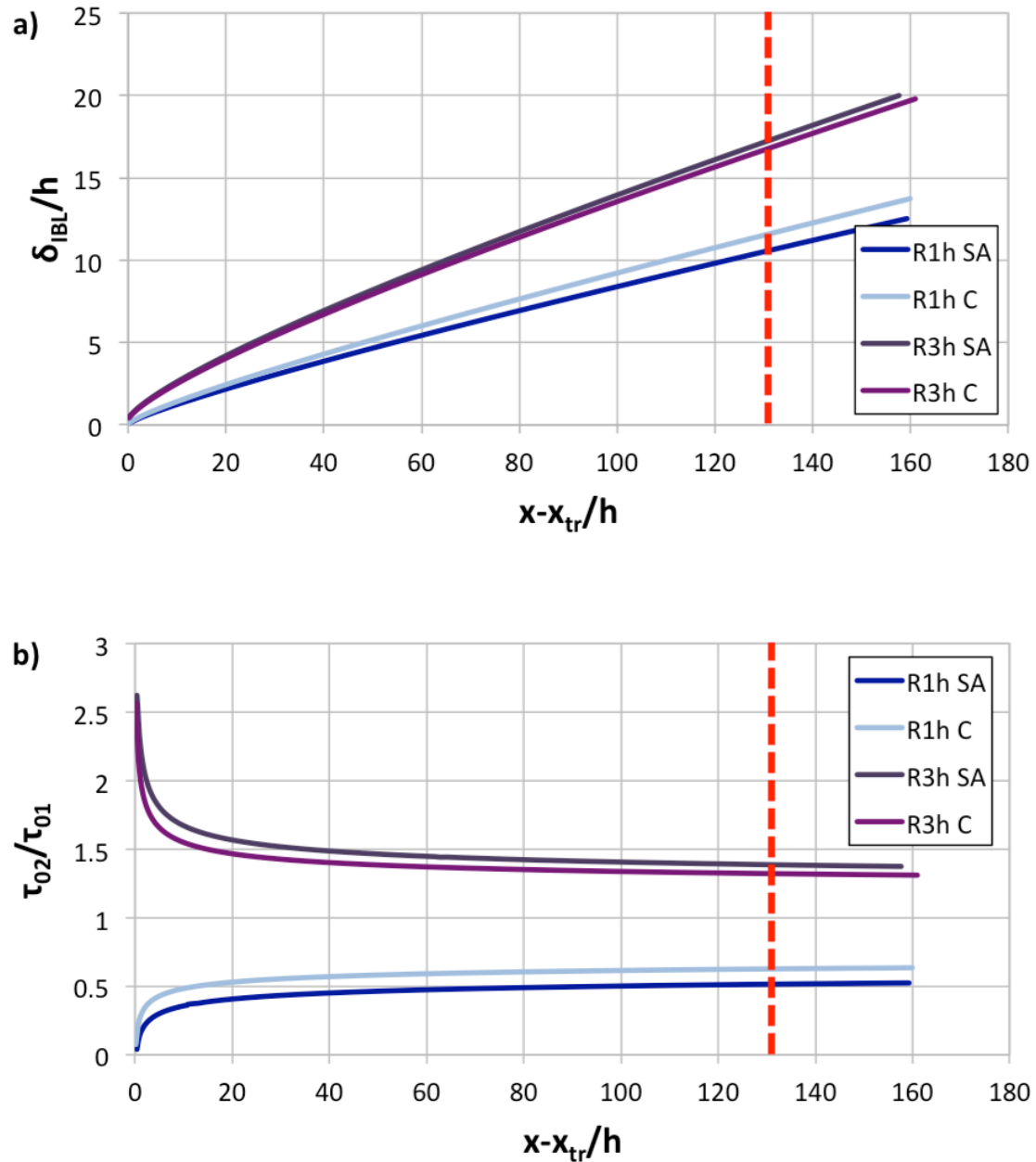
Figure 56   Estimated development of a) the depth of the IBL [3] and b) the shear stress [1] downstream of the terrain change with measurement location (▬ ▬), where SA = using spatially averaged and C = using centre profiles

By employing an initial x_{tr} = 13 m fetch of staggered cubes, the experimental setup used in the present work leads to a change in terrain for both the R1h and R3h configurations. This, in turn, leads to the development of an internal boundary layer (IBL) which forms

downstream of the roughness transition. The goal in the present work is not to investigate in detail the effect of the surface change on the flow evolution but, rather, to characterize the basic properties of the flow in the measurement section (x = 19.5 m, see Figure 55) as well as to ensure that the flow has reach equilibrium state, at least in the lowest part of the boundary layer. For more details on flow over changing terrain, the reader is referred to chapter 4 of Kaimal and Finnigan [2]. Previous studies have shown that a discontinuity of surface roughness is always accompanied by a change in surface momentum flux, which affects the characteristics of both the mean velocity profile and the turbulence [2]. This terrain transition can be primarily characterized by the parameter $M = \log(z_{01}/z_{02})$ where z_{01} and z_{02} are the roughness lengths upstream and downstream of the roughness discontinuity, respectively. Based on the use of the parameter M, analytical models have been developed to describe the longitudinal evolution downstream of the transition of both the depth of the IBL (δ_{IBL}) and the ratio of surface stresses τ_{01}/τ_{02} [2]. In the present work, the model of Panofsky and Dutton [3] is employed to estimate the depth of the IBL as a function of the longitudinal distance $x - x_{tr}$ after the transition, where $\kappa = 0.4$ is the Von Karman constant and B_1 is a constant equal to 1.25 [2] (Equation 17).

Equation 17   Panofsky & Dutton [3] model to estimate depth of IBL

$$\frac{\delta_{IBL}}{(x - x_{tr})}\left[\log\left(\frac{\delta_{IBL}}{z_{02}}\right) - 1\right] = B_1\kappa$$

The evolution of τ_{01}/τ_{02} is estimated using the model proposed by Jensen [1] that gives a direct estimation of the stress ratio as a function of the local IBL depth (Equation 18).

Equation 18   Jensen [1] model to estimate stress ratio

$$\frac{\tau_{02}}{\tau_{01}} = \log\left(1 - \frac{M}{\frac{\delta_{IBL}}{z_{02}}}\right)$$

The results of these two models are shown in Figure 56 for both the R1h and R3h configurations, where z_{01} corresponds to the roughness length of the flow developing

over the cube array (Rcu) and z_{02} corresponds to the roughness length of the flow developing over either the R1h or the R3h configuration (see Section 3.2 and Table 3 for a complete description of the characteristics of the flows). The terrain transition leads to the development of an IBL, the depth of which extends beyond the PIV measurement area (Figure 56a). The largest IBL was obtained for the R3h configuration, which has the largest roughness length (Table 3, page 37) and corresponds to smooth to rough transition. As expected, the terrain discontinuity induces an overshoot in surface stress and the attainment of a new equilibrium as the flow adjusts to the new terrain (Figure 56b). After a distance of 40h, it can be considered that an equilibrium state has been reached. It is noticeable that, despite its simplicity, the prediction of τ_{01}/τ_{02} of the model proposed by Jensen [1] at the most downstream location (corresponding to the PIV measurement section) agrees very well with the value of the surface stress obtained directly from the estimation of the friction velocity based on the use of the shear stress profile, for both configurations. From these results, it thus can be considered that for the 3 configurations, the fetch is sufficient for the flow to reach an equilibrium state at the measurement section (x = 19.5 m). In the same manner, the estimated longitudinal integral length scales of the flow (Figure 15d) are noticeably smaller than the distance from the terrain transition, which confirms that the investigated canyon flows are free from the initial transition influence.

References

1. Jensen NO (1978) Change of surface roughness and the planetary boundary layer. Q.J.R Meteorol Soc 104:351-356

2. Kaimal JC, Finnigan JJ (1994) Atmospheric boundary layer flows: their structure and measurement. Oxford University Press, 304 pages

3. Panofsky HA, Dutton JA (1984) Atmospheric turbulence: models and methods for engineering applications, Wiley, 397 pages

Appendix C: Convergence of turbulence statistics for a 30 minute period

The convergence of statistics is important to consider as it shows us whether the averaging period results in reliable statistics. Figure 57 shows the convergence of mean streamwise velocity, all three turbulence intensities and Reynolds shear stress over a sample 30 minute period of field data. As demonstrated by the figures convergence is obtained over this time period for all of the statistics.
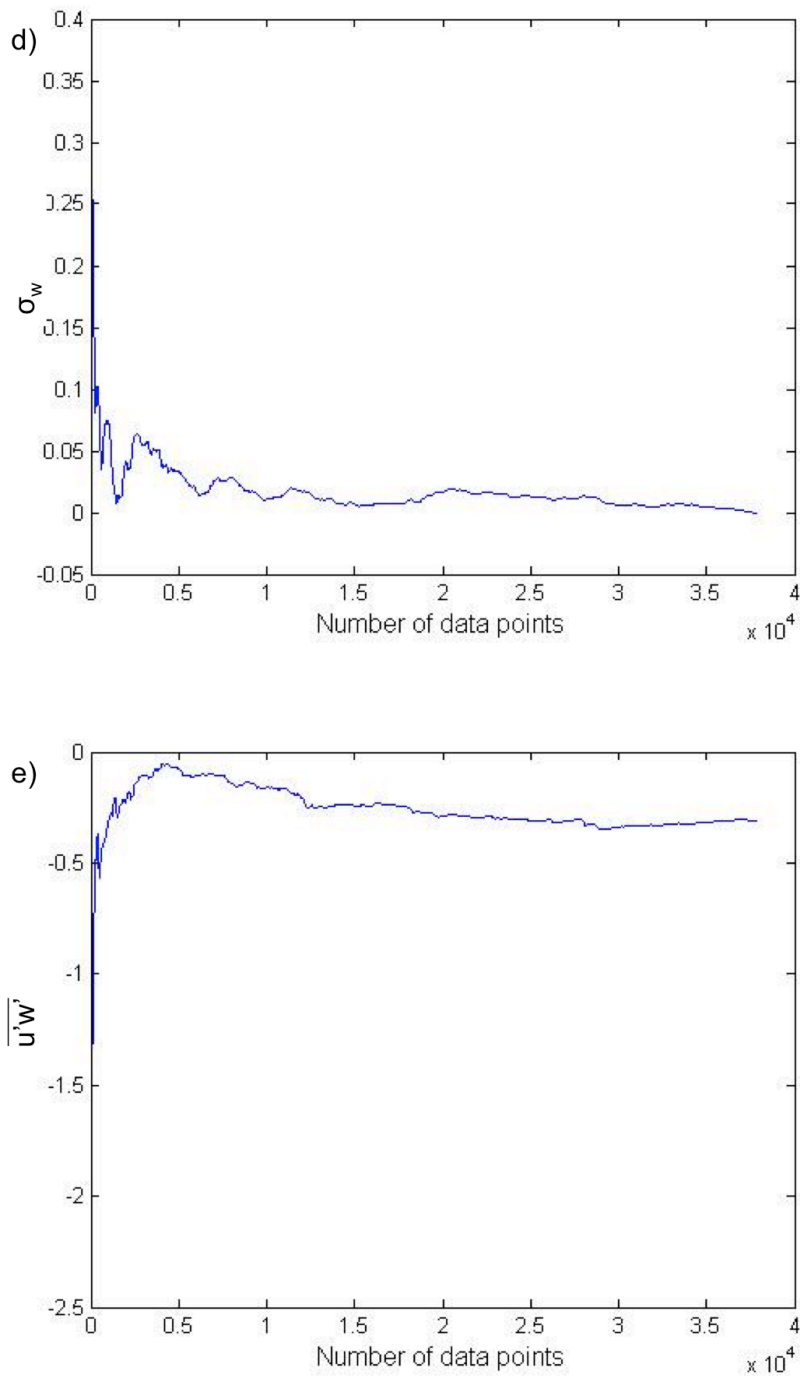

a)

b)

c)
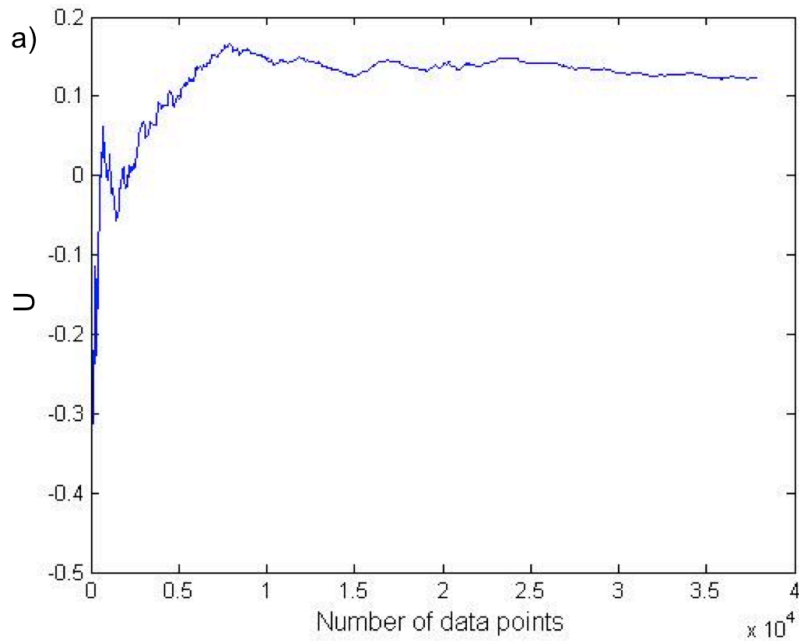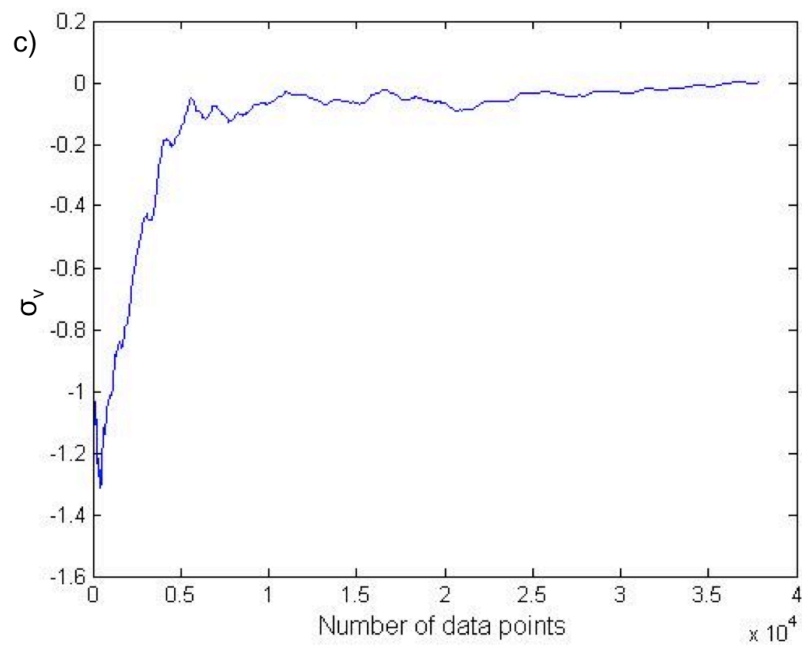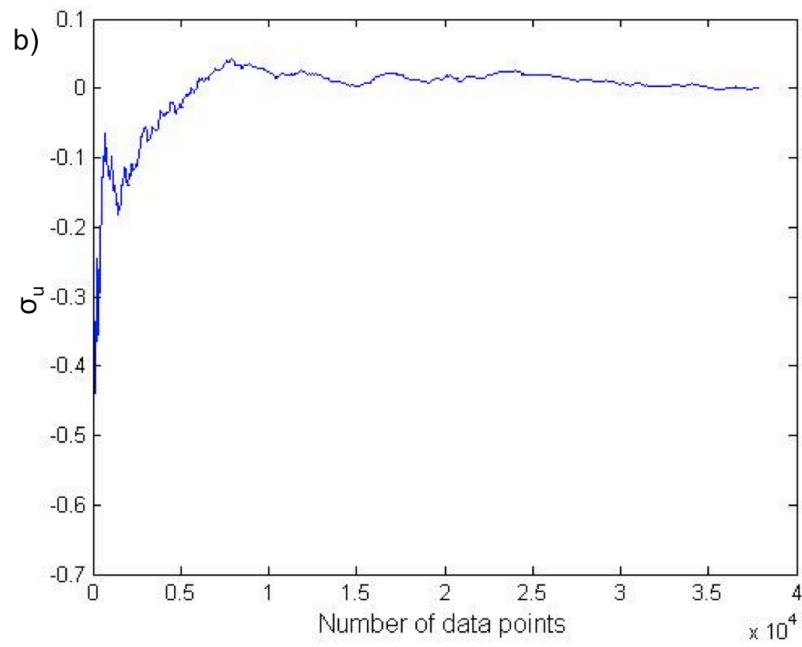
Figure 57   Example of convergence for a 30 minute period showing a) streamwise velocity; b) streamwise turbulence intensity; c) spanwise turbulence intensity and d) vertical turbulence intensity; e) Reynolds shear stress

Curriculum Vitae

Name: Karin Blackman

Post-secondary   University of Guelph
Education and   Guelph, Ontario, Canada
Degrees: 2007-2012 B.Eng.

                    The University of Western Ontario
                    London, Ontario, Canada
                    2012-2014 M.E.Sc.

Honours and   Province of Ontario Graduate Scholarship
Awards: 2013-2014

Related Work   Teaching Assistant
Experience   The University of Western Ontario
                    2012-2014

                    Junior Air Quality and Acoustics Scientist (Co-op)
                    Stantec Consulting Ltd.
                    2011

Publications:

Blackman, Karin, Perret, Laurent, and Savory, Eric. (2014) Effect of upstream flow regime on street canyon flow mean turbulence statistics. Journal of Environmental Fluid Mechanics, Submission Date: March, 2014.

Blackman, Karin, Perret, Laurent, and Savory, Eric. (2014) Wind tunnel modeling of upstream roughness arrays for street canyon flow studies. Proceedings of the Canadian Society for Mechanical Engineering International Congress, Toronto, CA, 1-4 June 2014.

Mubareka, Samira, Scott, James, Savory, Eric, Lin, William, Cuthbertson, Lauren, Blackman, Karin, and Roberto, Matthew. (2014) Western Cold and Flu (WeCoF) aerosol study – preliminary results. Proceedings of the Canadian Society for Mechanical Engineering International Congress, Toronto, CA, 1-4 June 2014.

Perret, Laurent, Blackman, Karin, and Savory, Eric. (2013) Effect of upstream flow regime on street canyon flow dynamics. Proceedings of International Workshop on Physical Modeling of Flow and Dispersion Phenomena, University of Surrey, UK, 16-18 September 2013.

Perret, Laurent, Savory, Eric, and Blackman, Karin. (2013) Towards a classification of street canyon regimes based on flow dynamics. Proceedings of European-African Conference on Wind Engineering, University of Cambridge, UK, 7-11 July 2013.